ELECTRONIC CORRELATION IN C_{60} AND OTHER MOLECULES

By

FEI LIN, B.Sc.Hons.

A Thesis
Submitted to the School of Graduate Studies
in Partial Fulfilment of the Requirements
for the Degree
Master of Science

McMaster University

MASTER OF SCIENCE (2003) McMaster University
(Condensed Matter) Hamilton, Ontario

TITLE: ELECTRONIC CORRELATION IN C_{60} AND OTHER MOLECULES

AUTHOR: Fei Lin,B.Sc.Hons.(Nanjing University, P.R. China)

SUPERVISOR: Dr. C. Kallin, Dr. A.J. Berlinsky

NUMBER OF PAGES: 1, 125

Abstract

In this thesis, we investigate the possibility that a purely electronic mechanism is the cause of superconductivity in C_{60} materials. Several computational methods are adopted to calculate the pair-binding energy. They are perturbation theory, exact diagonalization, Gutzwiller projection, and auxiliary field Monte Carlo. Results from these different methods are compared with each other both in a C_{60} molecule and in other smaller molecules in order to test conclusions about whether or not a purely electronic mechanism can lead to an attractive interactions between electrons in C_{60} molecules.

Besides this test of the superconductivity mechanism, we also explain in detail how to apply these different computational methods to C_{60} for the specific geometry of C_{60}. Clearly illustrating these computational methods is the second goal of this thesis.

Our final conclusion is that for both small and large Hubbard interaction U, there is pair binding in a single C_{60} molecule. For intermediate Hubbard interaction strength, there is no clear evidence for pair binding for the range of temperatures we explored. We suggest that the truncation of the Coulomb interaction, which is implicit in the Hubbard Hamiltonian, may suppress pair-binding of electrons in C_{60} and that it may be necessary to consider a model that includes the long range character of Coulomb interaction. This is a subject for further study.

Contents

List of Tables

List of Figures

Acknowledgements

In this acknowledgement, I should first thank my supervisors Professors Catherine Kallin and A. John Berlinsky for introducing me this interesting research project, otherwise, I would probably stay far away from the beautiful C_{60} molecule and never know what is happening there. I also thank them for suggesting me to study Gutzwiller projection for application in C_{60}. Because of this, I started to understand some results in the high Tc cuprates, where this projection operations have been used in some theoretical papers. This also opens my way to the practice of Monte Carlo simulations, which I learnt before but has never been applied to a real research project. I should also thank my supervisors John and Catherine for their patience in reading through the rather awkward draft, correcting the grammar errors and spelling mistakes in it, and pointing out the calculation mistakes.

Designing programs in a computer has occupied most of the research time. Often, errors were detected when I thought the programs were right, and then recalculations and replotting of graphs followed. This cost of energy has made me doubt the efficiency of my work. At this time talking with my wife Hong Tao is always important. I thank her for her accompany and encouragement, which sustained me through all these difficulties. I also want to thank my parents and my brother for their constant phone calls to ask about my research.

Thanks are also presented to Dr. Erik Sorensen, whose comments from the perspective of a computational physicist are helpful for my further study and research. As he is a member of the examination committee, I especially thank him for reading my thesis in this rather busy season of the year.

I also thank Dr. Amit Ghosal for providing me an excellent random number generator, and Patrick Byrne for providing me a latex thesis format.

Most of the Monte Carlo calculations were done in McMaster's supercomputer SHARCnet. The computation times in it are gratefully acknowledged.

Chapter 1

Geometry of C_{60} Molecule

C_{60} (Buckminsterfullerene), discovered [1] in 1985 by three Nobel laureates R.F. Curl, H.W. Kroto and R.E. Smalley, is regarded as the most symmetrical and beautiful molecule in the world. It was named after the famous architect Buckminster Fuller, because its structure resembles that of a dome built by the architect for the 1967 Expo in Montreal.

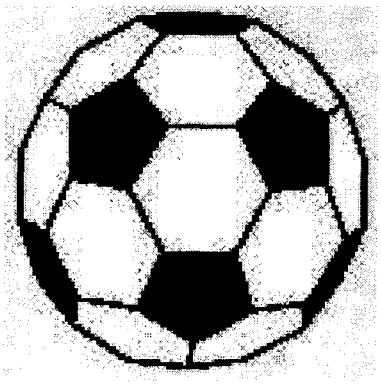

Figure 1.1: C_{60} molecule geometry.

The molecule is a closed cage, consisting of 12 pentagons and 20 hexagons. It has

the symmetry of the icosahedral point group with 120 symmetry operations, and all the 60 carbon atoms are equivalent in the sense that the symmetry operations can always bring one atom to the other. See Fig. 1.1 for a picture of the molecule.

X-ray analysis shows the diameter of the molecule to be approximately $7\mathring{A}$. Two kinds of bond lengths are present in C_{60}, the longer ones between a pentagon and a hexagon (single bonds, $1.46\mathring{A}$) and the shorter ones between two hexagons (double bonds, $1.40\mathring{A}$). When the molecules condense into a solid of fcc lattice (lattice constant $14\mathring{A}$), the shortest separation between two atoms on different molecules is about $3.1\mathring{A}$. There are two inequivalent molecule orientations allowed in pure C_{60} at low temperatures and they have a ratio of about 5 : 1 [2]. Most theoretical calculations assume a unidirection for all the molecules while Gelfand et al. [3, 4, 5] did consider orientation disorder. In this thesis, we will not touch this fcc lattice, but confine our calculations on a single molecule. We find it useful to list the coordinate, the nearest neighbor and next nearest neighbor data of the 60 atoms in a C_{60} molecule, which will be used for subsequent numerical calculations. The data are in Appendix M.

Chapter 2

Superconductivity and Pair Binding

With the development of techniques for producing larger and larger C_{60} samples during the late 1980's, there came the discovery of superconductivity in electron doped C_{60} [6, 7] in 1991. C_{60} doped with potassium has a superconductivity transition temperature of 18K in bulk material. Higher transition temperatures were found for C_{60} doped with rubidium (28K) and later 33K for $RbCs_2C_{60}$ and 40K for Cs_3C_{60} under pressure. Since then, more and more research has been done, both experimentally and theoretically [10], on C_{60} related materials. Despite the great effort devoted to it, the mechanism of the superconductivity in C_{60} related materials is still unclear. Whether it is a phonon mediated phenomenon, a purely electronic result or the combination of these two is still a subject of debate [10]. In this thesis, we carry out a study of what on earth causes superconductivity in this interesting material, and place our emphasis on how the pair binding energy is formed in C_{60}, which is, as in the BCS theory of conventional superconductors, thought to lead to superconductivity. Calculations here are based on the Hubbard model and hence on a purely electronic mechanism.

The pair binding energy, in the case of free C_{60} molecules, is defined as

$$E_b = (E(60) + E(62)) - 2E(61) \tag{2.1}$$

for electron doping or

$$E_b = (E(60) + E(58)) - 2E(59) \tag{2.2}$$

for hole doping. The numbers in the brackets refer to the electron numbers in a C_{60} molecule. Our criterion for the occurance of attractive interaction between electrons is that E_b is negative. This main quantity that we are going to calculate in the subsequent chapters has appeared in several papers. For example, Fye et al. [12] calculated hole binding energies in one-dimensional Hubbard chains using Bethe ansatz [13]. Fano et al. [14] calculated hole binding energies of a two-dimensional Hubbard model on a 4×4 cluster by exact diagonalization; and White et al. [15] exactly diagonalized the Hubbard model on small molecules, where both nearest and next nearest neighbor Coulomb interactions were taken into account. Especially, the paper of White et al. aimed at supporting a purely electronic mechanism of superconductivity in doped C_{60}, which had been previously proposed by Kivelson et al. [16, 17, 18] by perturbation calculations, but White et al. did not deal with C_{60} directly because it has too many sites (total 60) for exact diagonalization.

In our article, we will treat the C_{60} molecule directly and calculate the pair binding energy for either electrons or holes with various methods. Results from different methods are compared with each other in order to draw a sound conclusion concerning whether or not a purely electronic mechanism can induce pairing interactions between electrons or holes.

Calculations are also done on other molecules smaller than C_{60}. These smaller molecules include hydrogen, tetrahedron, cube, truncated tetrahedron, etc. Calculations on these molecules can, on the one hand, check the validity of the results from C_{60}, and on the other hand, provide us with more information on some aspects of electronic interactions, such as the spin-spin correlation energies. Our discussions will also include the concept of mesocale physics [19], which is believed to play an important role in both high temperature superconductors and other more complex systems.

Chapter 3

Model

In order to understand the physics underlying a phenomenon, models must be built. They must have the potential to contain the mechanism that causes the phenonmenon, and they should also be free of other unnecessary parameters to simplify calculations. The model that is most widely used in the study of high Tc superconductivity and also in other strongly correlated systems is the Hubbard model, which is believed by most people to capture the main physics. See, for example, the discussion of Anderson in [20].

The Hubbard model is usually written as

$$H = -t \sum_{<ij>,\sigma} (c^+_{i\sigma} c_{j\sigma} + h.c.) + U \sum_i n_{i\uparrow} n_{i\downarrow} - \mu \sum_i (n_{i\uparrow} + n_{i\downarrow}), \tag{3.1}$$

where, $c_{i,\sigma}(c^+_{i,\sigma})$ annihilates (creates) an electron on site i with spin σ; $n_{i\sigma}$ is the electron number on lattice site i with spin σ; t is the hopping integral between nearest sites, μ is the chemical potential and U is the Coulomb interaction between two electrons on the same lattice site; *h.c.* means Hermitian conjugate.

Some basic properties of the Hubbard Hamiltonian can be found easily: First, it conserves the total number of particles in the system. Second, it conserves the total spin at the system. Third, with a bit of work, one can show that at half filling, there is one additional symmetry in the Hamiltonian, i.e., particle-hole symmetry.

The difficulty in solving this model Eq.(3.1) results from the on-site Coulomb interaction term, i.e., $U \sum_i n_{i\uparrow} n_{i\downarrow}$. Generally, an analytic solution is not possible

at the level of mean field theory or for a one dimensional system, where an exact analytic solution is possible [13]. As a result, a lot of approximation schemes have been proposed to obtain at least some properties of the Hamiltonian. For example, the perturbation calculation in the small U case, Gutzwiller projection in the large U case, exact diagonalization of a system with a small number of lattice sites or Monte Carlo simulations. In this thesis, we will apply these techniques to study the pair-binding energy in C_{60} and other small or medium-sized molecules. We also make some comments on the strength and weakness of each of these techniques. For more introduction and discussion of the Hubbard model, we would refer interested readers to the book edited by M. Rasetti [21], where many computational approaches are reviewed.

The the Hubbard model neglects the long-range Coulomb interaction between electrons. There may be some justifications for this in C_{60} crystals [16], based on screening of the long-range Coulomb interaction by nearby electron clouds.

In the next chapter we will present detailed calculations for a single C_{60} molecule based on the Hubbard model. A large portion of the thesis is devoted to the discussion of various computational techniques used in model Hamiltonian calculations. For every computational method, we will briefly explain the main steps in these techniques, which will serve as a natural preparation for their application to C_{60}. Some minor steps, which might not be trivial to obtain, are put in the appendices. Thus one goal of this thesis is to explain things as clearly as possible in a pedagogical way.

Chapter 4

Perturbation Calculation

At the first attack on the Hubbard Hamiltonian Eq.(3.1), one might think of doing perturbation, regarding the on-site Coulomb interaction U as a small or not too large parameter compared to the energy band width in the single-electron picture. For instance, in a 2D square lattice, as long as U is less than $8t$ (the band width in single-electron picture), we will suppose that the on-site Coulomb interaction does not change the single-electron energy bands too much, and hence perturbation theory applies.

The calculation goes as follows: First, one neglects the U term, diagonalizing the Hamiltonian trivially for specific lattice configurations, and gets a set of energy bands and single-electron wave functions. Second, one fixes the chemical potential μ, i.e., the total number of particles in the system, and fills each energy band according to the Pauli principle. Third, one turns on the on-site interaction, and uses the wave functions obtained previously to calculate perturbatively (for the description of second order degenerate perturbation theory, see textbook [11]) the change of the energy bands and wave functions.

Returning to the problem of C_{60}, we find that the perturbation calculation based on the above scheme has been done by Chakravarty, Gelfand and Kivelson [16]. To make this thesis self-contained, we redo the perturbation, and explain the main results.

As we have mentioned, the symmetry of the C_{60} molecule is that of the icosahe-

dral group, and is nearly a spherical one. In the half-filled case, 60 electrons move independently within the big "π" molecular orbital that is formed by the 60 p_z atomic orbitals on the 60 carbon atoms. There are two kinds of hopping integrals in C_{60}: one is the hopping between two pentagons t', and the other is along the side of pentagons t. They have a ratio of $t'/t \approx 1.2$. An exact diagonalization of the non-interacting Hamiltonian gives 60 energy bands, and for the half- filled case, the 30 bands with the lowest energies are occupied. The lowest unoccupied molecular orbitals (LUMO) are 3-fold degenerate. The highest occupied molecular orbitals (HOMO) are 5-fold degenerate. The energy gap between them is $1.04t$ according to this single-electron picture. The detailed energy band information is drawn in Fig. 4.1.

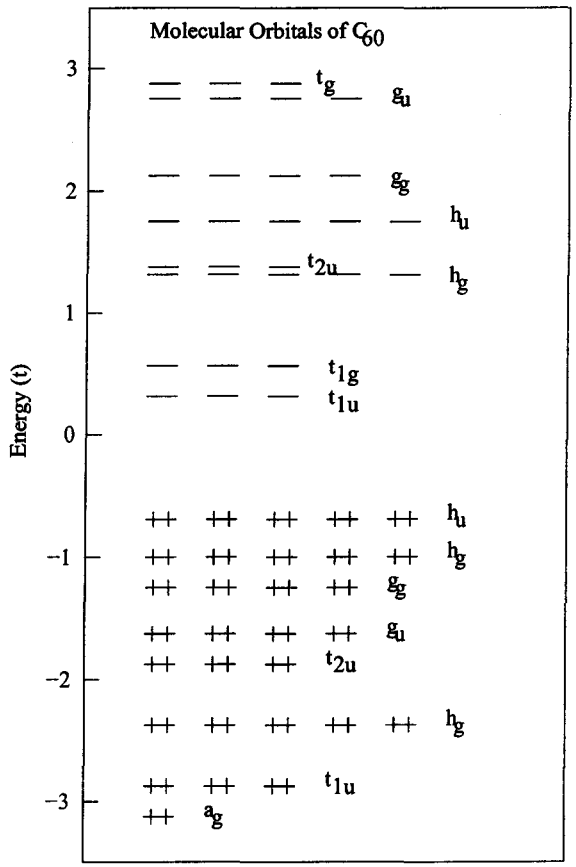

Figure 4.1: Huckel energy level diagram for neutral C_{60} molecule. The lowest 30 levels are occupied.

With the above information from the non-interacting Hamiltonian, we can proceed to include the on-site U term, and do a perturbation calculation to second order. The whole task in the perturbation calculation, is to add up all the intermediate states that can be accessed through the on-site perturbation U term. In second order perturbation theory, we need to consider two possibilities: one is that two electrons are excited to higher energy states first, then destroyed, and returned to original state or another lower energy state (two-particle excitation case); the other is that only one electron is excited to a higher energy state, followed by being destroyed again and returning to its original state or another degenerate state, while the other electron is destroyed in a band, and appears immediately in the same band again (one-particle excitation case). These two electronic processes are illustrated in Fig. 4.2.

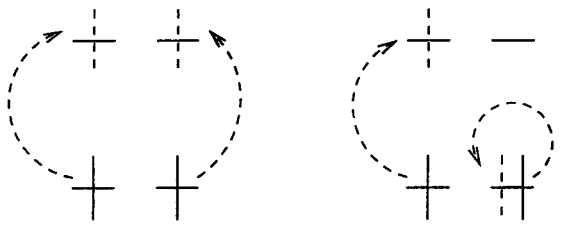

A. Two–particle excitation B. One–particle excitation

Figure 4.2: Two kinds of electronic excitation in perturbation calculations. The solid short lines are electrons in initial states, and the dashed lines are those in excited states.

For C_{60} molecules that are doped with electrons or holes, the perturbation calculation is basically the same, except that these calculations are more complicated and tedious in view of the degeneracy of the non-interacting wavefunctions. There are two ways to classify the degenerate wavefunctions. One is based on the symmetry of the C_{60} molecule. The other is based on the symmetry of the Hamiltonian under spin rotation. We first list Kivelson et al's results [16] in Table 4.1. Then we divide these wavefunctions into total spin $S_z = 0$ and $S_z = 1$ sectors (with two electrons or holes doping) according to the rotational symmetry of the Hamiltonian.

$E_{60}(L=0,S=0)$	$-100.80069+15(U/t)-0.74785(U/t)^2$
$E_{61}(L=1,S=1/2)$	$-100.80069+0.32166+15.5(U/t)-0.73772(U/t)^2$
$E_{62}(L=0,S=0)$	$-100.80069+0.32166\times 2+16.05(U/t)-0.74237(U/t)^2$
$E_{62}(L=1,S=1)$	$-100.80069+0.32166\times 2+16(U/t)-0.72557(U/t)^2$
$E_{62}(L=2,S=0)$	$-100.80069+0.32166\times 2+16.02(U/t)-0.73128(U/t)^2$
E_{59}	$-100.08003+14.5(U/t)-0.74535(U/t)^2$
$E_{62}(Sz=0)$	$-100.80069+0.32166\times 2+16.01(U/t)-1.48340(U/t)^2$
$E_{62}(Sz=1)$	$-100.80069+0.32166\times 2+16.00(U/t)-0.76447(U/t)^2$
$E_{58}(Sz=0)$	$-99.35938+13.98748(U/t)-0.78675(U/t)^2$
$E_{58}(Sz=1)$	$-99.35938+14(U/t)-0.75604(U/t)^2$

Table 4.1: Total electronic energies of a C_{60} molecule, either neutral, electron-doped or hole-doped (in units of t). The first 5 lines are taken from Kivelson et al's paper [16]. In the two electrons (holes) doping case, the last four energies are from the calculation with the classification of unperturbed wavefunctions based on the spin rotation symmetry of the Hamiltonian.

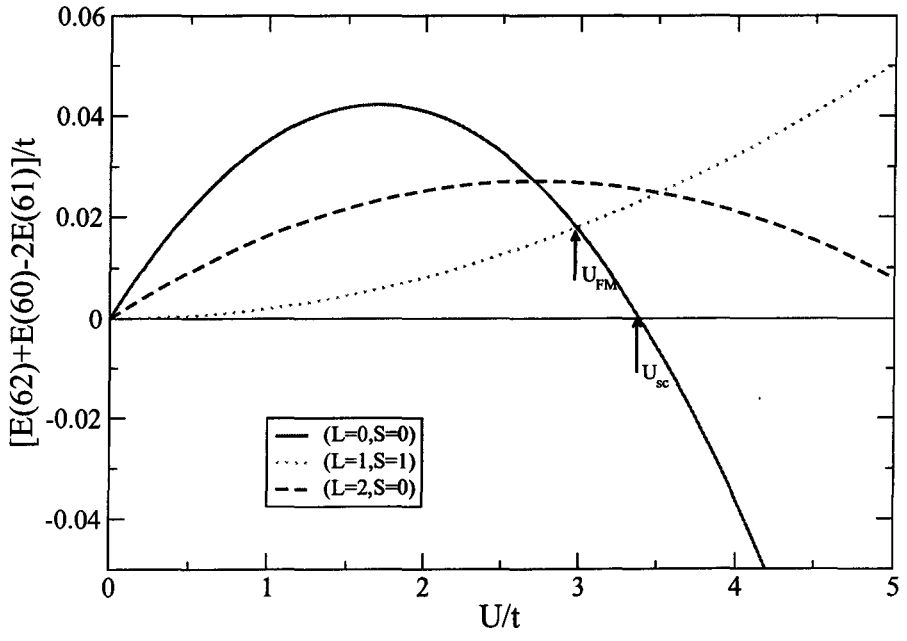

Figure 4.3: Pair-binding energy from perturbation calculation according to the molecule geometry of C_{60}. The data are taken from Kivelson et al's paper [16].

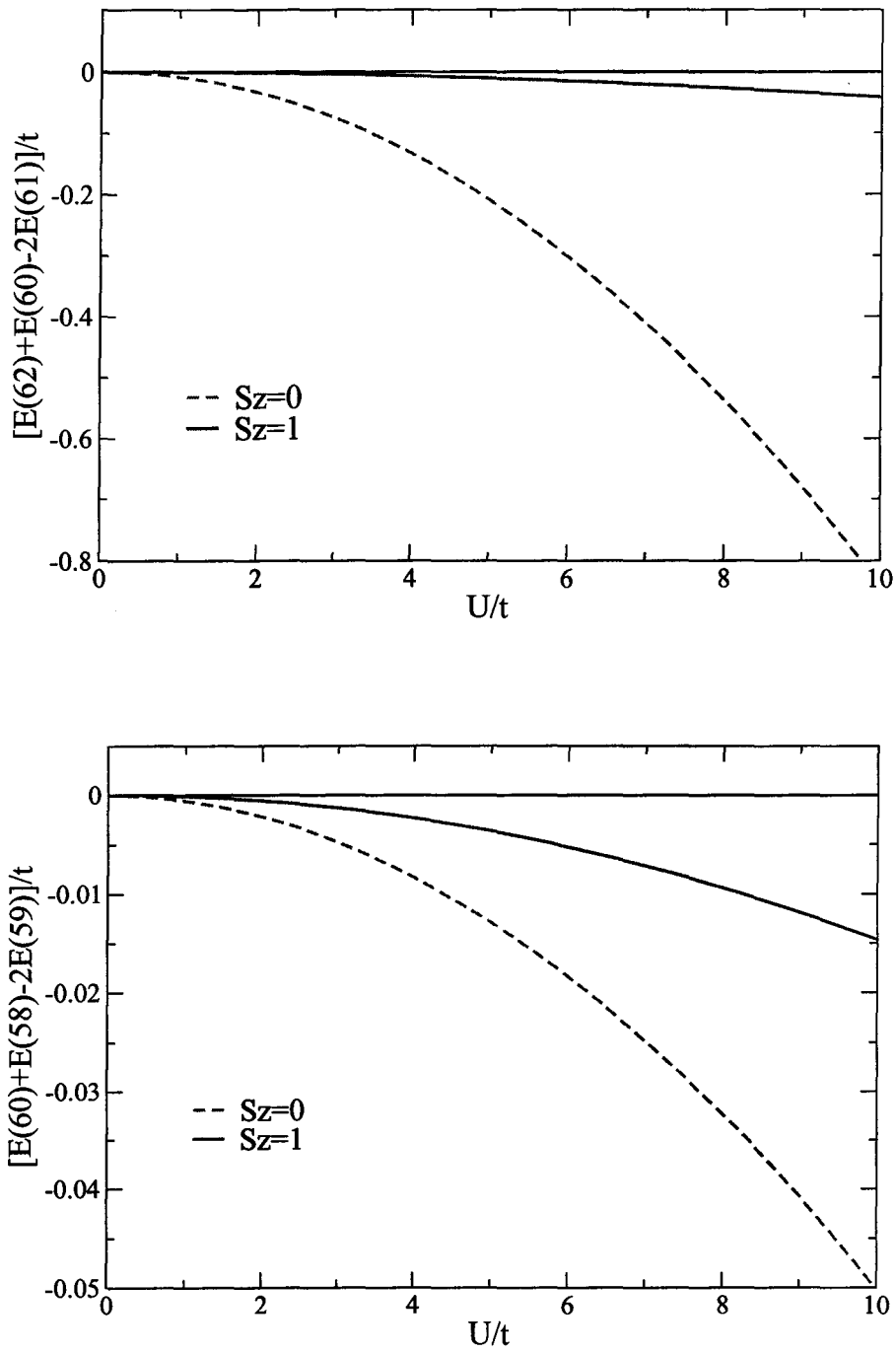

Figure 4.4: Pair-binding energy from perturbation calculation in electron- and hole-doped C_{60} according to the unperturbed wavefunctions classified by the spin rotation symmetry of the Hamiltonian.

From Fig. 4.3, we find that the pair binding does occur. For the electron doping case, the attractive interaction between electrons appears for an intermediate U value ($U_{sc} \approx 3.4t$). The transition between spin singlet and spin triplet is at about $U_{FM} = 3t$, and this has been discussed by Kivelson in terms of quantum transition between ferromagnetism and antiferromagnetism. In Fig. 4.4, where the unperturbed wavefunctions are divided into total spin $S_z = 0$ and $S_z = 1$ sectors, we see that $S_z = 0$ sector always has lower energy than the $S_z = 1$ sector.

Perturbation calculations on other smaller molecules are also performed, but we will not list them until in a later chapter where we discuss and compare different calculational approaches.

Chapter 5

Exact Diagonalization

As a way of approaching the solution of the Hubbard model, exact diagonalization has been applied to some small molecules or small clusters of atoms. The calculation begins with a counting of the number of states in the system. At every lattice site in the system, there are four kinds of occupation possibilities: doubly occupied, occupied by a spin-up electron, occupied by a spin-down electron and empty. Thus, the total number of basis wavefunctions (dimension of the Hilbert space) will be 4^n, where n is the number of lattice sites in the system. Although we can reduce some of these basis wavefunctions by applying some conservation laws, such as the total number of electrons in the system, and divide these wavefunctions into different total spin sectors, such as a sector with total spin $S_z = 0$ or a sector with total spin $S_z = \frac{\hbar}{2}$, we still have a huge number of basis wavefunctions to deal with, whenever $n > 8$. Some considerations on the geometrical symmetry of the lattice system can further block diagonalize the Hubbard Hamiltonian, and reduce the dimension of the matrix, as did by Dagotto et al. [22]. But we do not plan to incorporate these symmetry considerations here, and are satisfied with the maximum number of lattice sites we can reach, as these further considerations do not significantly reduce the computation tasks. The matrix formed by these basis wavefunctions will need a large amount of time to diagonalize even if we employ some special techniques that are to be discussed in the next sections, such as the Lanczos algorithm and Davidson algorithm. Before we do this, we first need to explain how to write down the matrix elements in the

matrix representation of the Hubbard Hamiltonian.

5.1 Matrix Representation of Hamiltonian

In the Configuration Interaction (CI) study of chemical bonding in Chemistry, one writes down the basis wavefunctions in a Slater determinant, including all possible permutations of electrons and atomic orbitals. However, we will not work with this representation but with the second quantization representation, which is more convenient for a model Hamiltonian calculations.

The antisymmetric property of the basis wavefunctions (Slater determinants) will be reflected in the anticommutation relation of the electronic creation and annihilation operators. To take into account this anticommutation nature, we need to define a definite ordering of lattice sites in the second quantization picture. We do this in the following way: (1) Every possible wavefunction is created by the application of an electronic creation operator on the vacuum. (2) The order of action of creation operators on the vacumm is from left to right according to the increase of the labelled site numbers. (3) The spin-up electron creation operator is placed to the left of the spin-down electron creation operator of the same site, if the site is doubly occupied. With this definition, the ambiguity of the second quantized wavefunctions are eliminated. We also employ some symbols to describe different occupation information at each site. For example, a doubly occupied site will be denoted by 2, a site occupied by one spin-up electron will be denoted by 1, a site occupied by one spin-down electron will be denoted by -1, and an empty site will be represented by 0. To summarize the above discussions, we give an example of a sample wavefunction in an N-site system.

$$|21-10\cdots 1>=c^{+}_{1\uparrow}c^{+}_{1\downarrow}c^{+}_{2\uparrow}c^{+}_{3\downarrow}\cdots c^{+}_{N\uparrow}|V>, \tag{5.1}$$

where $|V>$ represents the vacumm.

Having written down the basis wavefunctions in second quantization form, we need to calculate matrix elements of the Hamiltonian with respect to these basis wavefunctions. Suppose $|\alpha>$ and $|\beta>$ are two of the wavefunctions, and we want

to calculate $< \alpha|\hat{H}|\beta >$, where $\hat{H}$ is the Hubbard Hamiltonian Eq.(3.1). When $|\alpha >= |\beta >$, then the value of $< \alpha|\hat{H}|\beta >$ is just the total number of doubly occupied sites multiplied by the on-site Coulomb energy U. When $|\alpha > \neq |\beta >$, then the non-zero contribution to this matrix element comes from the kinetic energy term, and because of the bilinear nature of the kinetic energy operator, the difference between $|\alpha >$ and $|\beta >$ can only be in two sites, i and j. Different combinations of $|\alpha >$ and $|\beta >$ are listed in Table 5.1.

phase	$\|\alpha>$	$\|\beta>$	phase	$\|\alpha>$	$\|\beta>$
+1	$\|20>$	$\|1-1>$	-1	$\|20>$	$\|-11>$
+1	$\|02>$	$\|1-1>$	-1	$\|02>$	$\|-11>$
+1	$\|10>$	$\|01>$	-1	$\|21>$	$\|12>$
+1	$\|-10>$	$\|0-1>$	-1	$\|2-1>$	$\|-12>$

Table 5.1: Phase factors in the calculation of Hamiltonian matrix elements. In the representation of the basis wavefunctions, we include only the occupation information of sites i and j.

In Table 5.1, we consider only the two different sites i and j, and the same occupation information in other sites are not listed. To illustrate the different phase factors in the table, we discuss two combinations of basis wavefunctions below.

For $|\alpha >= |20 >$ and $|\beta >= |1-1 >$, the only non-zero contribution comes from $c^+_{i\downarrow}c_{j\downarrow}$ and its hermitian conjugate in the kinetic energy term. And

$$\begin{aligned} < 02|c^+_{i\downarrow}c_{j\downarrow}|1-1 > &= < 02|c^+_{i\downarrow}c_{j\downarrow}c^+_{i\uparrow}c^+_{j\downarrow}|V > \\ &= - < 02|c^+_{i\downarrow}c^+_{i\uparrow}|V > \\ &= < 02|c^+_{i\uparrow}c^+_{i\downarrow}|V > \\ &= < 02|20 > \\ &= 1. \end{aligned} \tag{5.2}$$

This gives the extra phase factor to be considered during the matrix element calcu-

lation. Similarly, for $|\alpha>=|20>$ and $|\beta>=|-11>$, we have

$$\begin{aligned} <02|c^+_{i\uparrow}c_{j\uparrow}|-11> &= <02|c^+_{i\uparrow}c_{j\uparrow}c^+_{i\downarrow}c^+_{j\uparrow}|V> \\ &= -<02|c^+_{i\uparrow}c^+_{i\downarrow}|V> \\ &= -<02|20> \\ &= -1. \end{aligned} \tag{5.3}$$

Certainly, besides these phase factors, we need to take into account the extra phase factors coming from the passing of the jth site operator, e.g. $c_{j\uparrow}$ in the above equation (for $j > i$), through the operators for sites between site i and j in the wavefunction $|\beta>$.

After the above calculations, we obtain a large sparse matrix to diagonalize. Dense techniques from the standard lapack package work well for a small or medium size matrix (typically for matrix dimensions less than 500), but for a large matrix, the dense technique is not efficient. We then resort to Lanczos or Davidson algorithms, designed for obtaining several extremal eigenvalues efficiently. These techniques will be discussed below.

5.2 Lanczos Algorithm

Lanczos theory was, as the name suggests, proposed by Lanczos in 1950 [23] and it was not applied to any practical calculations until the development of the computer algorithm. The Lanczos algorithm and also the Davidson algorithm to be discussed in the next section are useful when only a few extreme eigenvalues of a sparse matrix are needed. A good introduction of the Lanczos algorithm can be found in Golub and van Loan's book [24], so we will introduce only briefly how this algorithm works and place the emphasis on the physical ideas behind the theory.

5.2.1 Rayleigh-Ritz Variational Principle

Suppose we have a Hamiltonian H written in $N \times N$ matrix form and an N-dimensional wave vector $\vec{u}$, we will have

$$\lambda_1 \leq \lambda = \frac{< \vec{u}, H\vec{u} >}{< \vec{u}, \vec{u} >}, \tag{5.4}$$

where, λ_1 is the ground state energy of the Hamiltonian or the minimum eigenvalue of the Hamiltonian matrix and λ is the expectation value of H with respect to an arbitrary wave vector $\vec{u}$.

This is an interesting point, because this means a diagonalization problem can be transformed into a minimization problem, provided that we only need several extreme eigenvalues.

5.2.2 Iterative Method

The Lanczos algorithm is actually an iterative method. It starts with a random wave vector, and through iteration a better and better eigenvector can be achieved together with the lowest or highest eigenvalues. The rules for the iteration calculation can be found in the following way.

We have a set of orthonormal vectors $\{\vec{q}_i\}$, with $i = 1, 2, \cdots, j$, and the j^{th} approximate eigenvector $\vec{u}_j$ is spanned by these orthonormal vectors, i.e., $\vec{u}_j \in \text{space}\{\vec{q}_1, \cdots, \vec{q}_j\}$ and

$$\lambda(\vec{u}_j) = \frac{< \vec{u}_j H\vec{u}_j >}{< \vec{u}_j, \vec{u}_j >}. \tag{5.5}$$

The purpose of next iteration is to find a lower eigenvalue of the Hamiltonian. Since $\lambda(\vec{x})$ decreases most rapidly in the direction of $-\bigtriangledown \lambda(\vec{x})$, as can be seen from the expansion of the function

$$\lambda(\vec{x}) = \lambda(\vec{x}_0) + \bigtriangledown\lambda(\vec{x}_0) \cdot (\vec{x} - \vec{x}_0). \tag{5.6}$$

So, we require that $\vec{u}_j \in \{-\bigtriangledown \lambda(\vec{u}_{j-1})\}$. On the other hand, we have

$$\bigtriangledown\lambda(\vec{u}_{j-1}) = \frac{2}{\vec{u}_{j-1} \cdot \vec{u}_{j-1}}(H\vec{u}_{j-1} - \lambda(\vec{u}_{j-1})\vec{u}_{j-1}). \tag{5.7}$$

It is clear now that, in order to get a better estimate of the lowest eigenvalue, we must have $\vec{u}_j \in \text{span}\{\vec{u}_{j-1}, H\vec{u}_{j-1}\}$. And by induction, we finally arrive at

$$\text{span}\{\vec{q}_1, \cdots, \vec{q}_j\} = \text{span}\{\vec{q}_1, H\vec{q}_1, \cdots, H^{j-1}\vec{q}_1\}. \tag{5.8}$$

The right hand side of the above equation is called Krylov subspace in Mathematics and the remaining task is to find a way to calculate an orthonormal basis for this Krylov subspace, such as the set $\{\vec{q}_1, \cdots \vec{q}_j\}$.

5.2.3 Algorithm

The orthonormalization of the Krylov subspace can be achieved through the following tridiagonalization process. The proof of the validity is not given here but from the result of the tridiagonalization process, we will find that this process really gives us a set of orthonormal bases for the Krylov subspace. Here we outline such a tridiagonalization process.

As H is a real, symmetric matrix, there exists an orthogonal real matrix Q such that

$$Q^T H Q = D(\lambda_1, \cdots, \lambda_N), \tag{5.9}$$

where $D(\lambda_1, \cdots, \lambda_N)$ is a diagonal matrix, and Q^T denotes the transpose of Q (from Schur decomposition theorem in matrix theory). But our algorithm does not directly compute the diagonal matrix D, instead it first computes a partial transformation of the matrix H using a tridiagonal matrix T

$$Q^T H Q = T, \tag{5.10}$$

with

$$T = \begin{pmatrix} \alpha_1 & \beta_2 & 0 & \cdots & \cdots & \cdots & \cdots \\ \beta_2 & \alpha_2 & \beta_3 & 0 & \cdots & \cdots & \cdots \\ 0 & \beta_3 & \cdots & \cdots & \cdots & \cdots & \cdots \\ \cdots & 0 & \cdots & \cdots & \cdots & 0 & \cdots \\ \cdots & \cdots & \cdots & \cdots & \cdots & \beta_{J-1} & 0 \\ \cdots & \cdots & \cdots & 0 & \beta_{J-1} & \alpha_{J-1} & \beta_J \\ \cdots & \cdots & \cdots & \cdots & 0 & \beta_J & \alpha_J \end{pmatrix}, \tag{5.11}$$

and with

$$Q = [\vec{q}_1, \cdots, \vec{q}_J], \tag{5.12}$$

where the vectors $\vec{q}_j$ are column vectors, and where the number of iterations J is much smaller than the dimensionality of the original Hamiltonian H, $J \ll N$. Then, the algorithm finds the diagonal decomposition of T

$$T = S^T D S. \tag{5.13}$$

The elements of the diagonal matrix D are an estimate of the eigenvalues of H, and an estimate of the eigenvectors are given by $Y = [y_1, \cdots, y_J]$, with

$$Y = QS. \tag{5.14}$$

Eq.(5.10) can be written as

$$HQ = QT, \tag{5.15}$$

or

$$H\vec{q}_j = \beta_{j-1}\vec{q}_{j-1} + \alpha_j\vec{q}_j + \beta_j\vec{q}_{j+1} \tag{5.16}$$

for $j = 1, \cdots, J$. The orthogonality of the vectors $\vec{q}_j$ implies that

$$\alpha_j = \vec{q}_j^T H \vec{q}_j. \tag{5.17}$$

Furthermore, if we set

$$\vec{r}_j = (H - \alpha_j I)\vec{q}_j - \beta_{j-1}\vec{q}_{j-1} \tag{5.18}$$

and it is non-zero, then

$$\vec{q}_{j+1} = \frac{\vec{r}_j}{\beta_j}, \tag{5.19}$$

where $\beta_j = \pm\sqrt{<\vec{r}_j \cdot \vec{r}_j>}$. The iterative application of these equations, with a randomly chosen starting vector $\vec{q}_1$, defines the Lanczos iterative procedure. The total number of iterations J determines the accuracy of the computation. As this number increases, we can get not only more precise lowest or highest eigenvalues but also more eigenvalues different from the lowest or highest ones. We shall not discuss this in detail.

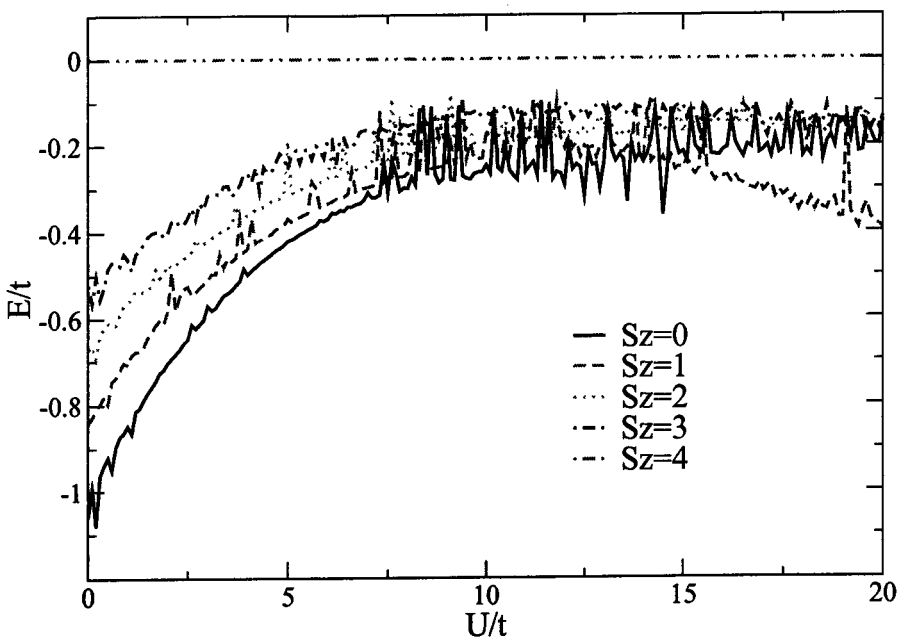

Figure 5.1: Ground state energy of a cube molecule from Lanczos algorithm.

5.2.4 Results and Discussion

As has been observed by other people [25, 26], state-of-the-art computer technology nowadays can perform the exact diagonalization of about 12 lattice sites. Although, some further progress can be made by some techniques, the total number of lattice sites that can be exactly diagonalized is still very limited. In our calculations, we apply the Lanczos technique to a cube molecule only, which has 8 lattice sites. The result is shown in Fig. 5.1.

Different curves in Fig. 5.1 represent different total spin sectors, $S_z = 0$, $S_z = \hbar$, etc. From the figure, and also compared with results from other calculations, for instance, the Davidson algorithm that is discussed below, we find that the Lanczos result is rather unstable. In view of this, we will study another similar algorithm that is built on the Lanczos algorithm but is more stable, fast, and accurate.

5.3 Davidson Algorithm

The theory of the Davidson algorithm can be found in [27], and it was proposed originally for the large-scale configuration interaction (CI) calculations of electronic wavefunctions. The algorithm is still of great interest now, but here we only briefly describe how to do the matrix diagonalization with this kind of algorithm.

1. If the kth eigenvalue is wanted, select a zeroth-order orthonormal subspace $\vec{b}_1$, $\vec{b}_2, \cdots, \vec{b}_l$ ($l \geq k$) spanning the dominant components of the first k eigenvectors. Form and save $H\vec{b}_1, H\vec{b}_2, \cdots, H\vec{b}_l$ and $(\vec{b}_i, H\vec{b}_j)=\hat{H}_{ij}$, $1 \leq i \leq j \leq l$. Diagonalize $\hat{H}$ using the dense technique for small matrices. Select the kth eigenvalue $\lambda_k^{(l)}$ and the corresponding eigenvector $\vec{\alpha}_k^{(l)}$.

2. Form $\vec{q}_M = \sum_{i=1}^{M} \alpha_{i,k}^{(M)}(H\vec{b}_i) - \sum_{i=1}^{M} \alpha_{i,k}^{(M)} \lambda_k^{(M)} \vec{b}_i$. Here M is the dimension of $\hat{H}$ used to find $\vec{\alpha}$ and λ.

3. Form $||\vec{q}_M||$ and check convergence by the formula, $\lambda_k^{(M)} - ||\vec{q}_M|| \leq \lambda_k \leq \lambda_k^{(M)}$.

4. Form $\xi_{I,(M+1)} = (\lambda_k^{(M)} - H_{II})^{-1} q_{I,M}$, $I = 1, \cdots, N$.

5. Form $\vec{d}_{(M+1)} = [\prod_{i=1}^{M}(1 - \vec{b}_i \vec{b}_i^T)]\xi_{(M+1)}$.

6. Form $\vec{b}_{(M+1)} = \vec{d}_{(M+1)}/||\vec{d}_{(M+1)}||$.

7. Form $H\vec{b}_{(M+1)}$.

8. Form $\hat{h}_{i,M+1} = (\vec{b}_i, H\vec{b}_{(M+1)})$, $i = 1, \cdots, M+1$.

9. Diagonalize $\hat{H}$ and return to step 2 with $\alpha_k^{(M+1)}$ and $\lambda_k^{(M+1)}$.

Again we confine ourselves in the cube molecule in half-filling and divide the spin configurations into different total Sz spin sectors. The result is put in Fig. 5.2. Note in this figure, we have compared Davidson result with the dense technique ("dsyev" subroutine in lapack) ones on some points, denoted by scatter points. They agree very well. When we extend the calculation to more lattice sites, for example the truncated tetrahedron (12 lattice sites), the same problem as the Lanczos technique is met:

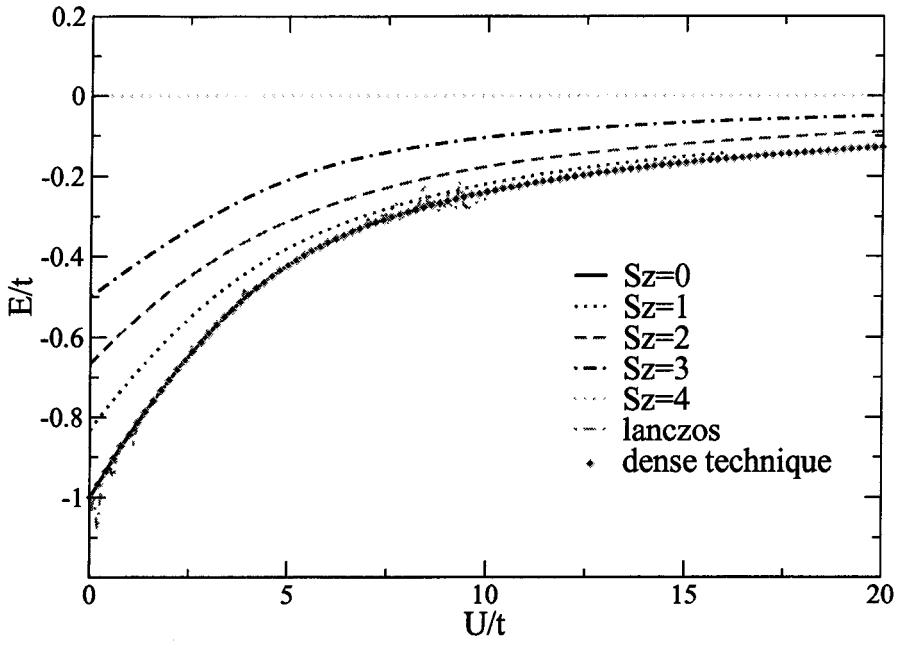

Figure 5.2: Ground state energy of a cube molecule from Davidson algorithm.

the memory of the computer is not big enough to accommodate such a big matrix (the maximum matrix is 853776×853776 for half-filling) diagonalization even when a supercomputer is resorted to. We rearrange the program and take out 500 rows of the matrix every time for calculation, which is roughly the maximum number of rows the computer memory can accommodate. But this reduced demand on computer memory results in the price of longer computer time in calculation. Despite this problem, we find that Davidson algorithm is more stable, accurate, and faster than the Lanczos one.

Chapter 6

$t - J$ Model and Gutzwiller Projection

As can be seen from its name, Gutzwiller projection was first proposed by Gutzwiller in one of his articles [28] on the Hubbard model. The projection is done in the limit of large U (again compared with the band width) and follows the idea that because of this large on-site Coulomb interaction, two electrons will not occupy the same lattice site. The projection is then followed by writing down a trial wavefunction, which must satisfy the condition that there are no doubly occupied sites in the lattice.

Due to the constraints of his time, Gutzwiller could not envision a practical application of his scheme, though he did obtain some approximate formulae analytically, which, we think, are not sufficient to understand many properties of the system. It was perhaps first pointed out by Horsch and Kaplan [29, 30] that when combined with the Monte Carlo technique, the energy of the system can be evaluated with respect to this kind of projected trial wavefunctions. Later Zhang et. al. [31] showed, through renormalized mean field theory, that in a two-dimensional lattice different trial wavefunctions are possible depending on different decoupling schemes and the Gutzwiller wavefunction (projected from a Fermi sea) is just one choice of such trial wavefunctions. Other trial wavefunctions that have been used include $|RVB>$ (Resonating Valence Bond) wavefunctions first proposed by Anderson [32] and $|SDW>$ (Spin Density Wave) wavefunctions. These two trial wavefunctions will be discussed

in Appendix C. Here we apply only the projected Fermi sea to C_{60} calculations; we reserve $|RVB>$ and $|SDW>$ for possible future studies.

In order to apply Gutzwiller projection and Monte Carlo simulation to the C_{60} problem, we need to first introduce what the projection actually means and the usual process of applying them. There is an excellent introduction of this kind of Gutzwiller calculation in Gros's paper [33, 34], and readers are referred to these papers for more applications of Gutzwiller projection.

6.1 Trial Wavefunction

The trial wavefunction that we are going to apply to C_{60} is a projected Fermi sea

$$|\Psi_{trial}>= P_{d=0}|\Phi_{HF}>, \tag{6.1}$$

with

$$P_{d=0} = \prod_i [1 - n_{i\uparrow}n_{i\downarrow}]. \tag{6.2}$$

Here $P_{d=0}$ is projection operator which projects the wavefunction into the Hilbert space without double occupancy, and

$$|\Phi_{HF}>= \det[\varphi_\uparrow(\vec{k},\vec{r})]\det[\varphi_\downarrow(\vec{k},\vec{r})] \tag{6.3}$$

is the Slater determinant of the Hartree-Fock-type ground state. The $(i,j)^{th}$ element of the determinants is written as

$$\varphi_\sigma(\vec{k}_i, \vec{r}_{j\sigma}), \tag{6.4}$$

where, $\vec{k}_i$ is understood as the ith irreducible representation of the icosahedral group, and $\vec{r}_{j\sigma}$ refers to the position of the j^{th} lattice site with a spin σ electron on it. The value of this matrix element is obtained when we diagonalize the non-interacting Hamiltonian for the C_{60} molecule.

In Gutzwiller's original formulation, the projection operator is

$$P = \prod_i (1 - (1-g)n_{i\uparrow}n_{i\downarrow}) \tag{6.5}$$

where g is a variational parameter that can be tuned for different physical situations. For example, when $g = 1$, there is no projection acting on the Hartree-Fock wavefunction, and we return to the ordinary Hartree-Fock theory. This would be the situation when the on-site interaction U is small. Another example would be $g = 0$, which eliminates all the doubly-occupied sites from the variational wavefunction and corresponds to an extremely large U case. Thus, different values of the parameter $g \in [0, 1]$ can be used in the calculation to find the lowest energy of the system and hence the best trial wave function. However, in this thesis, we will not include the parameter g in the calculation, because we will apply the Gutzwiller projection to the large U case, and hence any double occupancy in the system will be very expensive in energy. In the following discussion, we set $g = 0$.

6.2 $t - J$ Model

In the large U limit, some simplification of the Hubbard Hamiltonian Eq.(3.1) can be made through a unitary transformation, which is capable of eliminating the high energy processes (which include virtual hopping between doubly occupied sites and empty sites) and retaining the low energy processes (which include hoppings that do not change the total number of doubly occupied sites in the system). The final effective Hamiltonian obtained through the unitary transformation will be expressed in power series of t/U. In our calculation, we will keep terms to second order in t/U, because we recognize that the higher order terms describe processes in which more than 2 lattice sites are doubly occupied and hence are negligible.

We present detailed calculation of the unitary transformation in Appexdix A and list only main results here. The effective Hamiltonian that eliminates the high energy processes is

$$H_{eff} = e^{iS} H e^{-iS} \tag{6.6}$$

$$= H + i[S, H] + i^2/2[S, [S, H]] + \cdots, \tag{6.7}$$

where, H is the Hubbard Hamiltonian from Eq.(3.1). Up to second order in t/U,

H_{eff} takes the form

$$H_{eff} = T + H_{eff}^{(2)} + H_{eff}^{(3)}, \tag{6.8}$$

$$T = -t \sum_{<ij>,\sigma} (a_{i,\sigma}^{+} a_{j,\sigma} + h.c.) \tag{6.9}$$

$$H_{eff}^{(2)} = 4t^2/U \sum_{<ij>} (\vec{S}_i \cdot \vec{S}_j - n_i n_j/4) \tag{6.10}$$

$$H_{eff}^{(3)} = -t^2/U \sum_{i,\tau \neq \tau',\sigma} (a_{i+\tau,\sigma}^{+} a_{i,-\sigma}^{+} a_{i,-\sigma} a_{i+\tau',\sigma} + a_{i+\tau,-\sigma}^{+} a_{i,\sigma}^{+} a_{i,-\sigma} a_{i+\tau',\sigma}), \tag{6.11}$$

where, $a_{i,\sigma}^{+} = (1 - n_{i,-\sigma}) c_{i,\sigma}^{+}$, $n_{i,\sigma} = c_{i,\sigma}^{+} c_{i,\sigma}$, $i + \tau$ denotes a nearest neighbour of i, and $\vec{S}_i$ is the spin operator on site i. $H_{eff}^{(2,3)}$ are two- and three-site contributions, respectively. Note that in the above Hamiltonian, we have omitted the chemical potential μ which appeared in the previous Eq.(3.1). This is because we will work with a fixed number of electrons or we will work with the canonical partition function, not the grand canonical partition function. The chemical potential is thus redundant and is omitted.

The above effective Hamiltonian is valid only in the subspace of no doubly occupied sites, as can be seen from the conclusion in Appendix A. In the half-filled case, i.e., $n_i = 1$ for each lattice site i, the effective Hamiltonian reduces to the antiferromagnetic Heisenberg Hamiltonian, with a nearest neighbour coupling constant $J = 4t^2/U$. We will see in the numerical simulation that $H_{eff}^{(3)}$ is very small due to its three-site interactions.

6.3 Monte Carlo Algorithm

In the above discussions, we have confined ourselves to that part of Hilbert space where there are no doubly occupied lattice sites. Even in this subspace, we still encounter the problem of a large wavefunction basis for the single C_{60} molecule, where 60 lattice sites are present. For example, at half-filling with no double occupancy, we will have C_{60}^{30}, approximately 10^{17} basis wavefunctions. That is a tremendously large number. Thus, some kind of Monte Carlo algorithm should be devised to handle these wavefunctions.

6.3.1 Basis Wavefunctions

Suppose we have a trial wavefunction that we believe would be a good estimate of the true wavefunction, and we want to calculate the expectation value of the Hamiltonian with respect to this trial wavefunction. As we do not know the exact form of the trial wavefunction or it is hard to do calculations on this trial wavefunction directly, we will have to expand it in a complete wavefunction basis which we know, and evaluate probability amplitudes for each basis wavefunction. That is

$$< O > = \frac{< \Psi|O|\Psi >}{< \Psi|\Psi >} \tag{6.12}$$

$$= \sum_{\alpha,\beta} < \alpha|O|\beta > \frac{< \Psi|\alpha >< \beta|\Psi >}{< \Psi|\Psi >}. \tag{6.13}$$

In the expansion, α,β are states corresponding to specific configurations of the electron spins on each site, and can be written in terms of electron creation operators,

$$|\alpha >= c^{+}_{\vec{R}_1,\uparrow} \cdots c^{+}_{\vec{R}_{N_\uparrow},\uparrow} c^{+}_{\vec{R}'_1,\downarrow} \cdots c^{+}_{\vec{R}'_{N\downarrow},\downarrow} |0 >, \tag{6.14}$$

where $|0 >$ is a true vacuum. The form of $< \alpha|\Psi >$ depends on the choice of trial wavefunction $|\Psi >$, and in our calculation, the form of $< \alpha|\Psi >$ is just the Slater determinant, which has been previously given in Eq.(6.3). For other choices of trial wavefunctions, such as $|RVB >$ or $|SDW >$, we list their expressions for $< \alpha|\Psi >$ in Appendix C.

6.3.2 MC Weight

To proceed further, we need to change Eq.(6.13) a little.

$$< O > = \sum_{\alpha} (\sum_{\beta} \frac{< \alpha|O|\beta >< \beta|\Psi >}{< \alpha|\Psi >}) \frac{| < \alpha|\Psi > |^2}{< \Psi|\Psi >} \tag{6.15}$$

$$= \sum_{\alpha} f(\alpha)\rho(\alpha), \tag{6.16}$$

where,

$$f(\alpha) = \sum_{\beta} \frac{< \alpha|O|\beta >< \beta|\Psi >}{< \alpha|\Psi >} \tag{6.17}$$

$$\rho(\alpha) = \frac{| < \alpha|\Psi > |^2}{< \Psi|\Psi >}. \tag{6.18}$$

Note that, $\rho(\alpha)$ is always greater than 0 and

$$\sum_{\alpha} \rho(\alpha) = 1. \tag{6.19}$$

This suggests that we are able to use this factor as the weight for Monte Carlo simulation. The advantage is that we have no sign problem, which is usually met in fermion Monte Carlo simulations. The transition probability $T(\alpha \rightarrow \alpha')$ for going from one spatial configuration α to another configuration α' can be chosen as

$$T(\alpha \rightarrow \alpha') = \begin{cases} 1 & \text{if } \rho(\alpha') > \rho(\alpha); \\ \rho(\alpha')/\rho(\alpha) & \text{if } \rho(\alpha') < \rho(\alpha). \end{cases} \tag{6.20}$$

To make the Monte Carlo simulation as quick as possible, we will use some techniques to generate α' out of α by the interchange of two electrons with opposite spins. Through this technique, the time needed to compute the transition probability $T(\alpha \rightarrow \alpha')$ is cut down greatly. See the discussion in Appendix D.

By this procedure, a series of configurations $\{\alpha_1, \alpha_2, \cdots, \alpha_{N_{MC}}\}$ is generated, with N_{MC} the total number of MC steps. The expectation value of operator O is then given by

$$< O >= \frac{1}{N_{MC}} \sum_{i=1}^{N_{MC}} f(\alpha_i). \tag{6.21}$$

As the total number of MC steps is much less than the total number of spin configurations or the basis wave functions, we need to evaluate the error in our simulation. We do this by producing N_{run} independent MC runs, starting with different initial random spin configurations. Then the average expectation value of operator O in $|\Psi_{trial} >$ is given by

$$< \bar{O} >= \frac{1}{N_{run}} \sum_{j=1}^{N_{run}} < O >_j, \tag{6.22}$$

and the accuracy is defined by the standard deviation

$$\sqrt{\frac{1}{(N_{run}-1)} \sum_{j=1}^{N_{run}} (< O >_j - < \bar{O} >)^2}. \tag{6.23}$$

6.3.3 Evaluation of Physical Quantities

The physical quantities that we are going to evaluate are those operators from Eq.(6.9) to Eq.(6.11). As can be seen from Eq.(6.16), we need to do a counting of the non-zero $< \alpha|O|\beta >$. In order to calculate this quantity, we should first define a definite order of each product of creation operators as done in Eq.(6.14), where we put all the spin-up creation operators on the left and all the spin-down creation operators on the right, and ordered them according to their lattice site indices. This ordering is necessary to avoid ambiguity in the basis wavefuntions, and to take into account the anti-commutation relation of the fermion operators. We have seen this kind of ordering requirement before in the exact diagonalization chapter.

Next, we illustrate some examples on how to get the phase factor when we evaluate $< \alpha|O|\beta >$ with the ordering convention in Eq.(6.14).

1. $O = a^+_{i,\sigma}a_{j,\sigma}$ of the kinetic energy term in Eq.(6.10). For the expectation value to be non-zero, $|\alpha >$ and $|\beta >$ can differ in only two neighboring lattice sites, i.e., if $|\alpha >= \cdots c^+_{i\uparrow}\cdots 1_j \cdots |0>$, then $|\beta >= \cdots 1_i \cdots c^+_{j\uparrow}\cdots|0>$, with i,j the two nearest neighbors and 1 the unit operator. Let n_1 and n_2 be the number of spin-up creation operators to the left of lattice sites i and j respectively in wavefunction $|\beta >$ written using the ordering convention. A simple counting gives

$$a^+_{i\uparrow}a_{j\uparrow}|\beta >= \begin{cases} (-1)^{n_2+n_1}|\alpha >, & \text{for } i < j, \\ (-1)^{n_2+n_1-1}|\alpha >, & \text{for } i > j. \end{cases} \tag{6.24}$$

   The above two cases can be reduced to the same expression $(-1)^{n_{between}}|\alpha >$, where $n_{between}$ is the number of spin-up creation operators between lattice i and j in wavefunction $|\beta >$.

2. $O = \vec{S}_i \cdot \vec{S}_j$ of the potential energy term in Eq.(6.11). We divide this operator into diagonal and off-diagonal terms. The diagonal term $S^z_i S^z_j = \frac{1}{4}(c^+_{i\uparrow}c_{i\uparrow} - c^+_{i\downarrow}c_{i\downarrow})(c^+_{j\uparrow}c_{j\uparrow} - c^+_{j\downarrow}c_{j\downarrow})$ always has a phase factor of 1 and for non-zero average,

$|\beta>$ must be equal to $|\alpha>$. For the non-diagonal term, we have

$$\begin{aligned} S_i^x S_j^x + S_i^y S_j^y &= \frac{1}{2}(S_i^+ S_j^- + S_i^- S_j^+) \\ &= \frac{1}{2}(c_{i\uparrow}^+ c_{i\downarrow} c_{j\downarrow}^+ c_{j\uparrow} + h.c.). \end{aligned} \tag{6.25}$$

Let n_1, n_2 be the number of spin-up or spin-down creation operators to the left of lattice site i, and n_3, n_4 be the number of spin-up or spin-down creation operators to the left of lattice site j. Then we have

$$\begin{aligned} (c_{i\uparrow}^+ c_{i\downarrow} c_{j\downarrow}^+ c_{j\uparrow})|\beta> &= (-1)^{n_3+n_{up}-1+n_4+n_{up}-1+n_2+n_1}|\alpha> \\ &= (-1)^{n_{between1}+n_{between2}+1}|\alpha>, \end{aligned} \tag{6.26}$$

for $i < j$, where $n_{between1}$ ($n_{between2}$) is the number of spin-up (spin-down) creation operators between lattice site i and j in wavefunction $|\beta>$, and n_{up} is the total number of spin-up creation operators in $|\beta>$. Similarly, for $i > j$, we have

$$\begin{aligned} (c_{i\uparrow}^+ c_{i\downarrow} c_{j\downarrow}^+ c_{j\uparrow})|\beta> &= (-1)^{n_3+n_{up}-1+n_4+n_{up}-1+n_2+1+n_1+1}|\alpha> \\ &= (-1)^{n_{between1}+n_{between2}+1}|\alpha> . \end{aligned} \tag{6.27}$$

We see that in this case the phase factor is the same for either $i > j$ or $i < j$.

For the three-site interaction term $H_{eff}^{(3)}$ in Eq.(6.11), the analysis is a little complicated, but the final result is still simple. The phase factor is given by $(-1)^{n_{between1}+n_{between2}}$ for the first operator in $H_{eff}^{(3)}$ and $(-1)^{n_{between1}+n_{between2}+1}$ for the second operator in $H_{eff}^{(3)}$, where $n_{between1}$ is the number of spin-up creation operators between the two spin-up lattice sites (in $|\beta>$) and $n_{between2}$ is the number of spin-down creation operators between the two spin-down lattice sites (in $|\beta>$).

With the above rules, the expectation values of the effective Hamiltonian can be calculated easily with a computer.

6.4 Results for C_{60}

6.4.1 Pair-binding Energy

As mentioned above, we will confine ourselves to the Hartree-Fock-type wavefunction as in Eq.(6.1).

We describe briefly the calculation procedure for neutral C_{60}: First, we diagonalize the non-interacting Hamiltonian and get a set of eigenvectors that contain the geometric information of C_{60}. Second, we randomly choose an initial spin configuration on the 60 sites, with 30 up spins and 30 down spins. Third, combining the non-interacting eigenvectors and the spin configuration, we write down the projected Hartree-Fock wave function for the initial configuration. Fourth, we calculate the determinant of the initial wavefunction once. Fifth, we interchange one up-spin electron with one down-spin electron and get a new spin configuration. Then, with the technique introduced in Appendix D, we can calculate the transition probability very quickly.

We repeat the above procedure until N_{MC} Monte Carlo steps are passed. With this information, the expectation value of the Hubbard Hamiltonian can be evaluated. After N_{run} such runs, the averaged expectation value or the energy of the neutral C_{60} together with the error can be calculated.

The calculation for C_{60} that is doped with one or two holes can also be performed similarly, except that, in the two hole case, we have two kinds of total spin configurations, total spin z component $S_z = 0$ or $S_z = \hbar$. The results for all these cases are listed in Table 6.1, and the result for the hole binding energy $E_b = E(60) + E(58) - 2E(59)$ is drawn in Fig. 6.1.

6.4.2 Spin-spin Correlation Energy

In the above Gutzwiller projection formalism and the Monte Carlo procedure, the nearest neighbor spin-spin correlation energy $< \vec{S}_i \cdot \vec{S}_j >$ can be calculated easily and

E_{60}	$-(4t/U) \times 32.7(\pm 0.1)$
E_{59}	$-0.07(\pm 0.02) - (4t/U) \times 31.2(\pm 0.2)$
$E_{58}(S_z = 0)$	$-0.07(\pm 0.01) - (4t/U) \times 30.0(\pm 0.3)$
$E_{58}(S_z = 1)$	$-0.08(\pm 0.01) - (4t/U) \times 30.1(\pm 0.2)$
$E_b^{S_z=0}$	$0.07 - 1.2t/U$
$E_b^{S_z=1}$	$0.06 - 1.6t/U$

Table 6.1: Electronic energy of a C_{60} molecule, either neutral or hole-doped (in units of t) and pair-binding energy.

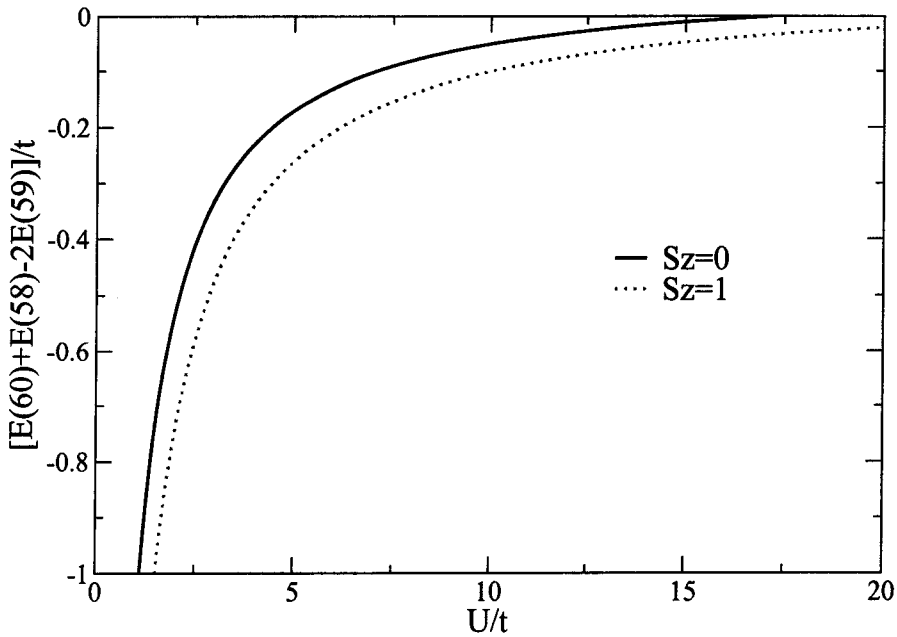

Figure 6.1: Pair-binding energy from Gutzwiller projection in hole-doped C_{60}.

$< \vec{S}_i \cdot \vec{S}_j >$	Gutz	SDW	RVB ($\Delta = 1.0$)
C_{60}	-0.113 ± 0.002	N.A.	N.A.
Icosahedron	-0.148	N.A.	N.A.
Truncated Tetrahedron	-0.311	N.A.	N.A.
Cube	-0.341	N.A.	N.A.
2D Square	-0.267 ± 0.003	-0.321 ± 0.001	-0.318 ± 0.002

Table 6.2: Nearest neighbor spin-spin correlation energy in various systems from Gutzwiller Monte Carlo calculations at half-filling. The values in the 2D square lattice are all taken from reference [34]. All data are in units of $J = 4t^2/U$. N.A. means "Not Available".

was produced at the same time that the ground state energy was obtained. We list the results in Table 6.2 together with those from other molecules and the two-dimensional square lattice, which are taken from Gros's paper [34].

We have also calculated the electron or hole binding energies for the molecules other than C_{60}. They are listed in Appendix E.

Chapter 7

Auxiliary Field Monte Carlo

In the earlier sections, we have introduced the method of Monte Carlo simulation in Gutzwiller projection. Here we will use it again in another scheme for solving the Hubbard model exactly. The scheme is called "auxiliary field Monte Carlo" and is based on Scalapino's papers [35, 36]. It was later refined by Hirsch [37, 38, 39]. Our notation here follows that of Hirsch.

The Hubbard model that will be considered here is still that of Eq.(3.1), where we rewrite H as a sum of two terms

$$H = H_0 + H_1, \tag{7.1}$$

where

$$H_1 = U \sum_i n_{i,\uparrow} n_{i,\downarrow} \tag{7.2}$$

is the interaction term and H_0 is the kinetic energy and chemical potential term. We have pointed out before that the difficulty in solving the Hubbard model lies in the on-site interactions. Thus if one could find a way to decouple this interaction term, then the difficulty will no longer exist. Actually this has been done by Hubbard [40] based on the identity from Stratonovich [41]

$$\exp(\frac{1}{2}A^2) = \frac{1}{\sqrt{2\pi}} \int dx \exp(-\frac{1}{2}x^2 - xA), \tag{7.3}$$

where A is a quantum-mechanical operator. This transformation decouples the interacting fermion operators and couples them to an auxiliary field. In order to use this

identity, we need to write the on-site interaction $n_{i\uparrow}n_{i\downarrow}$ the following way

$$n_{i\uparrow}n_{i\downarrow} = -\frac{1}{2}(n_{i\uparrow} - n_{i\downarrow})^2 + \frac{1}{2}(n_{i\uparrow} + n_{i\downarrow}), \tag{7.4}$$

where, we have used the property of fermion operators $n_{i\sigma}^2 = n_{i\sigma}$. Certainly, there are other ways to write identities to decouple on-site Coulomb interaction, like Eq.(7.4), but we think it is sufficient to use only one of them here.

As will be seen later, for the purpose of Monte Carlo simulations, the above continuous Hubbard-Stratonovich transformation is inferior to the discrete Hubbard-Stratonovich transformation that will be introduced below.

7.1 Discrete Hubbard-Stratonovich Transformation

The partition function for the Hubbard Hamiltonian is:

$$\begin{aligned} Z &= Tre^{-\beta H} \\ &= Tre^{-\beta(H_0+H_1)} \\ &= Tr\prod_{i=1}^{L} e^{-\Delta\tau(H_0+H_1)}, \end{aligned} \tag{7.5}$$

where we have treated β as imaginary time and divided it into L sections, i.e., $\beta = L\Delta\tau$. We have also used the fact that operators at different times commute.

Using the Suzuki-Trotter formula [42], we arrive at

$$Z \approx Tr\prod_{i=1}^{L} e^{-\Delta\tau H_0}e^{-\Delta\tau H_1} + O(\Delta\tau^2[H_0, H_1]). \tag{7.6}$$

As $\Delta\tau \to 0$, the error introduced by this approximation becomes negligible. So the magnitude of $\Delta\tau$ will be an important parameter in subsequent Monte Carlo calculations.

To proceed further, we need an identity

$$\exp(-\Delta\tau U n_{i\uparrow}n_{i\downarrow}) = \frac{1}{2}Tr_\sigma \exp[\lambda\sigma(n_{i\uparrow} - n_{i\downarrow}) - \frac{\Delta\tau U}{2}(n_{i\uparrow} + n_{i\downarrow})], \tag{7.7}$$

where

$$\tanh^2(\lambda/2) = \tanh(\Delta\tau U/4), \tag{7.8}$$

and $\sigma = \pm 1$ is the auxiliary Ising spin field index. The proof for this identity is given in Appendix F.

The partition function is then

$$\begin{aligned} Z &= Tr_\sigma Tr \prod_{l=1}^{L} e^{-\Delta\tau H_0} \exp[\sum_i (\lambda\sigma(n_{i\uparrow} - n_{i\downarrow}) \\ &\quad + \Delta\tau(\mu - \frac{U}{2})(n_{i\uparrow} + n_{i\downarrow}))] \\ &= Tr_\sigma Tr[\prod_{l=1}^{L} e^{-\Delta\tau H_{0\uparrow}} \exp\{\sum_i [\lambda\sigma + \Delta\tau(\mu - \frac{U}{2})] n_{i\uparrow}\}] \\ &\quad \times [e^{-\Delta\tau H_{0\downarrow}} \exp\{\sum_i [-\lambda\sigma + \Delta\tau(\mu - \frac{U}{2})] n_{i\downarrow}\}]. \end{aligned} \tag{7.9}$$

Denote

$$B_l(\alpha) = e^{-\Delta\tau K} e^{V^\alpha(l)}, \tag{7.10}$$

$$(K)_{ij} = \begin{cases} -t & \text{for } i,j \text{ nearest neighbours,} \\ 0 & \text{otherwise,} \end{cases} \tag{7.11}$$

$$V_{ij}^\alpha(l) = \delta_{ij}[\lambda\alpha\sigma_i(l) + \Delta\tau(\mu - U/2)], \tag{7.12}$$

and define the operators

$$D_l(\alpha) = e^{-\Delta\tau c_i^\dagger K_{ij} c_j} e^{c_i^\dagger V_i^\alpha(l) c_i}, \tag{7.13}$$

so that the partition function is

$$Z = Tr_\sigma Tr \prod_{\alpha=\pm 1} \prod_{l=1}^{L} D_l(\alpha). \tag{7.14}$$

We can take the trace over fermions explicitly, since there are only bilinear terms in fermion operators, and obtain

$$Z = Tr_\sigma \prod_\alpha \det[1 + B_L(\alpha) B_{L-1}(\alpha) \cdots B_1(\alpha)] \tag{7.15}$$

$$= Tr_\sigma \det O_\uparrow \det O_\downarrow. \tag{7.16}$$

The proof of this identity is taken from Hirsch's paper [39] and given in Appendix G. Special attention should be paid when we want to write down the matrix $B_l(\alpha)$ according to the definition of the exponential matrix. Details on how to write the matrix are given in Appendix H.

7.2 Monte Carlo Procedure

The partition function that we need to calculate has been reduced to Eq.(7.16). When the number of lattice sites is not small, the trace over the Ising spins is done numerically using a kind of Monte Carlo technique.

7.2.1 MC Weight and Transition Probability

From Eq.(7.16), we see that the Boltzmann weight can be easily taken as the product of determinants in the equation. For the half-filled case ($\mu = U/2$, see Appendix I for a proof), we can show that this Boltzmann weight is always positive and has no sign problem. Let's do a particle-hole transformation:

$$d_{i\sigma} = c^{+}_{i\sigma}, \tag{7.17}$$

$$c^{+}_{i\sigma}c_{i\sigma} = 1 - d^{+}_{i\sigma}d_{i\sigma}. \tag{7.18}$$

Then the expression for the determinant becomes

$$\begin{aligned} \det O_{\uparrow} &= Tr_c \prod_{l=1}^{L} e^{-\Delta\tau H_{0\uparrow}} e^{\lambda\sigma \sum_i c^{+}_{i\uparrow}c_{i\uparrow}} \\ &= Tr_d \prod_{l=1}^{L} e^{-\Delta\tau H_{0\uparrow}} e^{-\lambda\sigma \sum_i d^{+}_{i\uparrow}d_{i\uparrow}} e^{\lambda \sum_i \sigma_i(l)}, \end{aligned} \tag{7.19}$$

so

$$\det O_{\uparrow} = e^{\lambda \sum_{i,l} \sigma_i(l)} \det O_{\downarrow} \tag{7.20}$$

or

$$\det O_{\uparrow} \det O_{\downarrow} = e^{\lambda \sum_{i,l} \sigma_i(l)} (\det O_{\downarrow})^2 > 0. \tag{7.21}$$

And for the non-half-filled case, we have not found a way to prove whether the Boltzmann weight is positive or not, but we can still define it as

$$P(\sigma) = |\det O_{\uparrow} \det O_{\downarrow}|, \tag{7.22}$$

and from our experience, we have not yet found any negative weights that make our result unstable.

For the transition probability P, we use the usual Metropolis algorithm, i.e., the probability for flipping a given Ising spin is given by

$$P = R_\uparrow R_\downarrow, \tag{7.23}$$

where R_α is the ratio of the new determinant from the new Ising spin configuration to the old determinant from the old Ising spin configuration.

Techniques used to compute R_α are similar to those discussed in the Gutzwiller projection, and result from the idea that a local change of the field is much easier to calculate than a global one. We explain how to use these techniques in Appendix J.

7.2.2 Average of Physical Quantities

Consider now the evaluation of average quantities. Suppose we have operators P and Q, then the equal time correlation of these two operators is

$$\begin{aligned} << PQ >> &= \frac{Tr_\sigma TrPQ \prod_\alpha \prod_l D_l(\alpha)}{Z} \\ &= \frac{Tr_\sigma < PQ > \det O_\uparrow \det O_\downarrow}{Z}, \end{aligned} \tag{7.24}$$

$$< PQ > = \frac{TrPQ \prod_{l,\alpha} D_l(\alpha)}{\det O_\uparrow \det O_\downarrow}. \tag{7.25}$$

By using the transformation to normal modes, we can easily get the expression for the appropriate correlation functions in Eq.(7.25). For example, the single-particle Green's functions are given by

$$\begin{aligned} < c_i c_j^+ > &= \frac{Trc_i c_j^+ \prod_\nu e^{-c_\nu^\dagger l_\nu c_\nu}}{\prod_\nu (1+e^{-l_\nu})} \\ &= \sum_{\nu'} < \nu' | i >< j | \nu' > \frac{Trc_{\nu'} c_{\nu'}^+ \prod_\nu e^{-c_\nu^\dagger l_\nu c_\nu}}{\prod_\nu (1+e^{-l_\nu})} \\ &= \sum_{\nu'} < \nu' | i >< j | \nu' > \frac{1}{1+e^{-l_{\nu'}}} \\ &= [\frac{1}{1+B_L B_{L-1} \cdots B_1}]_{ij}, \end{aligned} \tag{7.26}$$

where we have suppressed the spin indices for simplicity. Similarly,

$$< c_i^+ c_j >= [B_L \cdots B_1 \frac{1}{1+B_L \cdots B_1}]_{ji}. \tag{7.27}$$

For two-particle Green's functions, it can be shown that Wick's theorem applies. For example,

$$< c^+_{i_1} c_{i_2} c^+_{i_3} c_{i_4} >=< c^+_{i_1} c_{i_2} >< c^+_{i_3} c_{i_4} > + < c^+_{i_1} c_{i_4} >< c^+_{i_2} c_{i_3} > . \qquad (7.28)$$

And for averages involving fermion operators of both spins, we can simply factorize them, since everything is diagonal in spins,

$$< n_{i\uparrow} n_{j\downarrow} >=< n_{i\uparrow} >< n_{j\downarrow} > . \qquad (7.29)$$

7.3 Results for C_{60}

The selection of parameters is according to Hirsch's paper [37], and a reasonable precision is achieved (about to the 3rd significant figures) when, for example, we set $\Delta\tau = 0.5$ for U equal or less than the value of $4t$. (Note $\beta = L\Delta\tau$) Certainly, the result converges to the exact answer as $L \to \infty$. The calculations are performed at different temperatures, and then the available data are used to find the pairing tendency towards zero temperature. The errors in the calculation can be estimated both by doing the Monte Carlo simulation several times (for statistical error) and for the formula provided by Fye [43] (the truncation error of using a finite $\Delta\tau$, the inverse of which will serve as the high energy cutoff). However, there is a way to minimize this truncation error, which is done trough an extrapolation to the zero $\Delta\tau$ limit at different temperatures. This is exactly what we have done in this thesis, and we will introduce this here for the case of C_{60} molecule, and in Appendix K for the case of the tetrahedron and cube molecules.

The chemical potential μ in the Hamiltonian is used to fix the electron number in the C_{60} molecule and will be substracted from the ground state energy estimation thereafter. The electron numbers of interest are 62, 61, 60, 59 and 58, which correspond to a filling factor of 1.033(62/60), 1.017(61/60), 1(60/60), 0.983(59/60) and 0.967(58/60), respectively. A standard program (subroutine "zbrent" in "Numerical Recipes") has been used in combination with the Monte Carlo procedure to determine the ground state energies of C_{60} molecules at different fillings and temper-

atures. We list in Table 7.1 energy data for pure and doped C_{60} molecules at different temperatures obtained through this process.

	n	$\Delta\tau$	L	μ	E
	58	0.25	2	1.733(2)	-0.087(4)
T=2.0	58	0.125	4	1.734(1)	-0.062(2)
	58	0.0625	8	1.735(2)	-0.054(5)
	58	0.03125	16	1.736(2)	-0.051(4)
					-0.049(1)
	58	0.5	2	1.714(4)	-0.455(9)
T=1.0	58	0.25	4	1.741(2)	-0.358(6)
	58	0.125	8	1.753(4)	-0.319(6)
	58	0.0625	16	1.751(2)	-0.307(5)
					-0.293(4)
	58	0.5	4	1.624(4)	-0.664(7)
T=0.5	58	0.25	8	1.683(2)	-0.525(5)
	58	0.125	16	1.699(1)	-0.475(5)
	58	0.0625	32	1.706(7)	-0.435(16)
					-0.412(4)
	58	0.5	8	1.397(14)	-0.731(8)
T=0.25	58	0.25	16	1.500(15)	-0.592(7)
	58	0.125	32	1.537(9)	-0.539(7)
	58	0.0625	40	1.556(1)	-0.515(12)
					-0.495(20)
	59	0.25	2	1.867(3)	-0.067(3)
T=2.0	59	0.125	4	1.867(1)	-0.040(3)
	59	0.0625	8	1.867(2)	-0.034(4)
	59	0.03125	16	1.868(1)	-0.032(3)
					-0.032(1)
	59	0.5	2	1.855(3)	-0.433(13)
T=1.0	59	0.25	4	1.870(1)	-0.338(7)
	59	0.125	8	1.873(1)	-0.301(6)
	59	0.0625	16	1.873(2)	-0.285(6)
					-0.271(1)

continued	n	$\Delta\tau$	L	μ	E
	59	0.5	4	1.792(2)	-0.647(6)
T=0.5	59	0.25	8	1.826(1)	-0.509(5)
	59	0.125	16	1.835(1)	-0.458(4)
	59	0.0625	32	1.838(1)	-0.426(11)
					-0.404(8)
	59	0.5	8	1.604(8)	-0.725(3)
T=0.25	59	0.25	16	1.685(9)	-0.582(4)
	59	0.125	32	1.710(5)	-0.526(9)
	59	0.1	40	1.711(1)	-0.514(8)
	59	0.0625	64	1.716(8)	-0.511(10)
					-0.493(8)
	60	0.25	2	2.001(3)	-0.044(3)
T=2.0	60	0.125	4	2.000(1)	-0.020(2)
	60	0.0625	8	2.000(1)	-0.011(3)
	60	0.03125	16	1.999(1)	-0.010(3)
					-0.008(2)
	60	0.5	2	1.989(6)	-0.429(8)
T=1.0	60	0.25	4	1.996(1)	-0.318(6)
	60	0.125	8	1.995(1)	-0.281(6)
	60	0.0625	16	1.996(1)	-0.269(6)
					-0.259(1)
	60	0.5	4	1.965(1)	-0.636(5)
T=0.5	60	0.25	8	1.975(1)	-0.491(6)
	60	0.125	16	1.979(2)	-0.422(12)
	60	0.0625	32	1.976(4)	-0.416(12)
					-0.392(20)
	60	0.5	8	1.922(2)	-0.704(6)
T=0.25	60	0.25	16	1.928(4)	-0.562(6)
	60	0.125	32	1.936(4)	-0.505(8)
	60	0.1	40	1.935(8)	-0.499(8)
	60	0.0625	64	1.933(8)	-0.493(8)
					-0.473(7)
	61	0.25	2	2.132(3)	-0.023(4)
T=2.0	61	0.125	4	2.132(1)	0.004(3)
	61	0.0625	8	2.132(1)	0.013(5)
	61	0.03125	16	2.131(1)	0.012(2)
					0.013(3)
	61	0.5	2	2.132(1)	-0.405(7)
T=1.0	61	0.25	4	2.121(2)	-0.291(6)
	61	0.125	8	2.118(1)	-0.254(5)
	61	0.0625	16	2.117(1)	-0.242(5)
					-0.232(1)
	61	0.5	4	2.141(2)	-0.608(5)
T=0.5	61	0.25	8	2.120(3)	-0.465(5)
	61	0.125	16	2.118(3)	-0.394(12)
	61	0.0625	32	2.114(2)	-0.397(7)
					-0.375(28)

continued	n	$\Delta\tau$	L	μ	E
	61	0.5	8	2.240(9)	-0.681(7)
T=0.25	61	0.25	16	2.168(5)	-0.540(7)
	61	0.125	32	2.154(2)	-0.486(9)
	61	0.1	40	2.140(5)	-0.474(14)
	61	0.0625	64	2.164(2)	-0.471(9)
					-0.450(7)
	62	0.25	2	2.266(5)	0.002(4)
T=2.0	62	0.125	4	2.264(1)	0.029(5)
	62	0.0625	8	2.263(2)	0.036(4)
	62	0.03125	16	2.263(1)	0.037(3)
					0.038(1)
	62	0.5	2	2.271(2)	-0.381(11)
T=1.0	62	0.25	4	2.248(2)	-0.269(8)
	62	0.125	8	2.242(2)	-0.228(5)
	62	0.0625	16	2.241(1)	-0.217(5)
					-0.205(4)
	62	0.5	4	2.309(4)	-0.582(6)
T=0.5	62	0.25	8	2.266(4)	-0.442(5)
	62	0.125	16	2.252(1)	-0.391(3)
	62	0.0625	32	2.246(3)	-0.367(8)
					-0.348(2)
	62	0.5	8	2.447(15)	-0.651(9)
T=0.25	62	0.25	16	2.347(8)	-0.510(4)
	62	0.125	32	2.331(5)	-0.453(7)
	62	0.1	40	2.327(1)	-0.455(11)
	62	0.0625	64	2.331(4)	-0.441(11)
					-0.425(8)

Table 7.1: C_{60} molecule energies per bond at different dopings, temperatures and $\Delta\tau$'s. All data are in units of t, the hopping integral. The parameter U is set to $4t$, n represents the total electron number in a C_{60} molecule, $T = 1/(\Delta\tau L)$ is the temperature, μ is the chemical potential, and E is the energy per bond of a C_{60} molecule filled with n electrons.

We first use the table data to extrapolate $\Delta\tau$ to zero value, which will give the single C_{60} molecule energies at each temperature for different electron dopings, see Fig. 7.1. - Fig. 7.5. Then, these energy values will be used to extrapolate the zero-temperature energy and calculate the electron or hole pair-binding energies at each temperature, see Fig. 7.6 and Fig. 7.7.

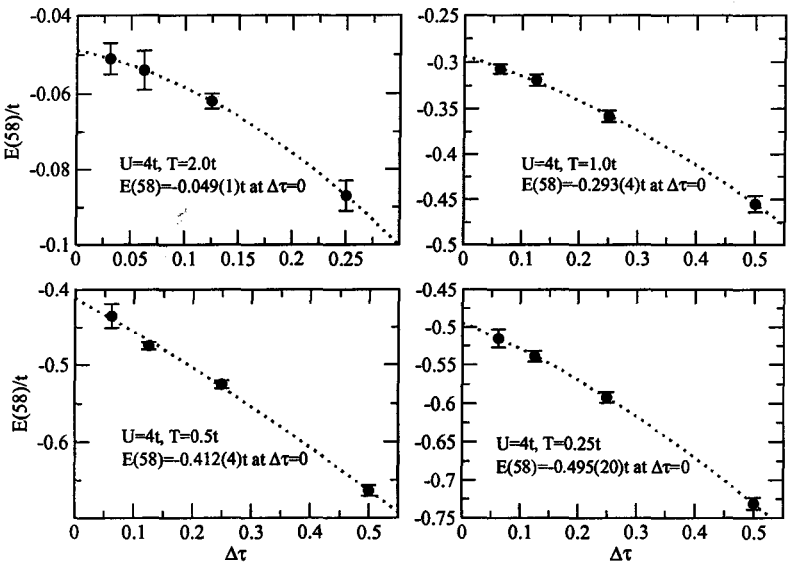

Figure 7.1: Extrapolation of energy per bond with $\Delta\tau$ at different temperatures for $U = 4t$ in a C_{60} molecule doped with 2 holes.

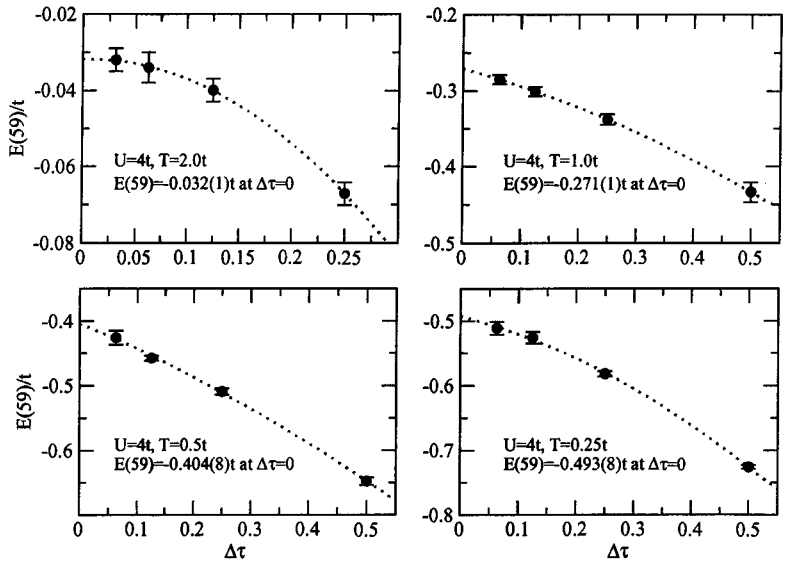

Figure 7.2: Extrapolation of energy per bond with $\Delta\tau$ at different temperatures for $U = 4t$ in a C_{60} molecule doped with 1 hole.

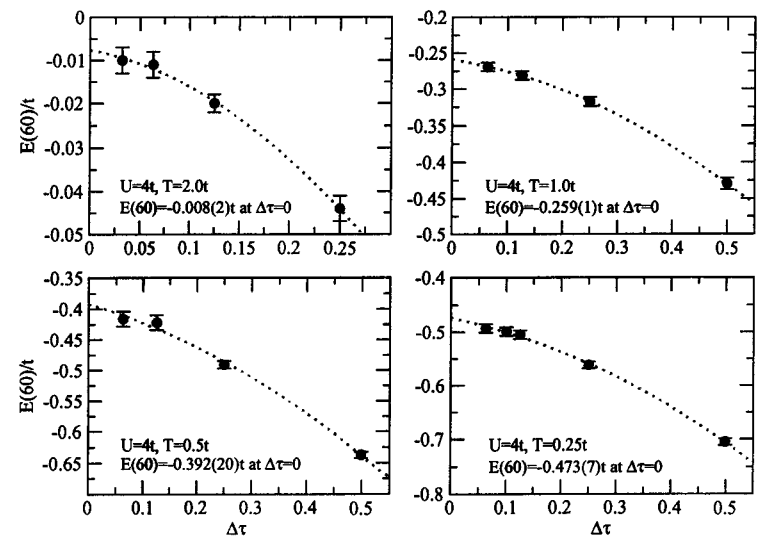

Figure 7.3: Extrapolation of energy per bond with $\Delta\tau$ at different temperatures for $U = 4t$ in a neutral C_{60} molecule.

From Fig. 7.7 we see that there are no definite trends of pair binding for either electrons or holes in a doped C_{60} molecule. We only show the errors for two points

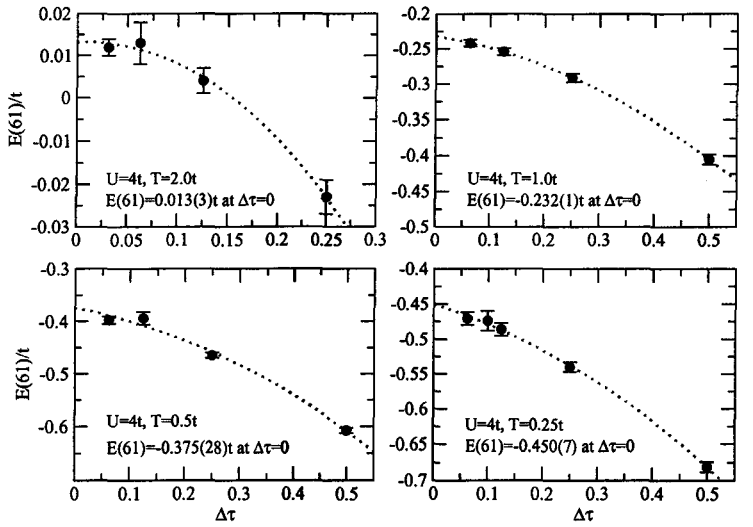

Figure 7.4: Extrapolation of energy per bond with $\Delta\tau$ at different temperatures for $U = 4t$ in a C_{60} molecule doped with 1 electron.

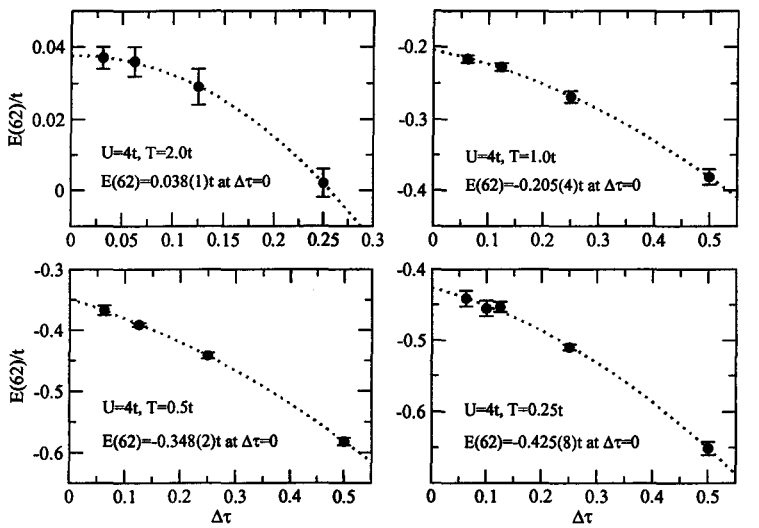

Figure 7.5: Extrapolation of energy per bond with $\Delta\tau$ at different temperatures for $U = 4t$ in a C_{60} molecule doped with 2 electrons.

in the hole-doping case, and the lower temperature points have larger errors, which are not shown for a clarity of the figure.

From the discussion in Appendix K, we believe that the auxiliary field Monte

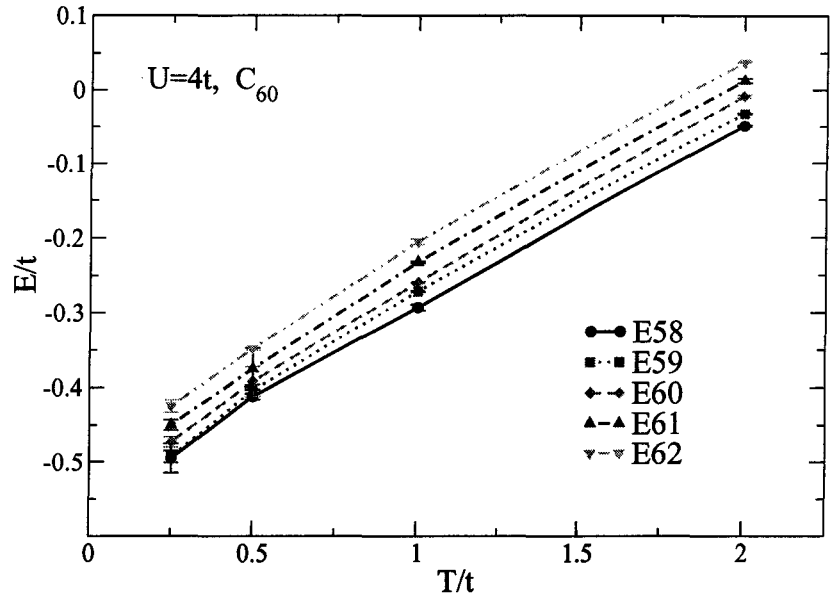

Figure 7.6: Energies of a C_{60} molecule at different temperatures and electron fillings; parameter $U = 4t$.

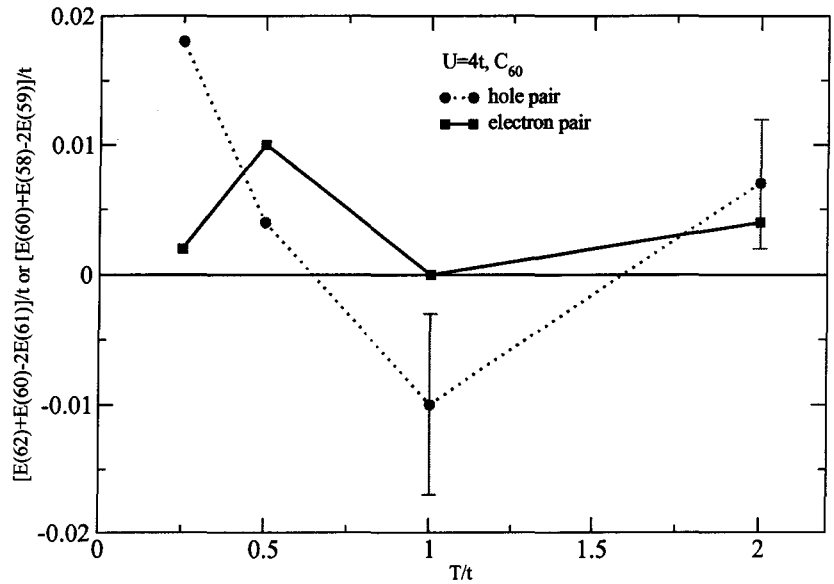

Figure 7.7: Pair binding energies for C_{60} molecule at different temperatures for $U = 4t$.

Carlo calculation can show a correct tendency of pair-binding when we go from high temperature to zero temperature. We thus tentatively conclude that for a single C_{60} molecule and in the range of temperatures reached ($0.25t \sim 2.0t$), there is no definite pair binding occurance for an intermediate Hubbard interaction $U = 4t$ if we base our calculation on the Hubbard Hamiltonian, which is a little disappointing. However, it is interesting to investigate and compare the differences between various calculational approaches. This will be the topic of discussion in the next chapter.

Chapter 8

Comparison of Different Calculational Methods

In the previous chapters, we have presented several different calculational methods for solving Hamiltonians involving Hubbard interactions. Some are approximate, such as the perturbation method and Gutzwiller projection, and some are exact, such as the Lanczos technique, the Davidson algorithm, and the discrete Hubbard-Stratonovich transformation. Generally, their results agree with each other qualitatively, but there are still some quantitatively appreciable differences. We believe these differences can not be neglected, and hence we devote this chapter of the thesis to this discussion.

8.1 Hydrogen Molecule

Our first comparison is made among the perturbation calculation, the Gutzwiller projection and the exact diagonalization on a hydrogen molecule in the half-filled case. As there are only two sites in the system, the ground state energy can be solved exactly and analytically. For a fixed number of electrons (2 electrons) in a hydrogen molecule, we have a total of 6 wavefunctions. Four of them can be grouped in a spin sector $S_z = 0$, and the other two can be divided into a $S_z = \hbar$ and a $S_z = -\hbar$ spin sector, respectively. Using these six wavefunctions as a basis and forming a matrix for the Hamiltonian, exact diagonalization of the matrix gives us the ground state

energy of the system

$$E_2^h = \frac{(\frac{U}{t}) - \sqrt{(\frac{U}{t})^2 + 16}}{2} t \tag{8.1}$$

for the Hubbard model and

$$E_2^{tj} = -J, \tag{8.2}$$

where $J = 4t^2/U$, for the $t - J$ model.

Perturbation calculation starts with a non-interacting Hamiltonain and is followed by a first order and second order perturbation. It is the same as in the C_{60} calculation except that in hydrogen, we can do all these calculations with a pencil. The result is

$$\begin{aligned} E_2 &= E^{(0)} + E^{(1)} + E^{(2)} \\ &= [-2 + \frac{1}{2}(\frac{U}{t}) - \frac{1}{16}(\frac{U}{t})^2]t. \end{aligned} \tag{8.3}$$

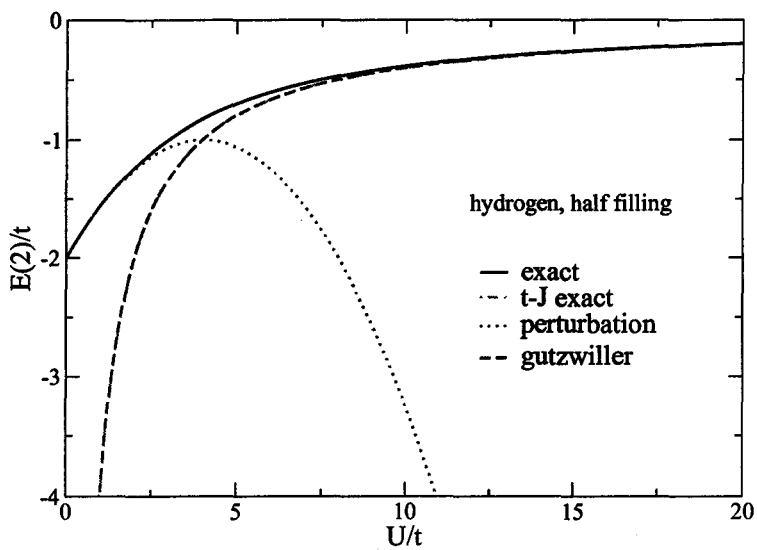

Figure 8.1: Ground state energy per bond of a half-filled hydrogen molecule from exact, perturbation and Gutzwiller calculation.

We plot the energy per bond from these two expressions versus U/t in Fig. 8.1 together with the result from Gutzwiller projection. We can see from the figure that

for a small value of U/t, the exact result agrees with the perturbation calculation, while in the large U/t regime, the Gutzwiller result behaves very well. In the large U/t limit, the Gutzwiller result coincides exactly with the exact diagonalization results of both the $t-J$ model and the Hubbard model.

Similar calculations can be performed for different total electron numbers on hydrogen. Please see Appendix L for details.

8.2 Tetrahedron Molecule

Similar calculations are performed on a tetrahedron molecule; the difference from the hydrogen molecule is that the calculations now have to be done using a computer. The ground state energy per bond from different methods is drawn in Fig. 8.2.

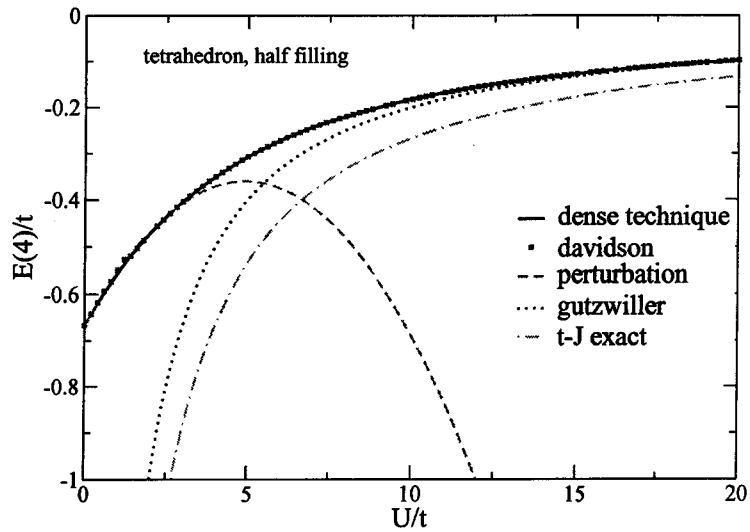

Figure 8.2: Ground state energy per bond of a half-filled tetrahedron molecule from various calculations.

In this figure, we find again that perturbation theory works well in the small U/t regime, while the Gutzwiller projection works well for large U/t. The $t-J$ model has a lower energy than the Hubbard model.

8.3 Cube Molecule

Another molecule that we have studied is the cube molecule, where there are 8 lattice sites. We plot the result for this molecule in Fig. 8.3.

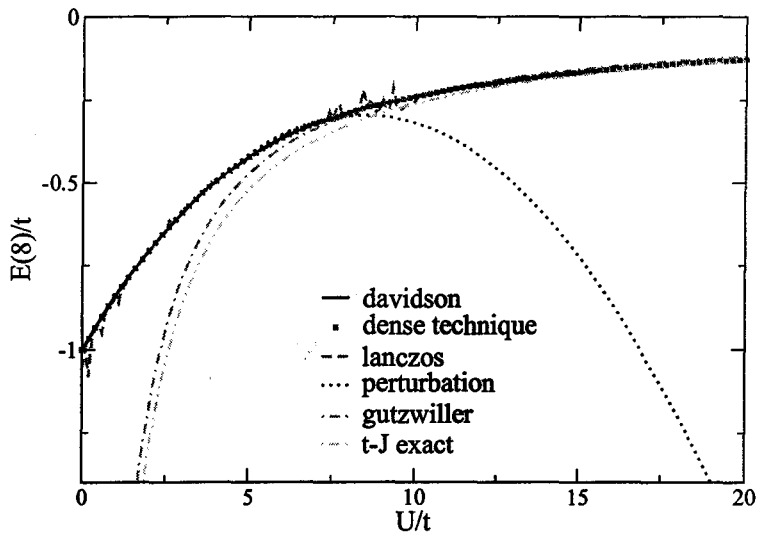

Figure 8.3: Ground state energy per bond of a half-filled cube molecule from various calculations.

The label "dense technique" means the diagonalization of the matrix used the standard program (subroutine "dsyev") from lapack. This curve may be regarded as exact and will be used to compare the other calculational approaches.

We note that results from the Davidson algorithm coincide exactly with the dense technique (Scatter points from dense technique lie exactly on the Davidson algorithm curve in Fig. 8.3). The Lanczos algorithm behaves reasonably well, compared with the "dense technique" result.

8.4 Checking of AMC Program

In this section, we check the results from the auxiliary field Monte Carlo program with the exact results for the hydrogen molecule. There was some check of auxiliary

field Monte Carlo simulation in Hirsch's paper, [37]; and the energy calculated there is the energy per site with periodic boundary conditions. Our auxiliary field Monte Carlo program, adopting the same boundary condition, will produce the same result as Hirsch did in [37]. The calculations are carried out for half-filling, and the results are listed in Table 8.1, where the parameter $\Delta\tau$ is in units of $1/t$. The units of the temperature and energy are t.

8.5 A Table

Table 8.2 provides a qualitative comparison of the different calculational approaches for solving the Hubbard model.

The table shows that different calculational approaches have their own characters. The simplist perturbation calculation is fast and easy and the results apply from small to maybe intermediate U/t.

The Gutzwiller projection is valid for large U/t regime, and the time spent in calculation is a little longer than for the perturbation calculation. We also suggest that the results in its validity regime is trustworthy, as can be seen from its comparison with the exact diagonalization in the large U/t regime. And the Gutzwiller projection also has the promise of doing a better job if we could find a more suitable trial wavefunction to approximate the true ground state or if we could find a way to write down the $|RVB>$ trial wavefunction in the C_{60} molecule.

As to the Lanczos or Davidson algorithm in exact diagonalization, the main problems are the limit of computer memory, to accommodate the basis wavefunctions in the system, and the limit of the CPU speed to carry out calculations quickly (Even when we employ a supercomputer, a lot of time is still needed for the large matrix operations). In the present situation, we can calculate the truncated tetrahedron or icosahedron (Both have 12 sites), although a large amount of time is required.

Our last method of approach is the auxiliary field Monte Carlo, and it has the advantage of being able to do calculations for large molecules, such as C_{60}, in a moderate cost of time and computer memory. Certainly, if we divide the imaginary time, i.e., β or $1/k_BT$ into large number of small sections $\Delta\tau$ and collect a large

hydrogen	k_BT	$\Delta\tau$	E/bond	exact
U=1	0.5	0.5	-1.1250(6)	
	0.5	0.25	-1.092(1)	
	0.5	0.125	-1.083(1)	
	0.5	0.0625	-1.081(1)	
	0.25	0.5	-1.551(2)	
	0.25	0.25	-1.510(1)	
	0.25	0.125	-1.499(1)	
	0.25	0.0625	-1.496(1)	-1.562
U=2	0.5	0.5	-0.923(2)	
	0.5	0.25	-0.802(2)	
	0.5	0.125	-0.769(2)	
	0.5	0.0625	-0.762(1)	
	0.25	0.5	-1.373(2)	
	0.25	0.25	-1.234(2)	
	0.25	0.125	-1.193(2)	
	0.25	0.0625	-1.182(2)	-1.236
U=4	0.5	0.5	-0.911(4)	
	0.5	0.25	-0.556(2)	
	0.5	0.125	-0.463(2)	
	0.5	0.0625	-0.438(2)	
	0.25	0.5	-1.319(4)	
	0.25	0.25	-0.912(3)	
	0.25	0.125	-0.783(4)	-0.828
U=6	0.5	0.5	-1.128(4)	
	0.5	0.25	-0.487(3)	
	0.5	0.125	-0.342(3)	
	0.5	0.0625	-0.303(3)	
	0.25	0.5	-1.507(14)	
	0.25	0.25	-0.758(9)	
	0.25	0.125	-0.549(10)	-0.606
U=8	0.5	0.5	-1.461(11)	
	0.5	0.25	-0.458(5)	
	0.5	0.125	-0.273(4)	
	0.5	0.0625	-0.224(3)	
	0.25	0.5	-1.640(59)	
	0.25	0.25	-0.682(79)	
	0.25	0.125	-0.399(50)	-0.472

Table 8.1: Comparison of exact diagonalization and auxiliary field Monte Carlo for the H_2 molecule. The exact results in the table are for $T = 0K$.

	Perturbation	Gutzwiller	Lanczos	Davidson	AMC
regime of U/t	small	large	all	all	all
accuracy	good $\forall N$	good $\forall N$	good $\forall N$	good $\forall N$	good $\forall N$
time	5	4	1	2	3

Table 8.2: Comparison of different calculational approaches. The amount of time decreases as number goes from 1 to 5.

amount of Monte Carlo data, we will approach the exact result. However, from our experience, a modest number of Monte Carlo data (1000 for tetrahedron, 10000 for cube and 100 for C_{60}) and a finite length of $\Delta\tau$ (0.5, 0.25, 0.125, 0.0625 etc.) at temperatures $2t$, t, $0.5t$, $0.25t$ etc. have produced a fairly good statistical result. Furthermore, from Appendix K, we find the auxiliary field Monte Carlo predicts a correct tendency for pair binding in both tetrahedron and cube molecules. We thus have confidence when we apply it to the C_{60} molecule.

8.6 Mesoscale Physics

Mesoscale physics is an interesting concept proposed by S. Chakravarty and S. Kivelson in [19]. They argue that a purely electronic mechanism of superconductivity requires structures at an intermediate or mesoscale system. The structures here include both the intermediate number of sites in the system and the intermediate magnitude of Hubbard interaction U. Their calculation is performed primarily on a one-dimensional Hubbard ring, and they found that for an intermediate number of lattice sites, the pair-binding energy achieves its maximum magnitude, and, when the number of lattice site is increased or decreased, the pair-binding tendency decreases. The second phenomenon is that for an intemediate Hubbard U, the pair-binding energy reaches its maximum magnitude (most attractive between electrons) and for smaller or larger U, it decreases (less attractive or repulsive).

The argument is interesting and it inspires our further investigation in this section. Our scheme is as following: we systematically perform calculations on a series of molecules that are of different sizes from hydrogen to C_{60} and then compare the pair-

binding energies to test the above argument; we also check results in different Hubbard U regimes for completeness. We believe that our results will be a useful test of this argument, although we understand the difference between the possible and necessary consequences of intermediate scale as stressed by Chakravarty and Kivelson in [19].

Our results on hydrogen from the analytic formula in Appendix L, and for tetrahedron and cube molecules from exact numerical calculations are plotted in Fig. 8.4, Fig. 8.5 and Fig. 8.6 for the cases of zero temperatures.

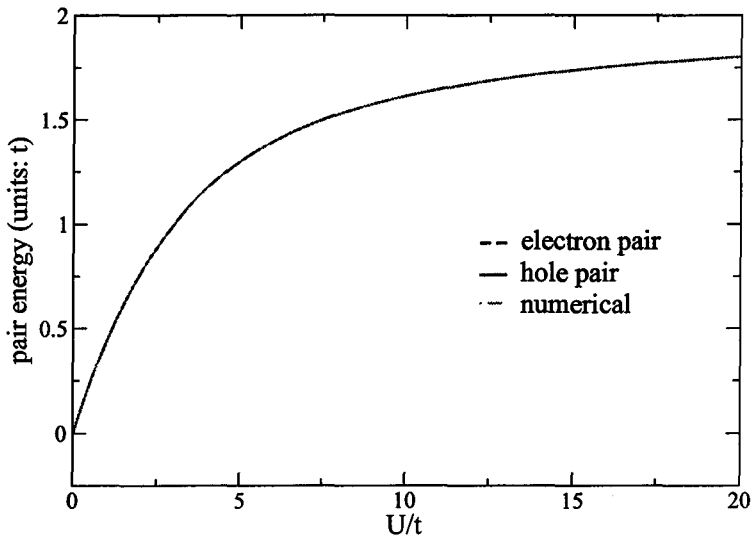

Figure 8.4: Pair binding energy per bond of a hydrogen molecule doped with electrons or holes at different Hubbard U from the exact analytic formula in Appendix L, and the exact numerical results.

Note that in Fig. 8.4, the analytic result coincides with the numerical result, which assures us again the correctness of our exact diagonalization programs that are applied to tetrahedron and cube molecules. In the large U limit, we see that the pair-binding energy calculated from Gutzwiller projected wavefunction (total $S_z = \hbar$ spin sector pair-binding energy) agrees roughly with the exact diagonalization result, see Fig. 8.7. We thus believe the pair binding energy calculated in the C_{60} molecule with the Gutzwiller projection technique is reliable to some extent.

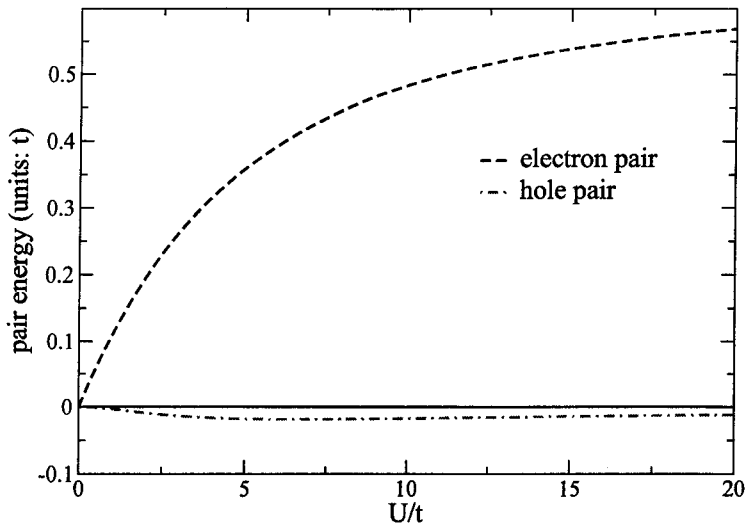

Figure 8.5: Pair binding energy per bond of a tetrahedron molecule doped with electrons or holes at different Hubbard U from the exact diagonalization.

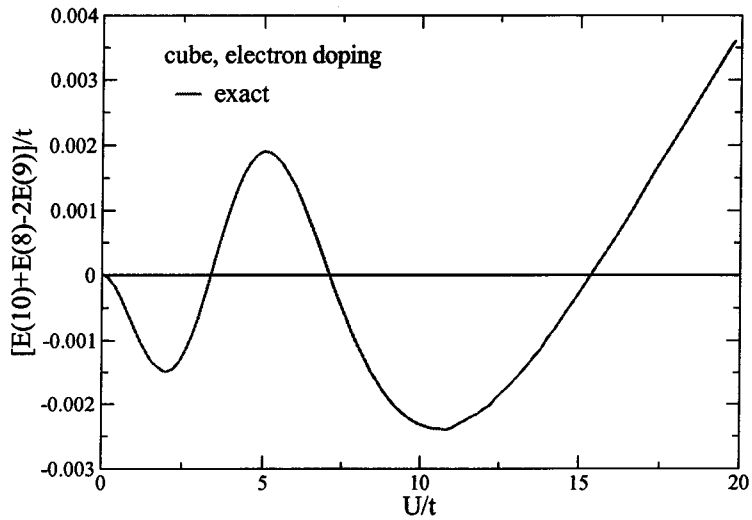

Figure 8.6: Pair-binding energy per bond of a cube molecule doped with electrons at different Hubbard U from the exact diagonalization.

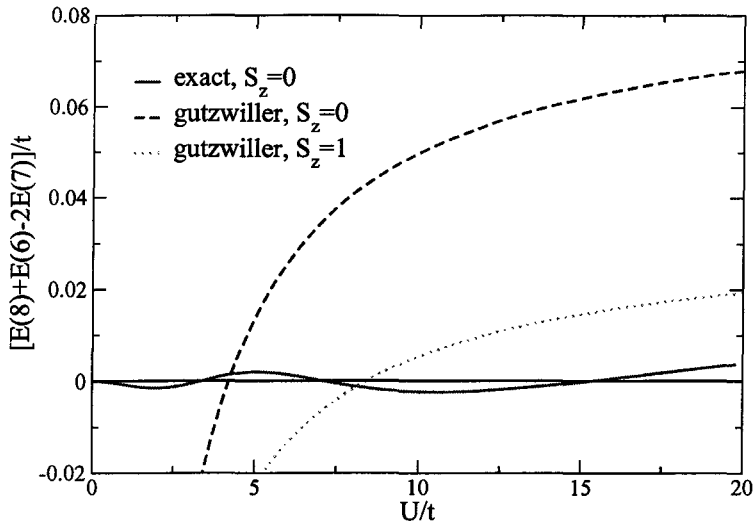

Figure 8.7: Pair-binding energy per bond of a cube molecule for singlet hole pairing state at different Hubbard U from the exact diagonalization compared to Gutzwiller-projected $t - J$ model for singlet and triplet hole pairings.

We see that from hydrogen to cube molecule, the pair binding occurs. And for the tetrahedron molecule, pair binding appears when the molecule is doped with holes, and the maximum strength of pair binding is for a Hubbard interaction strength of about $U = 5t$. For the cube molecule, both electron doping and hole doping give the same pairing tendency; and the maximum binding strength is at about $U = 10t$. We also see some pair binding possibilities in the intermediate strength of U from Appendix E, where a list of pair-binding energies as well as a figure (Fig. E.1) from Gutzwiller-projected wavefunctions are available.

Chapter 9

Conclusion

In this thesis, we have focused on the calculation of the pair-binding energy in a single C_{60} and other small molecules. Different methods have been applied to the Hubbard Hamiltonian, which is used to describe the electronic interactions inside these molecules.

The simplest perturbation calculation shows pair binding in some range of U values. Particularly, if we divide the unperturbed wavefunctions into two groups according to the symmetry of the Hubbard Hamiltonian, we find pair binding in small U regimes, and spin-singlet pairing is favored over the spin-triplet pairing.

When we enter the larger U region, we have to reconsider the validity of the perturbation calculation. In the extremely large U case, the reduction of the Hubbard Hamiltonian to the $t-J$ model is adopted. Variational Monte Carlo is then used, with the trial wavefunction constructed using the Gutzwiller projection. The calculation resulting from the Gutzwiller projected Fermi sea indicates that the pair-binding tendency in the single C_{60} molecule is in the spin-triplet channel.

Between the above two regions, there is the intermediate Hubbard interaction U regime, which corresponds to the real C_{60} material situation, and it is thus the most important regime to explore. However, neither of the above two methods can be used to draw conclusions about pair binding. Because of this, we introduce the auxiliary field Monte Carlo technique, which is essentially an exact method and can be applied to any value of Hubbard interaction. The auxiliary field Monte Carlo

program is checked by comparing it with the exact diagonalization result, and it shows satisfactory agreement. Auxiliary field Monte Carlo gives the correct tendency of pair binding in tetrahedral and cubic molecules. This agreement leads us to believe that the auxiliary field Monte Carlo data in the C_{60} molecule is reliable. Unfortunately, for the temperature range that we can reach with the Monte Carlo program, we find no clear evidence of pair binding for either electrons or holes. It is possible that at lower temperature pair binding can occur, but this regime is inaccessible to auxiliary field Monte Carlo, which suffers from a low temperature instability, as is common in thermodynamic Monte Carlo simulations.

The many-fermion problem in a single C_{60} molecule still needs further considerations; and it is desirable to improve the current Monte Carlo program to calculate not only with better statistics but also over a broader range of temperatures. Another conclusion is that the Hubbard Hamiltonian defined and explored in this thesis might not capture all the physical pictures about superconductivity in C_{60} materials. Further study on this problem will continue.

Bibliography

[1] H.W. Kroto, J.R. Heath, S.C. O'Brien, R.F. Curl and R.E. Smalley, Nature **381**, 162 (1985).

[2] W.F. David et al., Nature **353**, 147 (1991).

[3] M.P. Gelfand and J.P. Lu, Phys. Rev. Lett. **68**, 1050 (1992).

[4] M.P. Gelfand and J.P. Lu, Phys. Rev. B **46**, 4367 (1992).

[5] M.P. Gelfand and J.P. Lu, Phys. Rev. B **47**, 4149 (1993).

[6] A.F. Hebard et al., Nature **350**, 600 (1991).

[7] M.J. Rosseinsky et al., Phys. Rev. Lett. **66**, 2830 (1991).

[8] K. Tanigaki et al., Nature **352**, 222 (1991).

[9] T.T.M. Palstra et al., Solid State Commun. **93**, 327 (1995).

[10] O. Gunnarsson, Rev. Mod. Phys. **69**, 575 (1997) and references therein.

[11] L.D. Landau and E.M. Lifshitz, *Quantum Mechanics* (Pergamon Press, London) 1977, Chap.6.

[12] R.M. Fye, M.J. Martins and R.T. Scalettar, Phys. Rev. B **42**, 6809 (1990).

[13] E.H. Lieb and F.Y. Wu, Phys. Rev. Lett. **20**, 1445 (1968).

[14] G. Fano, F. Ortolani and A. Parola, Phys. Rev. B **42** ,6877 (1990).

[15] S.R. White, S. Chakravarty, M.P. Gelfand and S.A. Kivelson, Phys. Rev. B **45**, 5062 (1992).

[16] S. Chakravarty, M.P. Gelfand, and S. Kivelson, Science **254**, 970 (1991).

[17] S. Chakravarty and S. Kivelson, Europhys. Lett. **16** ,751 (1991).

[18] S. Chakravarty, S.A. Kivelson, M.I. Salkola and S. Tewari, Science **256**, 1306 (1992).

[19] S. Chakravarty and S.A. Kivelson, Phys. Rev. B **64**, 064511 (2001).

[20] P.W. Anderson, *The Theory of Superconductivity in the High-T_c Cuprates*, Ch.1, Princeton University Press, Princeton, New Jersy, 1997.

[21] edited by M. Rasetti, *The Hubbard Model: Recent Results*, World Scientific Publishing Co. Pte. Ltd., 1991.

[22] E. Dagotto, A. Moreo, F. Ortolani, D. Poilblanc, and J. Riera, Phys. Rev. B **45**, 10741 (1992).

[23] C. Lanczos, J. Res. Nat. Bur. Stand. **45**, 255 (1950).

[24] G.H. Golub and C.F. Van Loan, *Matrix Computations*, The Johns Hopkins University Press, Baltimore and London, 1989.

[25] H.Q. Lin (unpublished).

[26] S.R. White, S. Chakravarty, M. Gelfand, and S. Kivelson, Phys. Rev. B **45**, 5062 (1992).

[27] E.R. Davidson, J. Comp. Phys. **17**, 87 (1975).

[28] M.C. Gutzwiller, Phys. Rev. Lett. **10**, 159 (1963).

[29] P. Horsch and T.A. Kaplan, J. Phys. C **16**, L1203 (1983).

[30] P. Horsch and T.A. Kaplan, Bull. Am. Phys. Soc. **30**, 513 (1985).

[31] F.C. Zhang, C. Gros, T.M. Rice and H. Shiba, Supercond. Sci. Technol. **1**, 36 (1988).

[32] P.W. Anderson, Science **235**, 1196 (1987).

[33] C. Gros, R. Joynt, and T.M. Rice, Phys. Rev. B **36**, 381 (1987).

[34] C. Gros, Ann. Phys. **189**, 53 (1989).

[35] R. Blankenbecler, D.J. Scalapino and R.L. Sugar, Phys. Rev. D **24**, 2278 (1981).

[36] D.J. Scalapino and R.L. Sugar, Phys. Rev. B **24** , 4295 (1981).

[37] J.E. Hirsch, Phys. Rev. B **28**, 4059 (1983), and J.E. Hirsch, Phys. Rev. B **29**, 4159 (1984).

[38] J.E. Hirsch, Phys. Rev. Lett. **51**, 1900 (1983).

[39] J.E. Hirsch, Phys. Rev. B **31**, 4403 (1985).

[40] J. Hubbard, Phys. Rev. Lett. **3**, 77 (1959).

[41] R.L. Stratonovich, Dokl. Akad. Nauk SSSR **115** , 1097 (1957) [translation: Soviet Phys. -Doklady **2**, 416 (1958)].

[42] M. Suzuki, *Quantum Monte Carlo Methods, Solid State Sciences*, Vol. 74, ed. M. Suzuki (Springer, Berlin, 1986).

[43] R.M. Fye, Phys. Rev. B **33**, 6271 (1986).

[44] J.E. Hirsch and H.Q. Lin, Phys. Rev. B **37**, 5074 (1988).

[45] V.J. Emery, Phys. Rev. B **14**, 2989 (1976).

[46] J.E. Hirsch, Phys. Rev. Lett. **54**, 1317 (1985).

[47] P.W. Anderson, *Solid State Physics*, edited by F. Seitz and D. Turnbull (Academic Press Inc., New York, 1963), Vol.14, P99.

[48] Z.Z. Li, *Solid State Theory* (in Chinese, Advanced Education Press, Beijing, 1991), P.75.

[49] C. Castellani et al., Phys. Rev. Lett. **43**, 1957 (1979).

Appendix A

Unitary Transformation in Gutzwiller Projection

The Hubbard Hamiltonian Eq.(3.1) can be rewritten as

$$\begin{aligned} H &= T_h + T_d + T_{\rm mix} + V, \\ T_h &= -t \sum_{<i,j>,\sigma} (1-n_{i,-\sigma}) c^+_{i,\sigma} c_{j\sigma} (1-n_{j,-\sigma}) + h.c., \\ T_d &= -t \sum_{<i,j>,\sigma} n_{i,-\sigma} c^+_{i,\sigma} c_{j,\sigma} n_{j-\sigma} + h.c., \\ T_{\rm mix} &= -t \sum_{<i,j>,\sigma} n_{i,-\sigma} c^+_{i,\sigma} c_{j,\sigma} (1-n_{j,-\sigma}) + h.c. \\ &\quad -t \sum_{<i,j>,\sigma} (1-n_{i,-\sigma}) c^+_{i,\sigma} c_{j\sigma} n_{j,-\sigma} + h.c., \\ V &= U \sum_i n_{i\uparrow} n_{i,\downarrow}. \end{aligned} \tag{A.1}$$

T_h describes the transport of holes and T_d that of doubly occupied sites. They do not mix different Hubbard bands, while the term $T_{\rm mix}$ does so. We apply a unitary transformation to H,

$$\begin{aligned} H_{\rm eff} &= e^{iS} H e^{-iS} \\ &= H + i[S,H] + \cdots . \end{aligned} \tag{A.2}$$

The purpose of the transformation is that the term $T_{\rm mix}$, which represents the high-energy process, will disappear in lowest order. So this gives us the condition

$$i[S, T_h + T_d + V] = -T_{\rm mix}, \tag{A.3}$$

or if we write S explicitly

$$S = \sum_{n,m} |n> \frac{<n|T_{\rm mix}|m>}{i(\epsilon_n - \epsilon_m)} <m|, \tag{A.4}$$

where $|n>$, $|m>$ are eigenstates of $T_h + T_d + V$ with eigenvalues ϵ_n and ϵ_m. Although we do not exactly know the values of ϵ_n and ϵ_m, we can expect that for the large U limit, $\epsilon_n - \epsilon_m = \pm U + O(t)$. So we have

$$\begin{aligned} S &= \frac{it}{U} \sum_{<i,j>,\sigma} n_{i,-\sigma} c^+_{i,\sigma} c_{j,\sigma} (1 - n_{j,-\sigma}) \\ &\quad -\frac{it}{U} \sum_{<i,j>,\sigma} (1 - n_{i,-\sigma}) c^+_{i,\sigma} c_{j,\sigma} n_{j,-\sigma}. \end{aligned} \tag{A.5}$$

Note that in writing down the above equation, we have paid attention to the two kinds of different terms in $T_{\rm mix}$. For instance, terms like $n_{i,-\sigma} c^+_{i\sigma} c_{j\sigma} (1 - n_{j,-\sigma})$ should act on states $|m>$ without doubly occupied sites from left and states $<n|$ with one doubly occupied site from right; otherwise, it will give zero. So, such terms will be paired with $\epsilon_n - \epsilon_m = U$ in Eq.(A.4). Similarly, terms like $(1 - n_{i,-\sigma}) c^+_{i,\sigma} c_{j,\sigma} n_{j,-\sigma}$ should act on states $|m>$ with one doubly occupied site from left and states $<n|$ without doubly occupied sites from right, so they should be paired with $\epsilon_n - \epsilon_m = -U$ in Eq.(A.4).

If we take the effective Hamiltonian between states with no doubly occupied sites, we will have the desired result

$$\begin{aligned} H_{\rm eff} &= T_h + i[S, T_{\rm mix}] \\ &= T_h + \frac{4t^2}{U} \sum_{<i,j>} (\vec{S}_i \cdot \vec{S}_j - \frac{1}{4}). \end{aligned} \tag{A.6}$$

Actually to get Eq.(A.6), we still need some nontrivial steps, and we would like to give the details in the following lines. First, we know

$$i[S, T_{\rm mix}] = i(S T_{\rm mix} - T_{\rm mix} S). \tag{A.7}$$

Next, when we take the expectation value of the right hand side of Eq. (A.7) between two states with no doubly occupied sites, we find that in order to get a non-zero value, the application of the effective Hamiltonian should satisfy the conditions: in the first application of operators $T_{\rm mix}$ or S on the no-doubly-occupied-sites state, they will transfer a spin σ electron from site i to site j to create a state with only one doubly occupied site j; then in the second application of operators S or $T_{\rm mix}$, they will destroy this doubly occupied site j either by transferring a spin σ electron back to site i or by transferring a spin $-\sigma$ electron from site j to site i. This process can be represented in the following effective Hamiltonian

$$H_{\rm eff} = T_h - \frac{2t^2}{U} \sum_{<ij>\sigma} (c^+_{j\sigma} c_{i\sigma} c^+_{i\sigma} c_{j\sigma} + c^+_{j,-\sigma} c_{i,-\sigma} c^+_{i\sigma} c_{j\sigma}), \tag{A.8}$$

where the factor 2 comes from the commutation expression, i.e., one is from $ST_{\rm mix}$ and the other is from $T_{\rm mix}S$. So

$$\begin{aligned}
H_{\rm eff} &= T_h - \frac{2t^2}{U} \sum_{<ij>\sigma} (c^+_{j\sigma} c_{j\sigma} - c^+_{i\sigma} c_{i\sigma} c^+_{j\sigma} c_{j\sigma} - c^+_{i\sigma} c_{i,-\sigma} c^+_{j,-\sigma} c_{j\sigma}) \\
&= T_h - \frac{2t^2}{U} \sum_{<ij>} (c^+_{j\uparrow} c_{j\uparrow} + c^+_{j\downarrow} c_{j\downarrow} - c^+_{i\uparrow} c_{i\uparrow} c^+_{j\uparrow} c_{j\uparrow} - c^+_{i\downarrow} c_{i\downarrow} c^+_{j\downarrow} c^+_{j\downarrow} \\
&\quad - c^+_{i\uparrow} c_{i\downarrow} c^+_{j\downarrow} c_{j\uparrow} - c^+_{i\downarrow} c_{i\uparrow} c^+_{j\uparrow} c_{j\downarrow}) \\
&= T_h - \frac{2t^2}{U} \sum_{<ij>} [(\frac{1}{2} + S^z_j) + (\frac{1}{2} - S^z_j) - (\frac{1}{2} + S^z_i)(\frac{1}{2} + S^z_j) \\
&\quad - (\frac{1}{2} - S^z_i)(\frac{1}{2} - S^z_j) - S^+_i S^-_j - S^-_i S^+_j] \\
&= T_h - \frac{2t^2}{U} \sum_{<ij>} [\frac{1}{2} - 2S^z_i S^z_j - S^+_i S^-_j - S^-_i S^+_j] \\
&= T_h + \frac{4t^2}{U} \sum_{<ij>} (\vec{S}_i \cdot \vec{S}_j - \frac{1}{4}).
\end{aligned} \tag{A.9}$$

In the above equations, we have used the relations between creation (annihilation) operators and spin operators in a no-doubly-occupied-sites system. These relations are discussed in the next appendix.

Note that there is another way of reducing the Hubbard model in the large U limit to the $t-J$ model by a perturbation calculation as in Emery's paper [45] and also Hirsch's paper [46]. We refer interested readers to these papers.

Appendix B

Some Relations

In a half-filled system with no doubly occupied sites, we have the following equation [47, 48]

$$c_{i\uparrow}^{+}c_{i\uparrow} + c_{i\downarrow}^{+}c_{i\downarrow} = 1. \tag{B.1}$$

Let $\binom{1}{0}$ and $\binom{0}{1}$ represent spin up and down states on a site, respectively. And we know that

$$c_{\uparrow}^{+}c_{\uparrow}\binom{1}{0} = \binom{1}{0}, \quad c_{\uparrow}^{+}c_{\uparrow}\binom{0}{1} = 0, \tag{B.2}$$

where we have suppressed the site index for simplicity. Thus we can define the matrix representation of $c_{\uparrow}^{+}c_{\uparrow}$ as

$$c_{\uparrow}^{+}c_{\uparrow} = \begin{pmatrix} 1 & 0 \\ 0 & 0 \end{pmatrix}. \tag{B.3}$$

Similarly, we have

$$c_{\downarrow}^{+}c_{\downarrow} = \begin{pmatrix} 0 & 0 \\ 0 & 1 \end{pmatrix}, \tag{B.4}$$

$$c_{\uparrow}^{+}c_{\downarrow} = \begin{pmatrix} 0 & 1 \\ 0 & 0 \end{pmatrix}, \tag{B.5}$$

$$c_{\downarrow}^{+}c_{\uparrow} = \begin{pmatrix} 0 & 0 \\ 1 & 0 \end{pmatrix}. \tag{B.6}$$

Recall Pauli matrices

$$\hat{\sigma}^z = \begin{pmatrix} 1 & 0 \\ 0 & -1 \end{pmatrix}, \tag{B.7}$$

$$\hat{\sigma}^x = \begin{pmatrix} 0 & 1 \\ 1 & 0 \end{pmatrix}, \tag{B.8}$$

$$\hat{\sigma}^y = \begin{pmatrix} 0 & -i \\ i & 0 \end{pmatrix}, \tag{B.9}$$

and the relation between them and spin operators

$$S^z = \tfrac{1}{2}\hat{\sigma}^z, \quad S^x = \tfrac{1}{2}\hat{\sigma}^x, \quad S^y = \tfrac{1}{2}\hat{\sigma}^y. \tag{B.10}$$

Recall also the definition of spin raising and lowering operators

$$\begin{cases} S^+ &= S^x + iS^y \\ S^- &= S^x - iS^y. \end{cases} \tag{B.11}$$

We find, when taking into account Eq.(B.1) and anti-commutation relations of c operators, that

$$\begin{cases} S^z &= \tfrac{1}{2}(c_\uparrow^+ c_\uparrow - c_\downarrow^+ c_\downarrow) \\ S^+ &= c_\uparrow^+ c_\downarrow \\ S^- &= c_\downarrow^+ c_\uparrow, \end{cases} \tag{B.12}$$

or

$$\begin{cases} c_\uparrow^+ c_\uparrow &= \tfrac{1}{2}(1 + 2S^z) \\ c_\downarrow^+ c_\downarrow &= \tfrac{1}{2}(1 - 2S^z) \\ c_\uparrow^+ c_\downarrow &= S^+ \\ c_\downarrow^+ c_\uparrow &= S^-. \end{cases} \tag{B.13}$$

Appendix C

Other Trial Wavefunctions in Gutzwiller Projection

In the Gutzwiller projection technique, there are some other kinds of trial wavefunctions usually used besides the projected Fermi sea, such as the Resonating Valence Bond (RVB) wavefunction and the Spin Density Wave (SDW). They usually appear in the $2D$ square lattice geometries.

C.1 $|RVB>$ Wavefunction

The $|RVB>$ wavefunction is formed by a Gutzwiller projection on a BCS wavefunction

$$\begin{aligned} |RVB> &= P_{D=0}|BCS>, \\ &= P_{D=0}\prod_k (u_k + v_k c^+_{k\uparrow} c^+_{-k\downarrow}|0> \end{aligned} \tag{C.1}$$

where as before

$$P_{D=0} = \prod_i (1 - n_{i\uparrow} n_{i\downarrow}). \tag{C.2}$$

The parameters in the BCS wavefunction are given by

$$\begin{aligned} u_k^2 &= \frac{1}{2}(1+\frac{\xi_k}{\sqrt{\xi_k^2+\Delta_k^2}}) \\ v_k^2 &= \frac{1}{2}(1-\frac{\xi_k}{\sqrt{\xi_k^2+\Delta_k^2}}) \\ \xi_k &= -2t(\cos k_x+\cos k_y)-\mu \end{aligned} \tag{C.3}$$

for a $2D$ square lattice. It is easy to show that

$$\begin{aligned} \frac{v_k}{u_k} &= \frac{\Delta_k}{\xi_k+\sqrt{\xi_k^2+\Delta_k^2}} \\ &\equiv a_k. \end{aligned} \tag{C.4}$$

The parameter Δ_k can have different expressions

$$\Delta_k = \begin{cases} \Delta, & s-\text{wave}, \\ \Delta(\cos k_x-\cos k_y), & d-\text{wave}, \\ \Delta(\cos k_x+\cos k_y)-\mu, & \text{extended s-wave}. \end{cases} \tag{C.5}$$

Now we are ready to derive an expression for $<\alpha|\Psi>$, where $|\alpha>$ is the real space spin configuration in previous chapter. Let's concentrate on N lattice sites and half-filling,

$$|N>=P_N|RVB>. \tag{C.6}$$

P_N is a projection operator that projects $|RVB>$ into the subspace with fixed number of N particles. So

$$|N>=P_NP_{D=0}\prod_k(u_k+v_kc_{k\uparrow}^+c_{-k\downarrow}^+)|0>. \tag{C.7}$$

Recall our definition before: $v_k/u_k=a_k$.

$$\begin{aligned} |N> &= P_NP_{D=0}\prod_k u_k\prod_k(1+a_kc_{k\uparrow}^+c_{-k\downarrow}^+)|0> \\ &= \text{const.}\times P_{D=0}\prod_{k=k_1}^{k_{N/2}}(1+a_kc_{k\uparrow}^+c_{-k\downarrow}^+)|0> \\ &= \text{const.}\times P_{D=0}\prod_{k=k_1}^{k_{N/2}}a_kc_{k\uparrow}^+c_{-k\downarrow}^+|0> \\ &= \text{const.}\times P_{D=0}(\sum_k a_kc_{k\uparrow}^+c_{-k\downarrow}^+)^{N/2}|0>. \end{aligned} \tag{C.8}$$

Note that in our calculation we are interested in terms like: $< \alpha|\Psi > / < \beta|\Psi >$, and the constant in the expression will not affect our calculation. We can hence omit it for simplicity.

$$|N >= P_{D=0}(\sum_{k} a_k c_{k\uparrow} c_{-k\downarrow})^{N/2}|0> . \tag{C.9}$$

After a Fourier transformation:

$$a(\vec{R}_i) = \frac{1}{N}\sum_{k} a_k e^{-i\vec{k}\cdot\vec{R}_i}, \tag{C.10}$$

or

$$\begin{cases} a_k = \sum_{\vec{R}_i} a(\vec{R}_i) e^{i\vec{k}\cdot\vec{R}_i} \\ c^{+}_{k\sigma} = \sum_{\vec{R}_i} e^{i\vec{k}\cdot\vec{R}_i} c^{+}_{\vec{R}_i\sigma}, \end{cases}$$

we get

$$|N >= P_{D=0}[\sum_{\vec{R}'_j}\sum_{\vec{R}_l} a(\vec{R}'_j - \vec{R}_l) c^{+}_{\vec{R}_l\uparrow} c^{+}_{\vec{R}'_j\downarrow}]^{N/2}|0>, \tag{C.11}$$

where $\{\vec{R}_l\}$ is a set of lattice sites occupied by spin-up electrons and $\{\vec{R}'_j\}$ is the set of lattice sites occupied by spin-down electrons. Recall the expression of $|\alpha>$ in Eq.(6.14). A careful inspection gives (for $N_\uparrow = N_\downarrow = N_\sigma = N/2$)

$$< \alpha|N >= \det \begin{pmatrix} a(\vec{R}'_{1\downarrow} - \vec{R}_{1\uparrow}) & a(\vec{R}'_{1\downarrow} - \vec{R}_{2\uparrow}) & \cdots & a(\vec{R}'_{1\downarrow} - \vec{R}_{N_\sigma\uparrow}) \\ a(\vec{R}'_{2\downarrow} - \vec{R}_{1\uparrow}) & a(\vec{R}'_{2\downarrow} - \vec{R}_{2\uparrow}) & \cdots & a(\vec{R}'_{2\downarrow} - \vec{R}_{N_\sigma\uparrow}) \\ \vdots & \vdots & \vdots & \vdots \\ a(\vec{R}'_{N_\sigma\downarrow} - \vec{R}_{1\uparrow}) & a(\vec{R}'_{N_\sigma\downarrow} - \vec{R}_{2\uparrow}) & \cdots & a(R'_{N_\sigma\downarrow} - \vec{R}_{N_\sigma\uparrow}) \end{pmatrix}. \tag{C.12}$$

C.2 $|SDW>$ Wavefunction

In two dimensions, the spin density wave is given by

$$|SDW >= P_{D=0} \prod_{k\in \text{Fermi sea},\sigma} (u_k c^{+}_{k,\sigma} + \text{sign}(\sigma) v_k c^{+}_{k+Q,\sigma})|0> \tag{C.13}$$

with

$$\begin{cases} u_k^2 = \frac{1}{2}(1 - \frac{\epsilon_k}{\sqrt{\epsilon_k^2 + \Delta_{AF}^2}}) \\ v_k^2 = \frac{1}{2}(1 + \frac{\epsilon_k}{\sqrt{\epsilon_k^2 + \Delta_{AF}^2}}), \end{cases} \tag{C.14}$$

where

$$\epsilon_k = -2t(\cos k_x + \cos k_y), \tag{C.15}$$

and Δ_{AF} is the antiferromagnetic order parameter.

With the above spin density trial wavefunction, we can write down the amplitude $< \alpha|SDW >$ of a specific real space configuration $|\alpha >$. Suppose we have a spin configuration $(N_\downarrow, N_\uparrow)$, where $N_\uparrow$ and $N_\downarrow$ are number of spin-up or -down electrons in the system, then the amplitude $< \alpha|SDW >$ is the product of the determinant of an $N_\downarrow \times N_\downarrow$ matrix $(A_{\alpha,\downarrow})$ and the determinant of an $N_\uparrow \times N_\uparrow$ matrix $(A_{\alpha,\uparrow})$. The (j,l)th element of these matrices is given by

$$u_{k_j}\exp(i\vec{k}_j \cdot \vec{R}_{l,\sigma}) + \mathrm{sign}(\sigma)v_{k_j}\exp(i(\vec{k}_j + \vec{Q}) \cdot \vec{R}_{l,\sigma}), \tag{C.16}$$

where $\vec{k}_j$ is the jth wavevector occupied, $\vec{R}_{l,\sigma}$ the lth lattice site occupied by a spin-σ electron, and $\vec{Q}$ is equal to (π,π). To make the calculation easier, it is advantageous to assume $u_k = u_{-k}$ and $v_k = v_{-k}$ and define

$$\begin{aligned}
a_k(\vec{R}_{j,\downarrow}) &= u_k\exp(i\vec{k} \cdot \vec{R}_{j,\downarrow}) - v_k\exp(i(\vec{k} + \vec{Q}) \cdot \vec{R}_{j,\downarrow}) && \text{(C.17)}\\
a_k(\vec{R}_{l,\uparrow}) &= u_k\exp(i\vec{k} \cdot \vec{R}_{l,\uparrow}) + v_k\exp(i(\vec{k} + \vec{Q}) \cdot \vec{R}_{l,\uparrow}) && \text{(C.18)}\\
a(\vec{R}_{j,\downarrow}, \vec{R}_{l,\uparrow}) &= \sum_{k\in\text{Fermi sea}} a_k(\vec{R}_{l,\uparrow})a_{-k}(\vec{R}_{j,\downarrow}). && \text{(C.19)}
\end{aligned}$$

With these definitions, Eq.(C.13) can be rewritten as

$$\begin{aligned}
|SDW > &= P_{D=0} \prod_{k\in\text{Fermi sea}} \sum_{\vec{R}_{j,\downarrow},\vec{R}_{l,\uparrow}} a_k(\vec{R}_{l,\uparrow})a_{-k}(\vec{R}_{j,\downarrow})c^+_{\vec{R}_{l,\uparrow},\uparrow}c^+_{\vec{R}_{j,\downarrow},\downarrow}|0 >\\
&= P_{D=0}(\sum_{\vec{R}_{j,\downarrow},\vec{R}_{l,\uparrow}} a(\vec{R}_{j,\downarrow},\vec{R}_{l,\uparrow})c^+_{\vec{R}_{l,\uparrow},\uparrow}c^+_{\vec{R}_{j,\downarrow},\downarrow})^{N/2}|0 >\\
&= \sum_\alpha < \alpha|SDW > |\alpha > . && \text{(C.20)}
\end{aligned}$$

And the amplitude $< \alpha|SDW >$ then has the form

$$< \alpha|SDW >= \det \begin{pmatrix}
a(\vec{R}_{1\downarrow},\vec{R}_{1\uparrow}) & a(\vec{R}_{1\downarrow},\vec{R}_{2\uparrow}) & \cdots & a(\vec{R}_{1\downarrow},\vec{R}_{N_\sigma\uparrow})\\
a(\vec{R}_{2\downarrow},\vec{R}_{1\uparrow}) & a(\vec{R}_{2\downarrow},\vec{R}_{2\uparrow}) & \cdots & a(\vec{R}_{2\downarrow},\vec{R}_{N_\sigma\uparrow})\\
\vdots & \vdots & \vdots & \vdots\\
a(\vec{R}_{N_\sigma\downarrow},\vec{R}_{1\uparrow}) & a(\vec{R}_{N_\sigma\downarrow},\vec{R}_{2\uparrow}) & \cdots & a(R_{N_\sigma\downarrow},\vec{R}_{N_\sigma\uparrow})
\end{pmatrix} \tag{C.21}$$

for an equal number of spin-up and -down electrons.

Appendix D

Techniques for Calculating $< \alpha | \Psi >$

In the Gutzwiller projection section, we have pointed out that to make our Monte Carlo simulation efficient, we can generate a new spin configuration $|\alpha >_{i+1}$ out of the old configuration $|\alpha >_i$ by interchanging the positions of two electrons that have opposite spins. We also pointed out that the physical quantity that is of interest to our calculation is the ratio of the new and old amplitudes ${}_{i+1} < \alpha|\Psi > / {}_i < \alpha|\Psi >$. Denote two matrices as $A_{\alpha_{i+1}}$ and A_{α_i}, respectively, and suppose that the two electrons that interchange position with each other are sitting on $\vec{R}'_{l,\downarrow}$ and $\vec{R}_{j,\uparrow}$; then we have

$$A_{\alpha_{i+1}} = A_{\alpha_i} + \Delta A_1 + \Delta A_2, \tag{D.1}$$

where A_{α_i} is given by Eq.(C.12) and ΔA_1 and ΔA_2 differ from each other by one column and one row; if we replace $\vec{R}'_l$ with $\hat{\vec{R}}'_l$ and $\vec{R}_j$ with $\hat{\vec{R}}_j$, then the difference of two matrices are given by

$$\Delta A_1 = \begin{pmatrix} 0 & \cdots & 0 & a(\vec{R}'_1 - \hat{\vec{R}}_j) - a(\vec{R}'_1 - \vec{R}_j) & 0 & \cdots & 0 \\ 0 & \cdots & 0 & a(\vec{R}'_2 - \hat{\vec{R}}_j) - a(\vec{R}'_2 - \vec{R}_j) & 0 & \cdots & 0 \\ \vdots & \vdots & \vdots & \vdots & \vdots & \vdots & \vdots \\ 0 & \cdots & 0 & a(\vec{R}'_{N_\sigma} - \hat{\vec{R}}_j) - a(\vec{R}'_{N_\sigma} - \vec{R}_j) & 0 & \cdots & 0 \end{pmatrix} \tag{D.2}$$

and

$$\Delta A_2 = \begin{pmatrix} 0 & \cdots & 0 \\ \vdots & \vdots & \vdots \\ 0 & \cdots & 0 \\ a(\hat{\vec{R}}_l' - \vec{R}_1) - a(\vec{R}_l' - \vec{R}_1) & \cdots & a(\hat{\vec{R}}_l' - \vec{R}_{N_\sigma}) - a(\vec{R}_l' - \vec{R}_{N_\sigma}) \\ 0 & \cdots & 0 \\ \vdots & \vdots & \vdots \\ 0 & \cdots & 0 \end{pmatrix}. \quad \text{(D.3)}$$

We digress now to some mathematics before we discuss how to calculate $_{i+1} < \alpha|\Psi >$ out of $_i < \alpha|\Psi >$. Suppose we have $N \times N$ matrix A and its inverse B, i.e., $AB = BA = I$, and we have $N \times N$ matrix A' and its inverse B', $A'B' = B'A' = I$. A' differs from A by one column, say the jth column. We write

$$A' = A + \Delta A, \quad \text{(D.4)}$$

where

$$\Delta A = \begin{pmatrix} 0 & \cdots & 0 & \Delta A_{1j} & 0 & \cdots & 0 \\ 0 & \cdots & 0 & \Delta A_{2j} & 0 & \cdots & 0 \\ \vdots & \vdots & \vdots & \vdots & \vdots & \vdots & \vdots \\ 0 & \cdots & 0 & \Delta A_{Nj} & 0 & \cdots & 0 \end{pmatrix}. \quad \text{(D.5)}$$

Multiplying B' from right in Eq.(D.4), we get

$$I = AB' + \Delta A \cdot B'. \quad \text{(D.6)}$$

Multiplying B from left in Eq.(D.6), we find

$$B = B' + B\Delta A \cdot B'. \quad \text{(D.7)}$$

Eq.(D.7) is a Dyson-like equation and will be useful in simplifying our amplitude ratio calculations.

Now suppose we want to calculate a quantity Q, which is defined as

$$Q = \frac{\det(A')}{\det(A)}, \quad \text{(D.8)}$$

then what should we do? We know from the matrix properties the following identity:

$$Q = \frac{\det A^{'}}{\det A} = \frac{\det B}{\det B^{'}} = \det(BA^{'}). \tag{D.9}$$

From the Dyson-like equation Eq.(D.7), we know

$$\begin{aligned} BA^{'} &= (B^{'} + B\Delta AB^{'})A^{'} \\ &= I + B\Delta A. \end{aligned} \tag{D.10}$$

Thus

$$Q = \det(I + B\Delta A). \tag{D.11}$$

We need the expression for $B\Delta A$, which is given by

$$B\Delta A = \begin{pmatrix} 0 & \cdots & 0 & X1 & 0 & \cdots & 0 \\ 0 & \cdots & 0 & X2 & 0 & \cdots & 0 \\ \vdots & \vdots & \vdots & \vdots & \vdots & \vdots & \vdots \\ 0 & \cdots & 0 & X_N & 0 & \cdots & 0 \end{pmatrix}, \tag{D.12}$$

where

$$X_m = \sum_{i=1}^{N} B_{mi}\Delta A_{ij}, \quad m = 1, 2, \cdots, N. \tag{D.13}$$

So

$$I + B\Delta A = \begin{pmatrix} 1 & 0 & \cdots & 0 & X1 & 0 & \cdots & 0 \\ 0 & 1 & \cdots & 0 & X2 & 0 & \cdots & 0 \\ \vdots & \vdots & \vdots & \vdots & \vdots & \vdots & \vdots & \vdots \\ 0 & 0 & \cdots & 0 & 1+X_j & 0 & \cdots & 0 \\ \vdots & \vdots & \vdots & \vdots & \vdots & \vdots & \vdots & \vdots \\ 0 & 0 & \cdots & 0 & X_N & 0 & \cdots & 1 \end{pmatrix}. \tag{D.14}$$

The value of Q is hence trivially given by

$$\begin{aligned} Q &= \det(I + B\Delta A) \\ &= 1 + X_j. \end{aligned} \tag{D.15}$$

So if we know A, B and ΔA, and use the above method to calculate Q, we need only N operations, which is compared with the N^3 operations of calculating $\det A^{'}$ from $A^{'}$. The time needed to calculate Q is greatly reduced.

Another question we will discuss is how to calculate $B^{'}$ if we know matrix A, B and ΔA. The problem can be solved by looking at the Dyson-like equation Eq.(D.7), which gives

$$\begin{aligned} B^{'} &= B - B\Delta AB^{'} \\ &= B - B\Delta A(B - B\Delta AB^{'}) \\ &= B - B\Delta AB + B\Delta AB\Delta AB^{'} \\ &= \cdots \\ &= B - (B\Delta A - (B\Delta A)^2 + \cdots + (-1)^{m+1}(B\Delta A)^m + \cdots)B. \end{aligned} \tag{D.16}$$

Recall Eq.(D.12). It is easy to show that for an arbitrary integer m

$$\begin{aligned} (B\Delta A)^m &= \begin{pmatrix} 0 & \cdots & 0 & X_1X_j^{m-1} & 0 & \cdots & 0 \\ 0 & \cdots & 0 & X_2 2X_j^{m-1} & 0 & \cdots & 0 \\ \vdots & \vdots & \vdots & \vdots & \vdots & \vdots & \vdots \\ 0 & \cdots & 0 & X_N X_j^{m-1} & 0 & \cdots & 0 \end{pmatrix} \\ &= (B\Delta A)X_j^{m-1}. \end{aligned} \tag{D.17}$$

Thus

$$\begin{aligned} B^{'} &= B - B\Delta AB(1 - X_j + \cdots + (-1)^{m+1}X_j^{m-1} + \cdots) \\ &= B - B\Delta AB/(1 + X_j), \end{aligned} \tag{D.18}$$

or written in another way

$$B^{'}_{ml} = B_{ml} - \frac{X_m}{1 + X_j}B_{jl}. \tag{D.19}$$

After the above mathematical preparation, we can now return to Eq.(D.1), where ΔA_1 has only one column non-zero values and ΔA_2 has only one row non-zero values. Also suppose the inverse of matrix A_{α_i} is B_{α_i} and the inverse of matrix $A_{\alpha_{i+1}}$ is $B_{\alpha_{i+1}}$, i.e.

$$A_{\alpha_i}B_{\alpha_i} = B_{\alpha_i}A_{\alpha_i} = I \tag{D.20}$$

$$A_{\alpha_{i+1}}B_{\alpha_{i+1}} = B_{\alpha_{i+1}}A_{\alpha_{i+1}} = I. \tag{D.21}$$

The question is if we know A_{α_i}, B_{α_i}, ΔA_1 and ΔA_2, how to calculate Q and $B_{\alpha_{i+1}}$ efficiently? The parameter Q is as before defined as

$$Q = \frac{\det A_{\alpha_{i+1}}}{\det A_{\alpha_i}}. \tag{D.22}$$

We need to define an intermediate matrix $M = A_{\alpha_i} + \Delta A_1$, then with the method just mentioned above, we can calculate $\det M/\det A_{\alpha_i}$ and M^{-1} the inverse of M very easily. Note that

$$A_{\alpha_{i+1}} = M + \Delta A_2. \tag{D.23}$$

If we do a transpose on the above equation, we get

$$A^T_{\alpha_{i+1}} = M^T + \Delta A_2^T, \tag{D.24}$$

where ΔA_2^T now is a matrix that has only one column non-zero values. So we can apply the same technique as above on this equation and find the values for $\det(A^T_{\alpha_{i+1}})/\det M^T$ and $(A^T_{\alpha_{i+1}})^{-1}$ conveniently. Thus

$$\begin{aligned} Q &= \frac{\det A_{\alpha_{i+1}}}{\det A_{\alpha_i}} \\ &= \frac{\det(A^T_{\alpha_{i+1}})}{\det M^T} \cdot \frac{\det M}{\det A_{\alpha_i}}. \end{aligned} \tag{D.25}$$

Finally, the general properties of matrix will help us find

$$B_{\alpha_{i+1}} = A^{-1}_{\alpha_{i+1}} = ((A^T_{\alpha_{i+1}})^{-1})^T. \tag{D.26}$$

Appendix E

A List of Binding Energy

Here, we list some hole pair-binding energies for different molecules. Also see the following figure for pair-binding energies.

Icosahedron:	
	$E(12)+E^s(10)-2E(11)=0.19529-0.55541(4t/U)+0.03044(t/U)$
	$E(12)+E^T(10)-2E(11)=0.11900-0.20894(4t/U)-0.14801(t/U)$
Truncated Tetrahedron:	
	$E(12)+E^s(10)-2E(11)=0.25972-0.48407(4t/U)-0.13865(t/U)$
	$E(12)+E^T(10)-2E(11)=0.15133-0.32768(4t/U)-0.36148(t/U)$
Cube:	
	$E(8)+E^s(6)-2E(7)=1.03158-0.93828(4t/U)-0.58652(t/U)$
	$E(8)+E^T(6)-2E(7)=0.4-0.63377(4t/U)-0.83631(t/U)$

Table E.1: Hole spin singlet or triplet pair-binding energies per bond for different molecules from Gutzwiller projection calculation. All data are in units of t.

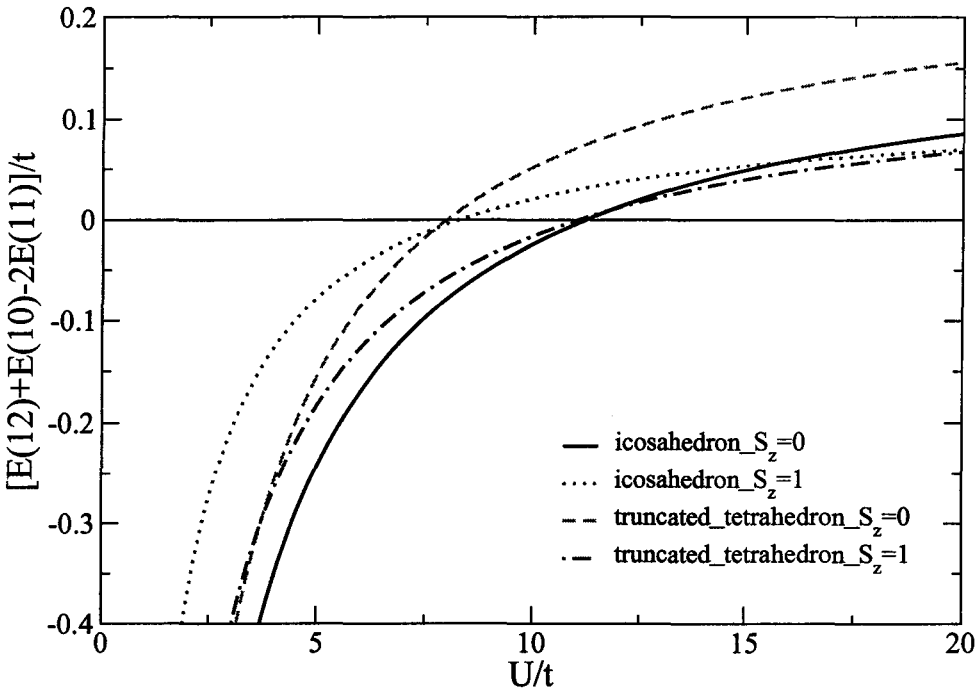

Figure E.1: Hole spin singlet or triplet pair-binding energies per bond of a truncated tetrahedron or icosahedron molecule.

Appendix F

Derivation of Eq.(7.7)

The discrete Hubbard-Stratonovich transformation in Eq.(7.7) will be proved in this section.

Recall Eq.(7.4)

$$n_{i\uparrow}n_{i\downarrow} = -\frac{1}{2}(n_{i\uparrow} - n_{i\downarrow})^2 + \frac{1}{2}(n_{i\uparrow} + n_{i\downarrow}). \tag{F.1}$$

We then have

$$\exp(-\Delta\tau U n_\uparrow n_\downarrow) = \exp[\frac{U\Delta\tau}{2}(n_\uparrow - n_\downarrow)^2 - \frac{U\Delta\tau}{2}(n_\uparrow + n_\downarrow)]. \tag{F.2}$$

We concentrate on term $\exp[\frac{U\Delta\tau}{2}(n_\uparrow - n_\downarrow)^2]$. A Taylor expansion gives

$$\begin{aligned}
\exp[\frac{U\Delta\tau}{2}(n_\uparrow - n_\downarrow)^2] &= 1 + \frac{1}{1!}[\frac{U\Delta\tau}{2}(n_\uparrow - n_\downarrow)^2] + \frac{1}{2!}[\frac{U\Delta\tau}{2}(n_\uparrow - n_\downarrow)^2]^2 + \cdots \\
&= 1 + \{\frac{1}{1!}(\frac{U\Delta\tau}{2}) + \frac{1}{2!}(\frac{U\Delta\tau}{2})^2 + \frac{1}{3!}(\frac{U\Delta\tau}{2})^3 + \cdots\} \\
&\quad \times (n_\uparrow - n_\downarrow)^2 \\
&= 1 + \{\exp(\frac{U\Delta\tau}{2}) - 1\}(n_\uparrow - n_\downarrow)^2,
\end{aligned} \tag{F.3}$$

where we have noted that for $k = 1, 2, 3, \cdots$ we have the following properties of fermion operators

$$\begin{cases} (n_\uparrow - n_\downarrow)^{2k} = (n_\uparrow - n_\downarrow)^2 \\ (n_\uparrow - n_\downarrow)^{2k+1} = (n_\uparrow - n_\downarrow). \end{cases} \tag{F.4}$$

Let $\exp(\frac{U\Delta\tau}{2}) - 1 = \cosh(2a) - 1$ or equivently

$$\tanh^2 a = \tanh(\frac{U\Delta\tau}{4}), \tag{F.5}$$

we have

$$\begin{aligned}
e^{\frac{U\Delta\tau}{2}(n_\uparrow - n_\downarrow)^2} &= 1 + \{\cosh(2a) - 1\}(n_\uparrow - n_\downarrow)^2 \\
&= 1 + \{\frac{1}{2!}(2a)^2 + \frac{1}{4!}(2a)^4 + \cdots\}(n_\uparrow - n_\downarrow)^2 \\
&= \frac{1}{2}\{1 + \frac{1}{1!}[2a(n_\uparrow - n_\downarrow)] + \frac{1}{2!}[2a(n_\uparrow - n_\downarrow)]^2 + \frac{1}{3!}[2a(n_\uparrow - n_\downarrow)]^3 \\
&\quad + \cdots\} + \frac{1}{2}\{1 + \frac{1}{1!}[-2a(n_\uparrow - n_\downarrow)] + \frac{1}{2!}[-2a(n_\uparrow - n_\downarrow)]^2 \\
&\quad + \frac{1}{3!}[-2a(n_\uparrow - n_\downarrow)]^3 + \cdots\} \\
&= \frac{1}{2}\{e^{2a(n_\uparrow - n_\downarrow)} + e^{-2a(n_\uparrow - n_\downarrow)}\} \\
&= \frac{1}{2}Tr_{\{\sigma\}}\exp[2a\sigma(n_\uparrow - n_\downarrow)].
\end{aligned} \tag{F.6}$$

Combining the above Eq.(F.6) and Eq.(F.2), we find that Eq.(7.7) is proved.

Appendix G

Derivation of Eq.(7.16)

The derivation of Eq.(7.16) here is taken from Hirsch's paper [39]. The equation follows from the identity

$$Tre^{-c_i^\dagger A_{ij} c_j} e^{-c_i^\dagger B_{ij} c_j} = \det(1 + e^{-A} e^{-B}), \tag{G.1}$$

where A and B are arbitrary matrices, and the summation over indices is assumed. To prove Eq.(G.1), we need to prove first the identity

$$e^{-c_i^\dagger A_{ij} c_j} e^{-c_i^\dagger B_{ij} c_j} = e^{-\sum_\nu c_\nu^\dagger l_\nu c_\nu}, \tag{G.2}$$

where $\lambda_\mu = e^{-l_\mu}$ are the eigenvalues of the matrix $e^{-A}e^{-B}$. From Eq.(G.2), Eq.(G.1) follows immediately, since

$$\begin{aligned} Tre^{-\sum_\nu c_\nu^\dagger l_\nu c_\nu} &= Tr \prod_\nu e^{-c_\nu^\dagger l_\nu c_\nu} \\ &= \prod_\nu (1 + e^{-l_\nu}) \\ &= \det(1 + e^{-A} e^{-B}). \end{aligned} \tag{G.3}$$

To prove Eq.(G.2), we show that an arbitrary many-particle state propagates in the same way using the expression on either side. Consider first a single-particle state

$$|\phi> = \sum_j a_j c_j^\dagger |0> \tag{G.4}$$

with a_j arbitrary numbers, and $|0>$ the true vacuum state. Let $|\mu>$ be the basis where the matrix B is diagonal, i.e.,

$$B = \sum_{\mu} |\mu > b_\mu < \mu|, \tag{G.5}$$

and define new fermion coordinates

$$\begin{aligned} c_\mu &= \textstyle\sum_j < \mu | j > c_j, \\ c_\mu^+ &= \textstyle\sum_j < j | \mu > c_j^+, \end{aligned} \tag{G.6}$$

with inverse

$$\begin{aligned} c_j &= \textstyle\sum_\mu < j | \mu > c_\mu, \\ c_j^+ &= \textstyle\sum_\mu < \mu | j > c_\mu^+. \end{aligned} \tag{G.7}$$

With Taylor expansion and the properties of fermion operator, we can write the exponential of B as

$$e^{-c_i^+ B_{ij} c_j} = e^{-c_\mu^+ b_\mu c_\mu} = \prod_{\mu} [1 + (e^{-b_\mu} - 1) c_\mu^+ c_\mu]. \tag{G.8}$$

On applying this to the state Eq.(G.4), expanding c_j^+ in terms of c_μ^+, and using fermion anticommutation relations, we find

$$\begin{aligned} e^{-c_i^+ B_{ij} c_j} |\phi > &= \textstyle\sum_j a_j' c_j^+ |0>, \\ a_i' &= \textstyle\sum_j (e^{-B})_{ij} a_j. \end{aligned} \tag{G.9}$$

Similarly, in operating with both factors on the left-hand side of Eq.(G.2), one finds after some algebra

$$\begin{aligned} e^{-c_i^+ A_{ij} c_j} e^{-c_i^+ B_{ij} c_j} |\phi > &= \textstyle\sum_j a_j'' c_j^+ |0>, \\ a_i'' &= \textstyle\sum_j (e^{-B})_{ij} a_j, \end{aligned} \tag{G.10}$$

i.e., the amplitude of the propagated state is obtained by multiplying the original amplitude by the product of the matrices. Eq.(G.10) is valid in any basis, in particular in the one where $e^{-A} e^{-B}$ is diagonal. If we start with a state that is an eigenstate of $e^{-A} e^{-B}$:

$$|\phi > = c_\nu^+ |0>, \tag{G.11}$$

then

$$e^{-c_i^+ A_{ij} c_j} e^{-c_i^+ B_{ij} c_j} |\phi> = (e^{-A} e^{-B})_{\nu\nu} c_\nu^+ |0> = e^{-l_\nu} c_\nu^+ |0>, \tag{G.12}$$

which is the same as we obtain from the right-hand side of Eq.(G.2). Thus we have proved Eq.(G.2) when applied to single-particle states, and it remains to be shown that if we have more than one particle they propagate independently. Consider first the propagation by one factor. If we take a two-particle state

$$|\phi> = c_{\mu_1}^+ c_{\mu_2}^+ |0> \tag{G.13}$$

and propagate it with B, we have

$$e^{-c_i^+ B_{ij} c_j} |\phi> = \prod_\mu [1 + (e^{-B_\mu} - 1) c_\mu^+ c_\mu] c_{\mu_1}^+ c_{\mu_2}^+ |0> \tag{G.14}$$

$$= e^{-B_{\mu_1}} e^{-B_{\mu_2}} c_{\mu_1}^+ c_{\mu_2}^+ |0> . \tag{G.15}$$

Eq.(G.15) clearly holds if $\mu_1 \neq \mu_2$, since we pair μ_1 and μ_2 with their corresponding factors, and also if $\mu_1 = \mu_2$, since then both sides are zero due to the Pauli principle. Clearly then, the propagation of an arbitrary two-particle state is a superposition of each particle independently, and similarly for many-particle states. By using the argument repeatedly, it follows also for propagation through more than one factor, which completes the proof of Eq.(G.1). Of course, this is then trivially extended to more than two factors.

Appendix H

Exponential Matrix

We find it necessary to discuss the problem of exponential matrix, an example of which appears in Eq.(7.11) in the auxiliary field Monte Carlo chapter. In Eq.(7.11), kinetic energy matrix K is a non-diagonal matrix, while potential energy matrix V is a diagonal one. The techniques to write their respective exponential matrices $e^{-\Delta\tau K}$ and $e^{V^{\alpha}(l)}$ are different.

Suppose A is a common matrix, then the definition of e^{A} is

$$e^{A} = I + \frac{1}{1!}A + \frac{1}{2!}A^{2} + \frac{1}{3!}A^{3} + \cdots, \tag{H.1}$$

where I is a unit matrx.

If A is diagonal matrix, then according to this definition, it is easy to check that

$$e^{A} = \begin{pmatrix} e^{A_{11}} & 0 & 0 & \cdots & 0 \\ 0 & e^{A_{22}} & 0 & \cdots & 0 \\ 0 & 0 & e^{A_{33}} & \cdots & 0 \\ \vdots & \vdots & \vdots & \vdots & \vdots \\ 0 & 0 & 0 & 0 & e^{A_{NN}} \end{pmatrix}. \tag{H.2}$$

If A is non-diagonal matrix, then we assume that through a unitary transformation A can be reduced to a diagonal matrx D, i.e.,

$$B^{-1}AB = D. \tag{H.3}$$

We then have

$$\begin{aligned} B^{-1}e^{A}B &= B^{-1}(I+\frac{1}{1!}A+\frac{1}{2!}A^2+\frac{1}{3!}A^3+\cdots)B \\ &= I+\frac{1}{1!}D+\frac{1}{2!}D^2+\frac{1}{3!}D^3+\cdots . \end{aligned} \tag{H.4}$$

So

$$\begin{aligned} e^{A} &= B(I+\frac{1}{1!}D+\frac{1}{2!}D^2+\frac{1}{3!}D^3+\cdots)B^{-1} \\ &= B\begin{pmatrix} e^{D_{11}} & 0 & 0 & \cdots & 0 \\ 0 & e^{D_{22}} & 0 & \cdots & 0 \\ 0 & 0 & e^{D_{33}} & \cdots & 0 \\ \vdots & \vdots & \vdots & \vdots & \vdots \\ 0 & 0 & 0 & 0 & e^{D_{NN}} \end{pmatrix} B^{-1}. \end{aligned} \tag{H.5}$$

Appendix I

Chemical Potential

As is known to all, the chemical potential μ in the Hubbard model is included in the grand canonical partition function to fix the electron number in the system. The reason why $\mu = U/2$ corresponds to half-filling of the system has been stated in [49]. Here, we outline the proof.

In the derivation of the Hubbard Hamiltonian, Wannier functions are used to calculate the nearest neighbor hopping integrals, i.e. the hopping parameter t in the Hubbard Hamiltonian (3.1).

$$t = \int \phi_i^*(\vec{r})\phi_j(\vec{r})\, d\vec{r}, \tag{I.1}$$

where i and j denote nearest neighbor sites. Suppose that we shift the phase of the Wannier representation $\phi_i(\vec{r}) \rightarrow \phi_i'(\vec{r})\exp(i\alpha_i)$, then because these two representations describe the same physical system, the grand canonical partition function is invariant under such a phase change. Particularly, if we choose

$$\alpha_i - \alpha_j = \pi, \quad \text{for } i,j \text{ nearest neighbor}, \tag{I.2}$$

we will get $t' = -t$ and

$$Z_\mu(t') = Z_\mu(-t) = Z_\mu(t) = \mathrm{Tr}e^{-\beta(H_0 - \mu N_e)}, \tag{I.3}$$

where H_0 is the Hubbard model without the chamical potential term and $N_e = \sum_i n_i$ is the total electron number operator.

Next we do a particle-hole transformation on the Hubbard Hamiltonian, $c^+_{i\sigma} \to h_{i\sigma}$. It is easy to show that the Hubbard Hamiltonian undergoes the following transformation

$$H_0(t) - \mu N_e = H_0(-t) - (U-\mu)N_h + (U-2\mu)N_t. \tag{I.4}$$

Here N_t is the total number of lattice sites in the system, and $N_h = \sum_i h_i^+ h_i$ is the hole number operator. Thus

$$\begin{aligned} Z_\mu(t) &= \mathrm{Tr} e^{-\beta(H_0-\mu N_e)} \\ &= \mathrm{Trexp}[-\beta(H_0(-t) - (U-\mu)N_h + (U-2\mu)N_t)] \\ &= \exp[-\beta(U-2\mu)N_t] Z_{U-\mu}(t), \end{aligned} \tag{I.5}$$

where in the last step, we have used the property of Eq.(I.3). Taking the partial derivative of Eq.(I.5) with respect to μ, we obtain

$$\begin{aligned} < N_e > &= \frac{1}{\beta}\frac{\partial}{\partial\mu}\ln Z_\mu \\ &= \frac{1}{\beta}\frac{\partial}{\partial\mu}\ln\{\exp[-\beta(U-2\mu)N_t] Z_{U-\mu}(t)\} \\ &= 2N_t - \frac{1}{\beta}\frac{\partial}{\partial(U-\mu)}\ln Z_{U-\mu}(t), \end{aligned} \tag{I.6}$$

or

$$\frac{1}{\beta}\frac{\partial}{\partial(U-\mu)}\ln Z_{U-\mu}(t) = 2N_t - < N_e > . \tag{I.7}$$

At half-filling, i.e. $< N_e >= N_t$ (the average electron number per site is one), we will find

$$\begin{aligned} \frac{1}{\beta}\frac{\partial}{\partial(U-\mu)}\ln Z_{U-\mu}(t) &= N_t \\ &= < N_e > \\ &= \frac{1}{\beta}\frac{\partial}{\partial\mu}\ln Z_\mu(t), \end{aligned} \tag{I.8}$$

which certainly implies that $U - \mu = \mu$ or $\mu = U/2$.

Appendix J

Local Field Change Technique in MC

In the auxiliary field Monte Carlo section, we have deferred the discussion of the local field change technique to this appendix. A good reference can also be found in [35].

We assume that a change in the auxiliary Ising field element on a single lattice site i:

$$\phi_m(i) \rightarrow \phi_m(i) + \delta\phi_m(i) \tag{J.1}$$

at time slice $\tau_m = (m - 1/2)\Delta\tau$ induces a change in $V_m(i)$, which is the diagonal element of the Hamiltonian and is given by $V_m(i) = \lambda\sigma$ in our calculation, see Eq.(7.12). The local change is represented as

$$V_m(i,i) \rightarrow V_m(i) + \delta V_m(i). \tag{J.2}$$

The other elements of the V_m (and V_n, $n \neq m$ at different time slices) remain fixed. We then have a change $B_m \rightarrow B_m\Delta_m$, where the definition of B_m can be found in the previous section Eq.(7.11) and Δ_m is a diagonal matrix with

$$\begin{cases} \Delta_m(i,i) = e^{-\Delta\tau\delta V_m(i)} \equiv N_m(i) + 1, \\ \Delta_m(j,j) = 1, \text{for } j \neq i. \end{cases} \tag{J.3}$$

The ratio R, see Eq.(7.23) for definition, is

$$R = \frac{\det(I + B_{m-1} \cdots B_1 B_L \cdots B_m \Delta_m)}{\det(I + B_{m-1} \cdots B_1 B_L \cdots B_m)}, \tag{J.4}$$

where we have suppressed the spin index in B for simplicity, and we have assumed that the imaginary time has been divided into L time slices. Let

$$g_m = (I + B_{m-1} \cdots B_1 B_L \cdots B_m)^{-1}, \tag{J.5}$$

or

$$g_m^{-1} = I + B_{m-1} \cdots B_1 B_L \cdots B_m, \tag{J.6}$$

then we have

$$I + B_{m-1} \cdots B_1 B_L \cdots B_m \Delta_m = I + (g_m^{-1} - I)\Delta_m. \tag{J.7}$$

So the ratio R can be written as

$$R = \frac{\det(I + (g_m^{-1} - I)\Delta_m)}{\det g_m^{-1}}. \tag{J.8}$$

Thus

$$\begin{aligned} R &= \det(I + (g_m^{-1} - I)\Delta_m)\det g_m \\ &= \det[(I + (g_m^{-1} - I)\Delta_m) g_m] \\ &= \det[g_m (I + (g_m^{-1} - I)\Delta_m)] \\ &= \det[I + (I - g_m)(\Delta_m - I)]. \end{aligned} \tag{J.9}$$

Note that matrix $(\Delta_m - I)$ has only one non-zero element, i.e., the i^{th} diagonal element, which is $N_m(i)$. It follows that

$$R = 1 + [1 - g_m(i,i)] N_m(i). \tag{J.10}$$

So the ratio of the determinant R can be computed trivially as long as we know matrix g_m.

The next thing to consider is that suppose we accept the local field change according to the metropolis or heat bath algorithm, how can we calculate the new

green's function $\overline{g}_m$ quickly. First, we notice that if we accept the local field change $\phi_m(i) \to \phi_m(i) + \delta\phi_m(i)$, we then proceed to a new lattice site, which is still in the m^{th} time slice

$$\overline{g}_m = (I + B_{m-1} \cdots B_1 B_L \cdots B_m \Delta_m)^{-1}. \tag{J.11}$$

$\overline{g}_m$ can be calculated according to a Dyson-like equation, which is about the same as in the Gutzwiller projection.

The process goes as follows. From Eq.(J.11), we have

$$\begin{aligned} (\overline{g}_m)^{-1} &= I + B_{m-1} \cdots B_1 B_L \cdots B_m \Delta_m \\ &= I + (\overline{g}_m^{-1} - I)\Delta_m, \end{aligned} \tag{J.12}$$

or multiplying by $\overline{g}_m$ from right

$$I = \overline{g}_m + (g_m^{-1} - I)\Delta_m \overline{g}_m. \tag{J.13}$$

Then multiplying by g_m from left, we get

$$g_m = g_m \overline{g}_m + (I - g_m)\Delta_m \overline{g}_m. \tag{J.14}$$

After some collection, we find again the Dyson-like equation

$$\overline{g}_m = g_m - (I - g_m)(\Delta_m - I)\overline{g}_m. \tag{J.15}$$

This Dyson-like equation can then be solved by iteration as before

$$\begin{aligned} \overline{g}_m &= g_m - (I - g_m)[g_m - (I - g_m)(\Delta_m - I)\overline{g}_m] \\ &= \cdots \\ &= g_m - (I - g_m)(\Delta_m - I)\{I - (I - g_m)(\Delta_m - I) \\ &\quad + (I - g_m)^2(\Delta_m - I)^2 + \cdots\} g_m. \end{aligned} \tag{J.16}$$

We know that

$$\Delta_m = \begin{pmatrix} 1 & 0 & \cdots & 0 & 0 & 0 & \cdots & 0 \\ 0 & 1 & \cdots & 0 & 0 & 0 & \cdots & 0 \\ \vdots & \vdots & \vdots & \vdots & \vdots & \vdots & \vdots & \vdots \\ 0 & 0 & \cdots & 1 & 0 & 0 & \cdots & 0 \\ 0 & 0 & \cdots & 0 & N_m(i)+1 & 0 & \cdots & 0 \\ 0 & 0 & \cdots & 0 & 0 & 1 & \cdots & 0 \\ \vdots & \vdots & \vdots & \vdots & \vdots & \vdots & \vdots & \vdots \\ 0 & 0 & \cdots & 0 & 0 & 0 & \cdots & 1 \end{pmatrix}. \tag{J.17}$$

The matrix $(\Delta_m - I)$ then has only one non-zero diagonal element, i.e., the i^{th} element, and

$$(I - g_m)(\Delta_m - I) = \begin{pmatrix} 0 & \cdots & x_1 & \cdots & 0 \\ \vdots & \vdots & \vdots & \vdots & \vdots \\ 0 & \cdots & x_N & \cdots & 0 \end{pmatrix}, \tag{J.18}$$

where $x_k = (1 - g_m(k,i))N_m(i)$ for $k = 1, \cdots, N$. It is easy to show that for an arbitrary positive integer k,

$$(I - g_m)^k(\Delta_m - I)^k = (I - g_m)(\Delta_m - I)x_i^{k-1} \tag{J.19}$$

is always true. so

$$\begin{aligned} \bar{g}_m &= g_m - (I - g_m)(\Delta_m - I)\{1 - x_i + x_i^2 - x_i^3 + \cdots + (-1)^{k+1}x_i^k + \cdots\}g_m \\ &= g_m - (I - g_m)(\Delta_m - I)g_m/(1 + x_i), \end{aligned} \tag{J.20}$$

or written in matrix elements

$$\bar{g}_m = g_m(j,k) - \frac{[\delta_{ji} - g_m(j,i)]N_m(i)g_m(i,k)}{1 + [1 - g_m(i,i)]N_m(i)}. \tag{J.21}$$

After such updating is performed on every lattice site in the time slice $\tau_m = (m - \frac{1}{2})\Delta\tau$, we can go on to the next time slice by replacing the index m with $m+1$, and the green's function is

$$\begin{aligned} g_{m+1} &= (I + B_m \cdots B_1 B_L \cdots B_{m+1})^{-1} \\ &= B_m g_m B_m^{-1}. \end{aligned} \tag{J.22}$$

Appendix K

AMC Details on Tetrahedron and Cube Molecules

We will, in this appendix, introduce the details on how to perform extrapolations of tetrahedron and cube molecule energies in auxiliary field Monte Carlo calculation. We first list data in the following tables for various temperatures and on-site interaction strengths for tetrahedron and cube molecules. Then we will extract the pair-binding energy from them, and compare them with the exact diagonalization results, which are obtained through

$$< E >_T = \frac{\sum_i E_i e^{-E_i/T}}{\sum_i e^{-E_i/T}}, \tag{K.1}$$

where E_i is energy levels from exact diagonalization and we have set $K_B = 1$.

	n	$\Delta\tau$	L	μ	E
	2	0.05	10	-1.825(10)	-0.325(2)
$T = 2.0$	2	0.025	20	-1.813(15)	-0.324(2)
	2	0.0125	40	-1.819(14)	-0.325(2)
	2	0.00625	80	-1.816(21)	-0.327(2)
					-0.329(1)
	2	0.1	10	-0.974(11)	-0.612(4)
$T = 1.0$	2	0.05	20	-0.970(12)	-0.607(6)
	2	0.025	40	-0.975(13)	-0.605(6)
	2	0.0125	80	-0.971(13)	-0.605(7)
					-0.605(1)
	2	0.5	4	-0.760(3)	-0.925(1)
$T = 0.5$	2	0.25	8	-0.655(3)	-0.875(2)
	2	0.125	16	-0.621(3)	-0.848(2)
	2	0.0625	32	-0.611(4)	-0.839(2)
					-0.826(3)
	2	0.5	8	-0.613(4)	-0.966(1)
$T = 0.25$	2	0.25	16	-0.513(10)	-0.918(2)
	2	0.125	32	-0.478(12)	-0.891(3)
	2	0.0625	64	-0.468(14)	-0.885(2)
					-0.873(6)
	3	0.05	10	0.149(9)	-0.248(3)
$T = 2.0$	3	0.025	20	0.154(7)	-0.248(2)
	3	0.0125	40	0.152(10)	-0.247(3)
	3	0.00625	80	0.155(5)	-0.247(3)
					-0.246(1)
	3	0.1	10	0.619(8)	-0.502(7)
$T = 1.0$	3	0.05	20	0.626(8)	-0.499(3)
	3	0.025	40	0.624(8)	-0.497(4)
	3	0.0125	80	0.621(9)	-0.496(5)
					-0.495(1)
	3	0.5	4	1.038(11)	-0.724(2)
$T = 0.5$	3	0.25	8	1.255(2)	-0.756(2)
	3	0.125	16	1.337(4)	-0.673(3)
	3	0.0625	32	1.092(26)	-0.602(2)
					-0.518(2)
	3	0.5	8	1.254(4)	-0.757(2)
$T = 0.25$	3	0.25	16	1.336(3)	-0.672(2)
	3	0.125	32	1.354(3)	-0.636(3)
	3	0.0625	64	1.358(3)	-0.623(2)
					-0.609(2)
	4	0.1	5	2.097(1)	0.013(1)
$T = 2.0$	4	0.05	10	2.097(1)	0.018(2)
	4	0.025	20	2.096(1)	0.018(1)
	4	0.0125	40	2.096(1)	0.022(2)
					0.023(3)

	n	$\Delta\tau$	L	μ	E
	4	0.5	2	2.306(3)	-0.327(2)
$T = 1.0$	4	0.25	4	2.256(2)	-0.237(3)
	4	0.125	8	2.237(2)	-0.207(1)
	4	0.0625	16	2.233(4)	-0.199(2)
					-0.191(2)
	4	0.5	4	2.462(11)	-0.444(6)
$T = 0.5$	4	0.25	8	2.372(6)	-0.335(4)
	4	0.125	16	2.346(8)	-0.294(4)
	4	0.0625	32	2.405(10)	-0.302(8)
					-0.296(18)
	4	0.5	8	2.518(19)	-0.526(5)
$T = 0.25$	4	0.25	16	2.436(5)	-0.400(2)
	4	0.125	32	2.404(8)	-0.353(4)
	4	0.0625	64	2.389(5)	-0.340(3)
					-0.325(5)
	5	0.05	10	4.011(5)	0.499(1)
$T = 2.0$	5	0.025	20	4.012(9)	0.498(2)
	5	0.0125	40	4.013(9)	0.499(2)
	5	0.00625	80	4.012(8)	0.499(3)
					0.500(1)
	5	0.1	10	3.868(9)	0.336(1)
$T = 1.0$	5	0.05	20	3.860(7)	0.336(3)
	5	0.025	40	3.860(10)	0.338(3)
	5	0.0125	80	3.862(10)	0.338(2)
					0.339(1)
	5	0.5	4	4.074(2)	0.220(1)
$T = 0.5$	5	0.25	8	3.959(2)	0.241(1)
	5	0.125	16	3.922(4)	0.248(1)
	5	0.0625	32	3.914(1)	0.250(1)
					0.252(1)
	5	0.4	10	4.110(5)	0.189(3)
$T = 0.25$	5	0.25	16	4.018(3)	0.193(3)
	5	0.2	20	3.991(14)	0.192(3)
	5	0.125	32	3.969(4)	0.192(2)
	5	0.0625	64	3.957(3)	0.193(5)
					0.192(1)
	6	0.05	10	5.872(16)	1.143(1)
$T = 2.0$	6	0.025	20	5.871(10)	1.142(1)
	6	0.0125	40	5.875(17)	1.142(2)
	6	0.00625	80	5.871(20)	1.142(2)
					1.142(1)
	6	0.1	10	5.156(10)	1.053(4)
$T = 1.0$	6	0.05	20	5.152(14)	1.055(3)
	6	0.025	40	5.157(9)	1.053(2)
	6	0.0125	80	5.158(11)	1.054(3)
					1.053(1)

Continued	n	$\Delta\tau$	L	μ	E
	6	0.5	4	4.985(2)	1.011(2)
$T = 0.5$	6	0.25	8	4.964(2)	1.014(1)
	6	0.125	16	4.956(4)	1.016(2)
	6	0.0625	32	4.956(3)	1.015(2)
					1.016(2)
	6	0.5	8	4.956(2)	1.056(101)
$T = 0.25$	6	0.25	16	4.939(2)	0.998(5)
	6	0.2	20	4.937(8)	0.996(6)
	6	0.125	32	4.928(2)	0.995(7)
	6	0.0625	64	4.919(6)	0.984(40)
					0.998(8)

Table K.1: Data for extrapolation of ground state energy in a tetrahedron molecule for different number of filled electrons n. These data are obtained by setting the on-site Coulomb interaction $U = 4t$. The last column is energy per bond and is in units of t; the extrapolated energy at $\Delta\tau = 0$ limit is also shown immediately following the energy data for each $\Delta\tau$'s. The units of T are t, too. Numbers in brackets are errors of the last digits.

	n	$\Delta\tau$	L	μ	E
	2	0.5	2	-1.411(3)	-0.702(2)
$T = 1.0$	2	0.25	4	-1.403(4)	-0.694(3)
	2	0.125	8	-1.401(4)	-0.694(2)
	2	0.0625	16	-1.401(4)	-0.691(2)
					-0.691(3)
	2	0.5	4	-1.118(3)	-0.933(1)
$T = 0.5$	2	0.25	8	-1.256(6)	-0.916(2)
	2	0.125	16	-1.168(8)	-0.921(2)
	2	0.0625	32	-1.093(5)	-0.921(4)
					-0.927(4)
	2	0.5	8	-1.019(4)	-0.974(3)
$T = 0.25$	2	0.25	16	-1.177(6)	-0.960(2)
	2	0.125	32	-1.035(8)	-0.961(2)
	2	0.0625	64	-0.955(6)	-0.958(4)
					-0.960(4)

Continued	n	$\Delta\tau$	L	μ	E
	2	0.5	10	-1.008(5)	-0.973(1)
$T = 0.20$	2	0.25	20	-0.885(5)	-0.964(2)
	2	0.125	40	-0.882(4)	-0.963(3)
	2	0.0625	80	-0.926(4)	-0.961(4)
					-0.961(2)
	3	0.5	2	-0.096(3)	-0.664(2)
$T = 1.0$	3	0.25	4	-0.094(4)	-0.658(2)
	3	0.125	8	-0.095(2)	-0.655(2)
	3	0.0625	16	-0.095(3)	-0.654(2)
					-0.653(1)
	3	0.5	4	0.533(2)	-0.763(1)
$T = 0.5$	3	0.25	8	0.434(3)	-0.754(2)
	3	0.125	16	0.504(3)	-0.750(2)
	3	0.0625	32	0.520(5)	-0.749(2)
					-0.748(1)
	3	0.5	8	0.918(5)	-0.767(2)
$T = 0.25$	3	0.25	16	0.820(6)	-0.759(2)
	3	0.125	32	0.890(5)	-0.755(2)
	3	0.0625	64	0.900(3)	-0.756(3)
					-0.755(2)
	3	0.5	10	0.995(8)	-0.768(3)
$T = 0.20$	3	0.25	20	0.895(5)	-0.758(4)
	3	0.125	40	0.960(3)	-0.757(2)
	3	0.0625	80	0.972(1)	-0.755(2)
					-0.755(2)
	4	0.5	2	0.852(2)	-0.481(1)
$T = 1.0$	4	0.25	4	0.849(1)	-0.475(1)
	4	0.125	8	0.848(1)	-0.473(1)
	4	0.0625	16	0.848(1)	-0.472(1)
					-0.471(1)
	4	0.5	4	1.147(1)	-0.534(1)
$T = 0.5$	4	0.25	8	1.117(1)	-0.531(1)
	4	0.125	16	1.130(2)	-0.526(2)
	4	0.0625	32	1.128(1)	-0.525(2)
					-0.522(2)
	4	0.5	8	1.313(2)	-0.546(1)
$T = 0.25$	4	0.25	16	1.271(4)	-0.542(4)
	4	0.125	32	1.271(1)	-0.538(2)
	4	0.0625	64	1.265(3)	-0.538(1)
					-0.536(1)
	4	0.5	10	1.344(6)	-0.549(9)
$T = 0.20$	4	0.25	20	1.296(5)	-0.546(10)
	4	0.125	40	1.291(3)	-0.542(3)
	4	0.0625	80	1.283(2)	-0.543(3)
					-0.541(2)

Continued	n	$\Delta\tau$	L	μ	E
	5	0.5	2	1.670(1)	-0.241(1)
$T = 1.0$	5	0.25	4	1.665(1)	-0.236(1)
	5	0.125	8	1.663(1)	-0.235(1)
	5	0.0625	16	1.664(1)	-0.235(2)
					-0.235(1)
	5	0.5	4	1.658(1)	-0.274(1)
$T = 0.5$	5	0.25	8	1.681(1)	-0.273(1)
	5	0.125	16	1.656(1)	-0.270(1)
	5	0.0625	32	1.646(1)	-0.269(1)
					-0.267(1)
	5	0.5	8	1.661(6)	-0.289(1)
$T = 0.25$	5	0.25	16	1.684(1)	-0.291(3)
	5	0.125	32	1.658(1)	-0.290(2)
	5	0.0625	64	1.649(1)	-0.289(1)
					-0.288(1)
	5	0.5	10	1.663(2)	-0.300(10)
$T = 0.20$	5	0.25	20	1.684(4)	-0.298(1)
	5	0.125	40	1.659(1)	-0.298(1)
	5	0.0625	80	1.651(2)	-0.297(2)
					-0.297(1)
	6	0.5	2	2.492(2)	0.039(1)
$T = 1.0$	6	0.25	4	2.488(3)	0.041(1)
	6	0.125	8	2.488(3)	0.042(1)
	6	0.0625	16	2.489(4)	0.042(1)
					0.042(1)
	6	0.5	4	2.170(2)	0.020(2)
$T = 0.5$	6	0.25	8	2.204(3)	0.020(2)
	6	0.125	16	2.167(4)	0.022(1)
	6	0.1	20	2.147(2)	0.021(1)
	6	0.0625	32	2.152(4)	0.022(1)
					0.023(1)
	6	0.5	8	2.012(2)	0.010(1)
$T = 0.25$	6	0.25	16	2.049(2)	0.010(2)
	6	0.125	32	2.022(2)	0.011(2)
	6	0.0625	64	2.013(2)	0.010(1)
					0.010(1)
	6	0.5	10	1.978(2)	0.008(2)
$T = 0.20$	6	0.25	20	2.023(8)	0.006(2)
	6	0.125	40	2.002(3)	0.008(2)
	6	0.0625	80	1.994(2)	0.008(2)
					0.010(1)

Table K.2: Continued data table for a tetrahedron molecule. Now the parameter $U = 1t$.

	n	$\Delta\tau$	L	μ	E
	6	0.1	5	0.064(2)	-0.214(1)
$T = 2.0$	6	0.05	10	0.068(2)	-0.210(1)
	6	0.025	20	0.067(1)	-0.209(1)
	6	0.0125	40	0.067(3)	-0.210(1)
					-0.210(1)
	6	0.25	4	0.311(2)	-0.456(1)
$T = 1.0$	6	0.125	8	0.332(1)	-0.430(1)
	6	0.0625	16	0.337(2)	-0.424(1)
	6	0.03125	32	0.341(2)	-0.422(1)
					-0.422(1)
	6	0.5	4	0.276(2)	-0.664(1)
$T = 0.5$	6	0.25	8	0.388(2)	-0.585(1)
	6	0.125	16	0.423(1)	-0.555(1)
	6	0.0625	32	0.430(1)	-0.547(1)
					-0.538(3)
	6	0.5	8	0.244(3)	-0.719(1)
$T = 0.25$	6	0.25	16	0.390(1)	-0.640(1)
	6	0.125	32	0.434(2)	-0.609(2)
	6	0.0625	64	0.445(3)	-0.600(1)
					-0.590(3)
	7	0.1	5	1.024(1)	-0.128(1)
$T = 2.0$	7	0.05	10	1.026(1)	-0.124(1)
	7	0.025	20	1.027(1)	-0.123(1)
	7	0.0125	40	1.026(1)	-0.123(1)
					-0.123(1)
	7	0.25	4	1.102(1)	-0.395(1)
$T = 1.0$	7	0.125	8	1.118(1)	-0.364(1)
	7	0.0625	16	1.123(1)	-0.355(1)
	7	0.03125	32	1.124(1)	-0.353(1)
					-0.352(1)
	7	0.5	4	0.943(2)	-0.644(1)
$T = 0.5$	7	0.25	8	1.049(2)	-0.535(2)
	7	0.125	16	1.081(1)	-0.496(1)
	7	0.0625	32	1.087(2)	-0.486(1)
					-0.475(4)
	7	0.5	8	0.772(2)	-0.716(1)
$T = 0.25$	7	0.25	16	0.912(1)	-0.604(1)
	7	0.125	32	0.952(1)	-0.563(1)
	7	0.0625	64	0.960(2)	-0.550(2)
					-0.537(3)
	8	0.1	5	2.000(0)	0.010(1)
$T = 2.0$	8	0.05	10	2.000(0)	0.014(1)
	8	0.025	20	2.000(0)	0.015(1)
	8	0.0125	40	2.000(0)	0.015(1)
					0.015(1)

Continued	n	$\Delta\tau$	L	μ	E
	8	0.5	2	2.000(0)	-0.372(1)
$T = 1.0$	8	0.25	4	2.000(0)	-0.270(1)
	8	0.125	8	2.000(0)	-0.236(1)
	8	0.0625	16	2.000(0)	-0.227(1)
	8	0.03125	32	2.000(0)	-0.223(1)
					-0.219(3)
	8	0.5	4	2.000(0)	-0.654(1)
$T = 0.5$	8	0.25	8	2.000(0)	-0.431(1)
	8	0.125	16	2.000(0)	-0.387(2)
	8	0.0625	32	2.000(0)	-0.374(1)
					-0.378(2)
	8	0.5	8	2.000(0)	-0.686(2)
$T = 0.25$	8	0.25	16	2.000(0)	-0.543(2)
	8	0.125	32	2.000(0)	-0.492(2)
	8	0.0625	64	2.000(0)	-0.478(2)
					-0.463(4)
	9	0.1	5	2.976(1)	0.205(1)
T=2.0	9	0.05	10	2.974(1)	0.209(1)
	9	0.025	20	2.975(1)	0.210(1)
	9	0.0125	40	2.974(1)	0.211(1)
					0.211(1)
	9	0.25	4	2.898(1)	-0.062(1)
T=1.0	9	0.125	8	2.882(2)	-0.031(1)
	9	0.0625	16	2.878(1)	-0.022(1)
	9	0.03125	32	2.877(1)	-0.020(1)
					-0.019(1)
	9	0.5	4	3.057(2)	-0.311(1)
T=0.5	9	0.25	8	2.950(1)	-0.202(1)
	9	0.125	16	2.921(2)	-0.164(1)
	9	0.0625	32	2.914(1)	-0.154(2)
					-0.144(4)
	9	0.5	8	3.227(2)	-0.384(2)
T=0.25	9	0.25	16	3.088(3)	-0.269(2)
	9	0.125	32	3.048(2)	-0.230(2)
	9	0.0625	64	3.039(1)	-0.218(2)
					-0.207(2)
	10	0.1	5	3.934(1)	0.453(1)
T=2.0	10	0.05	10	3.932(2)	0.456(1)
	10	0.025	20	3.933(2)	0.457(1)
	10	0.0125	40	3.932(1)	0.457(1)
					0.457(1)
	10	0.25	4	3.690(2)	0.211(1)
T=1.0	10	0.125	8	3.667(2)	0.235(1)
	10	0.0625	16	3.660(2)	0.243(1)
	10	0.03125	32	3.659(1)	0.245(1)
					0.247(1)

Continued	n	$\Delta\tau$	L	μ	E
	10	0.5	4	3.725(1)	0.003(1)
T=0.5	10	0.25	8	3.611(1)	0.082(1)
	10	0.125	16	3.580(1)	0.111(1)
	10	0.0625	32	3.570(1)	0.119(1)
					0.128(3)
	10	0.5	8	3.757(2)	-0.052(2)
T=0.25	10	0.25	16	3.608(2)	0.026(1)
	10	0.125	32	3.567(1)	0.057(2)
	10	0.0625	64	3.556(1)	0.064(3)
					0.074(5)

Table K.3: Continued data table for a cube molecule. The parameter $U = 4t$.

Extrapolations of the data in Table K.1, K.2 and K.3 are shown in Fig. K.1, K.2 and K.3 below:

And with the above extrapolation data, the energy of the system in different dopings can be shown in Fig. K.4, K.5, K.6, K.7. and K.8.

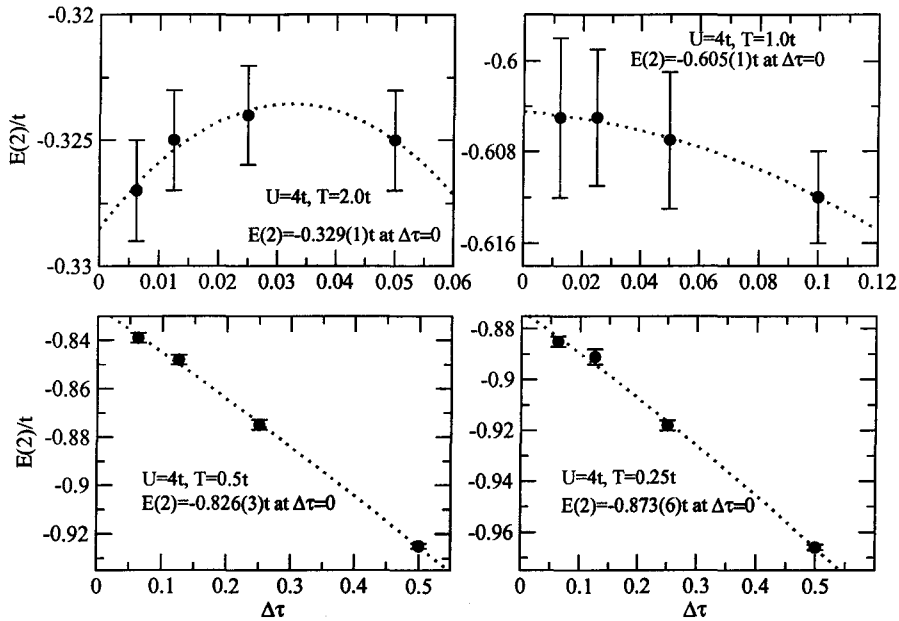
E(2)/t
U=4t, T=2.0t
E(2)=-0.329(1)t at Δτ=0
U=4t, T=1.0t
E(2)=-0.605(1)t at Δτ=0
U=4t, T=0.5t
E(2)=-0.826(3)t at Δτ=0
U=4t, T=0.25t
E(2)=-0.873(6)t at Δτ=0
Δτ

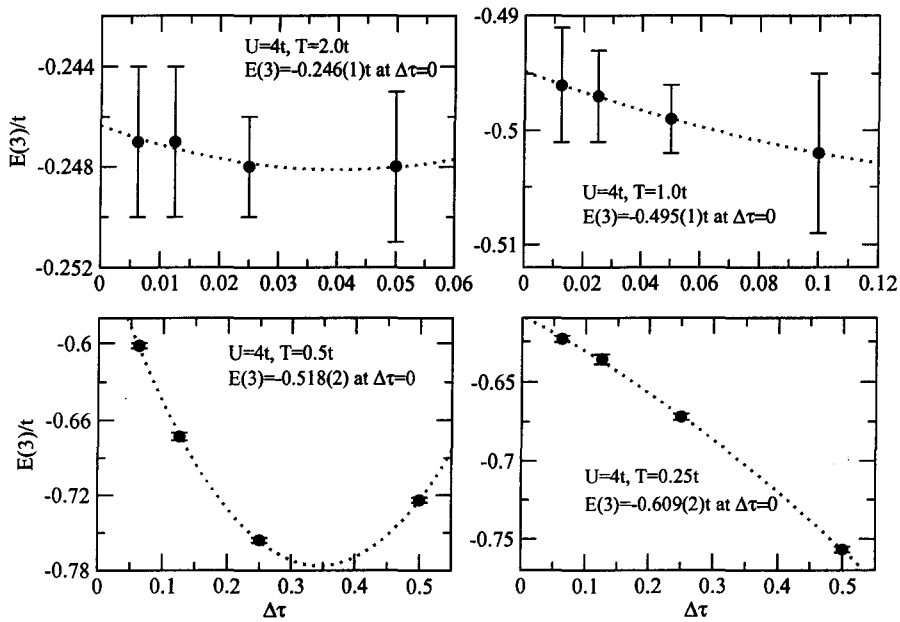
E(3)/t
U=4t, T=2.0t
E(3)=-0.246(1)t at Δτ=0
U=4t, T=1.0t
E(3)=-0.495(1)t at Δτ=0
U=4t, T=0.5t
E(3)=-0.518(2) at Δτ=0
U=4t, T=0.25t
E(3)=-0.609(2)t at Δτ=0
Δτ

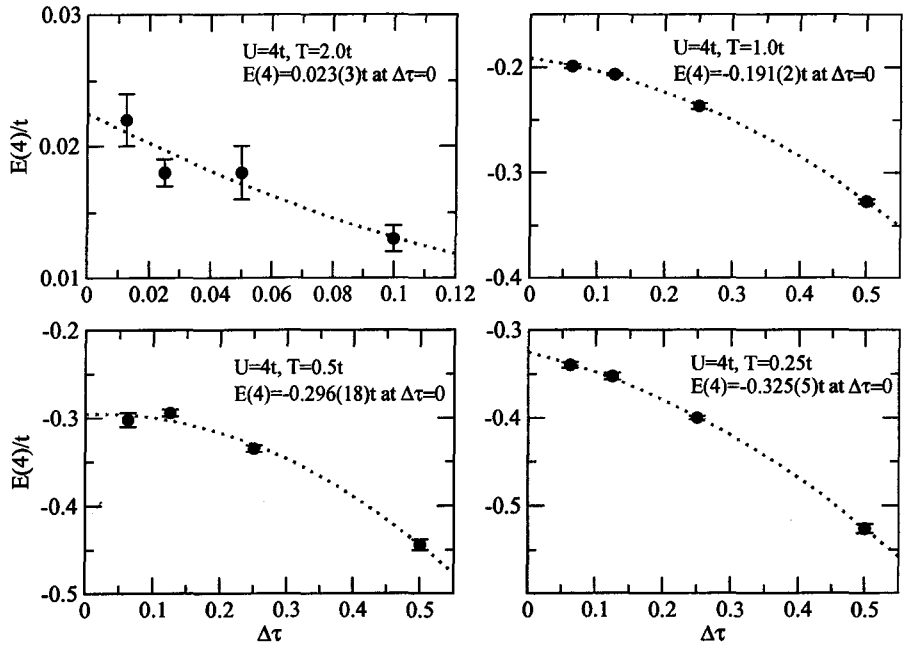
U=4t, T=2.0t
E(4)=0.023(3)t at Δτ=0
U=4t, T=1.0t
E(4)=-0.191(2)t at Δτ=0
U=4t, T=0.5t
E(4)=-0.296(18)t at Δτ=0
U=4t, T=0.25t
E(4)=-0.325(5)t at Δτ=0
E(4)/t
Δτ

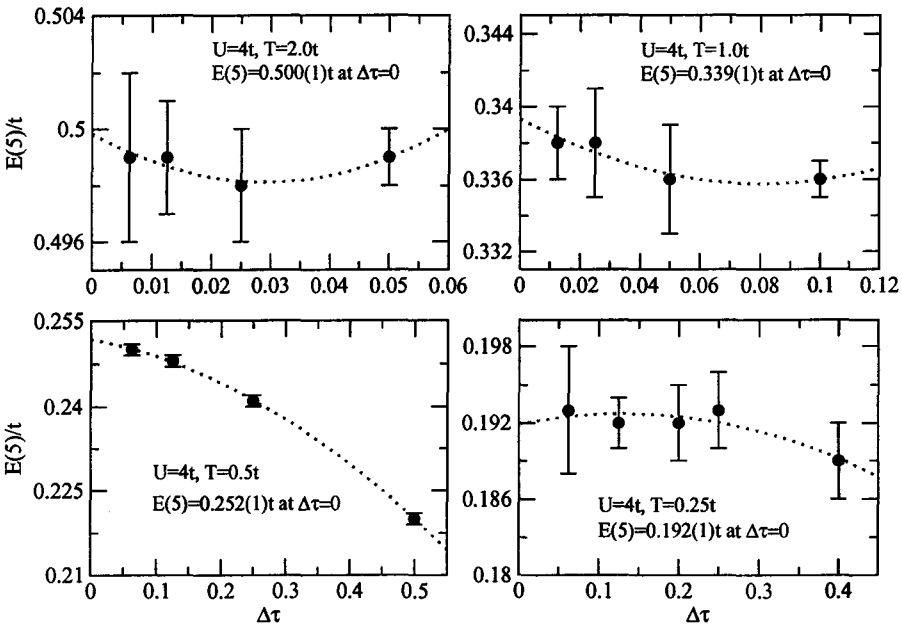
U=4t, T=2.0t
E(5)=0.500(1)t at Δτ=0
U=4t, T=1.0t
E(5)=0.339(1)t at Δτ=0
U=4t, T=0.5t
E(5)=0.252(1)t at Δτ=0
U=4t, T=0.25t
E(5)=0.192(1)t at Δτ=0
E(5)/t
Δτ

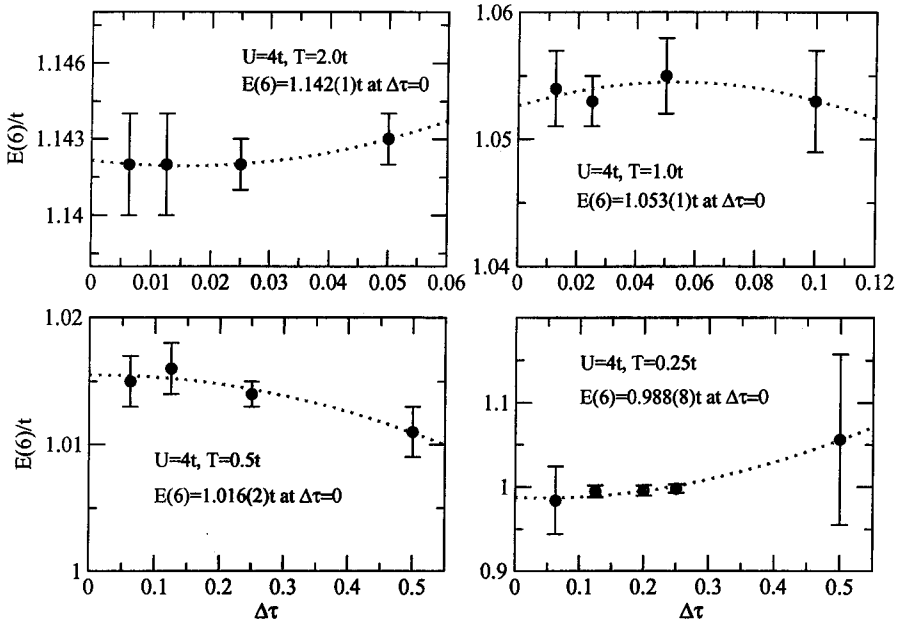

Figure K.1: Extrapolation of energy per bond with $\Delta\tau$ at different temperatures and electron fillings for $U = 4t$ in a tetrahedron molecule.

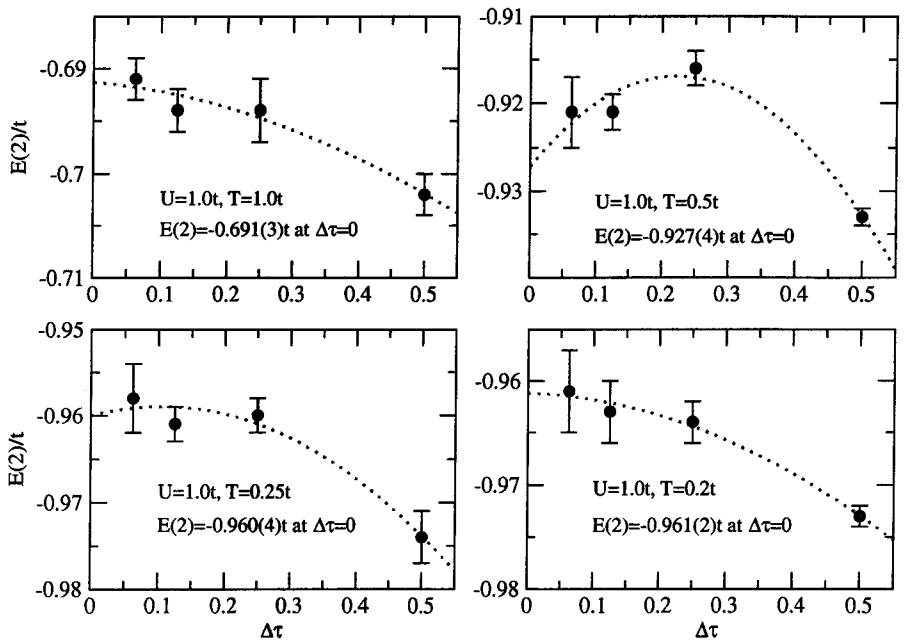

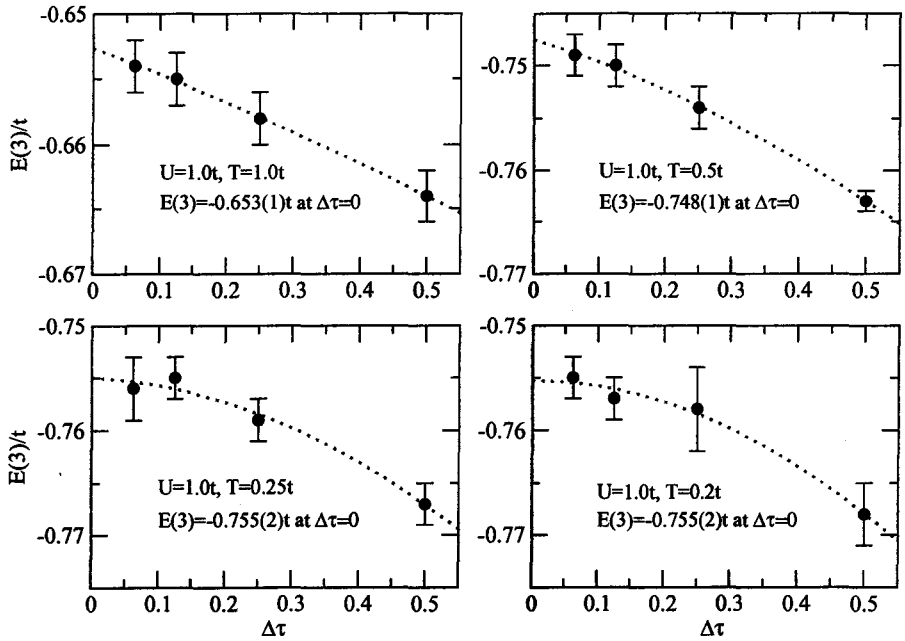
E(3)/t
U=1.0t, T=1.0t
E(3)=-0.653(1)t at Δτ=0
U=1.0t, T=0.5t
E(3)=-0.748(1)t at Δτ=0
U=1.0t, T=0.25t
E(3)=-0.755(2)t at Δτ=0
U=1.0t, T=0.2t
E(3)=-0.755(2)t at Δτ=0
Δτ

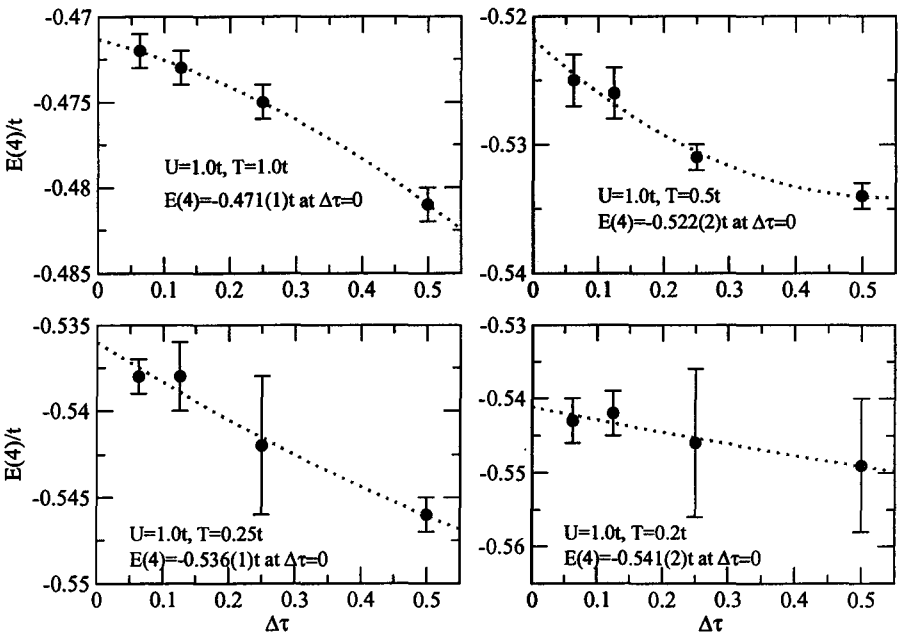
E(4)/t
U=1.0t, T=1.0t
E(4)=-0.471(1)t at Δτ=0
U=1.0t, T=0.5t
E(4)=-0.522(2)t at Δτ=0
U=1.0t, T=0.25t
E(4)=-0.536(1)t at Δτ=0
U=1.0t, T=0.2t
E(4)=-0.541(2)t at Δτ=0
Δτ

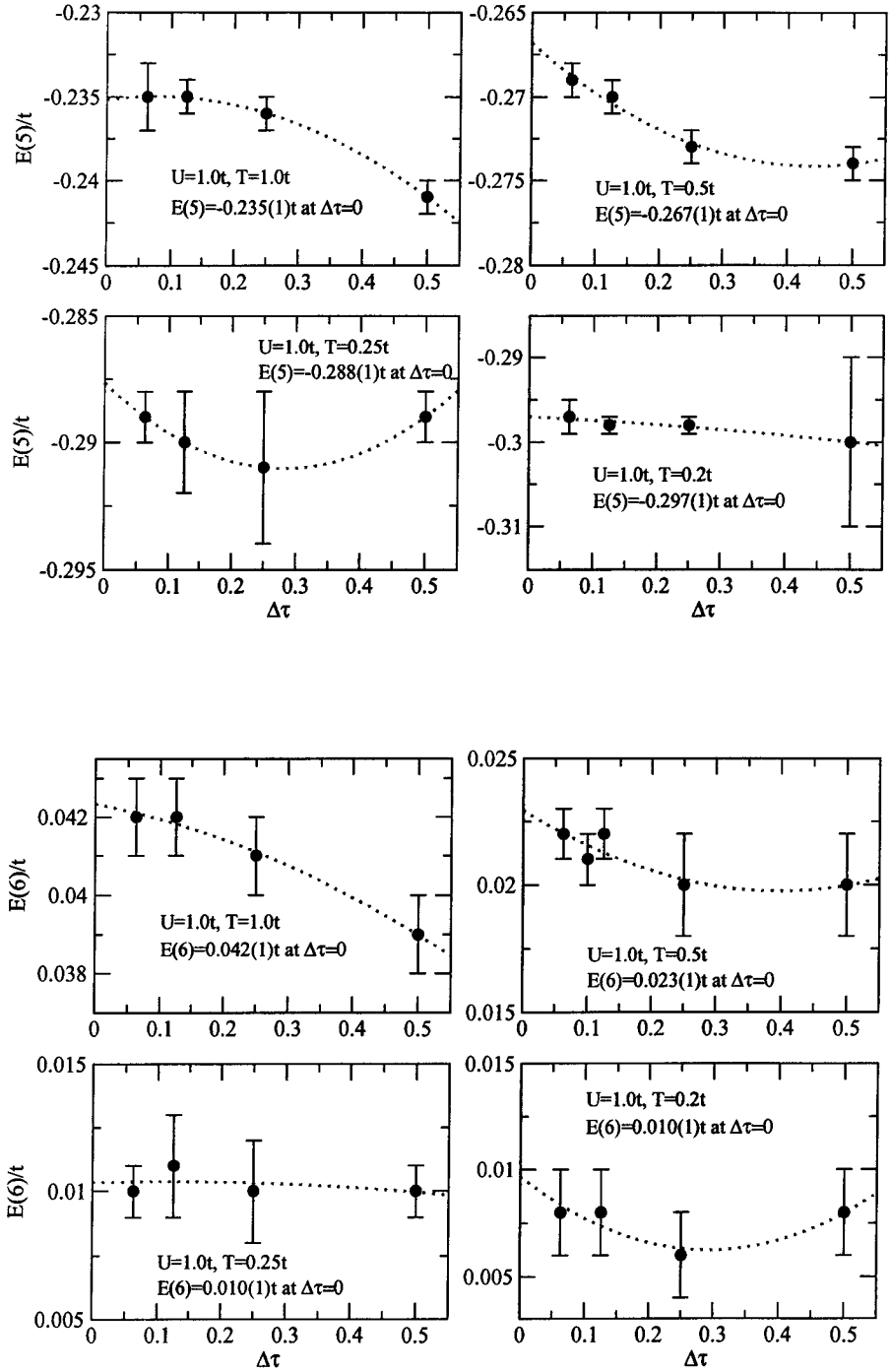

Figure K.2: Extrapolation of energy per bond with $\Delta\tau$ at different temperatures and electron fillings for $U = 1t$ in a tetrahedron molecule.

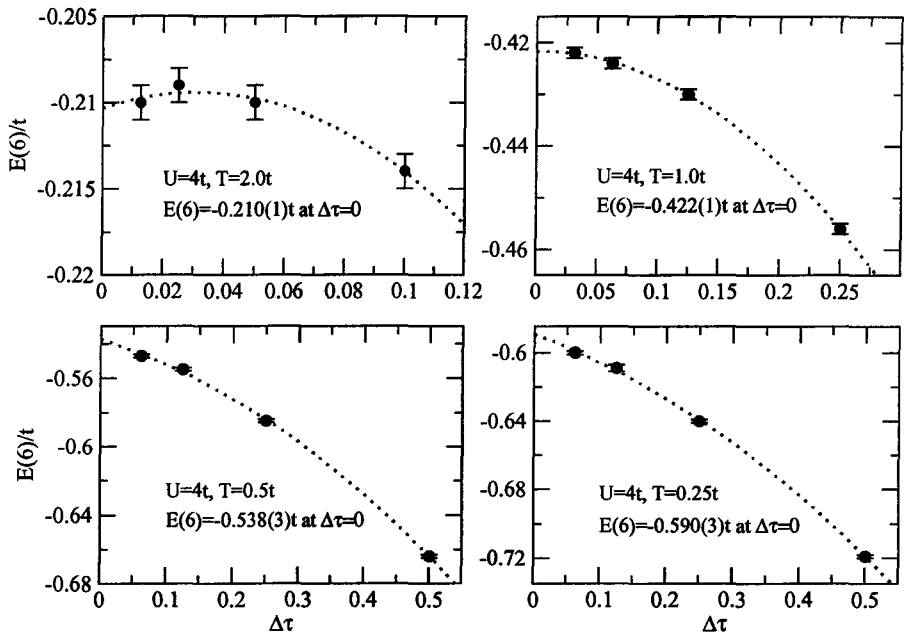
E(6)/t
U=4t, T=2.0t
E(6)=-0.210(1)t at Δτ=0
U=4t, T=1.0t
E(6)=-0.422(1)t at Δτ=0
U=4t, T=0.5t
E(6)=-0.538(3)t at Δτ=0
U=4t, T=0.25t
E(6)=-0.590(3)t at Δτ=0
Δτ

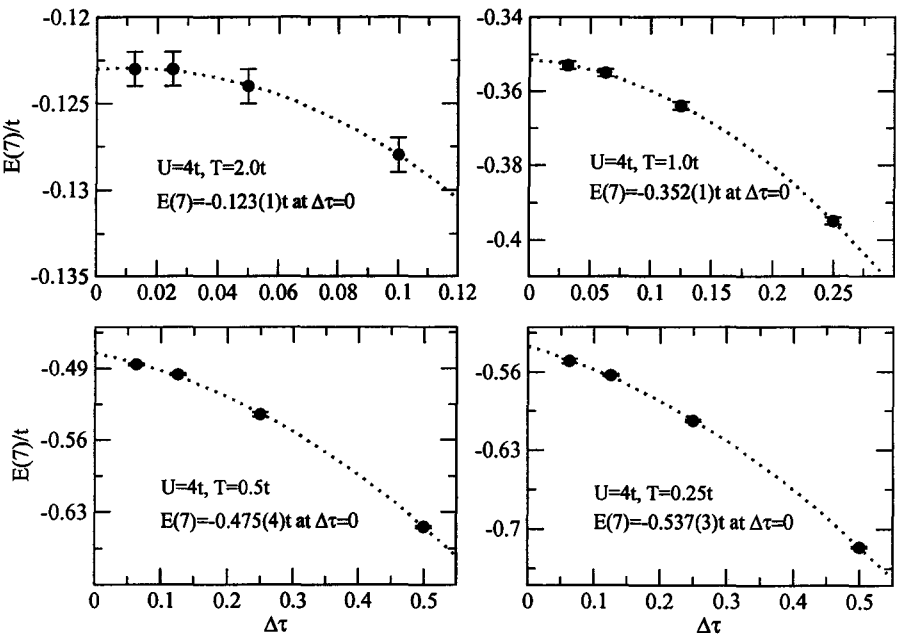
E(7)/t
U=4t, T=2.0t
E(7)=-0.123(1)t at Δτ=0
U=4t, T=1.0t
E(7)=-0.352(1)t at Δτ=0
U=4t, T=0.5t
E(7)=-0.475(4)t at Δτ=0
U=4t, T=0.25t
E(7)=-0.537(3)t at Δτ=0
Δτ

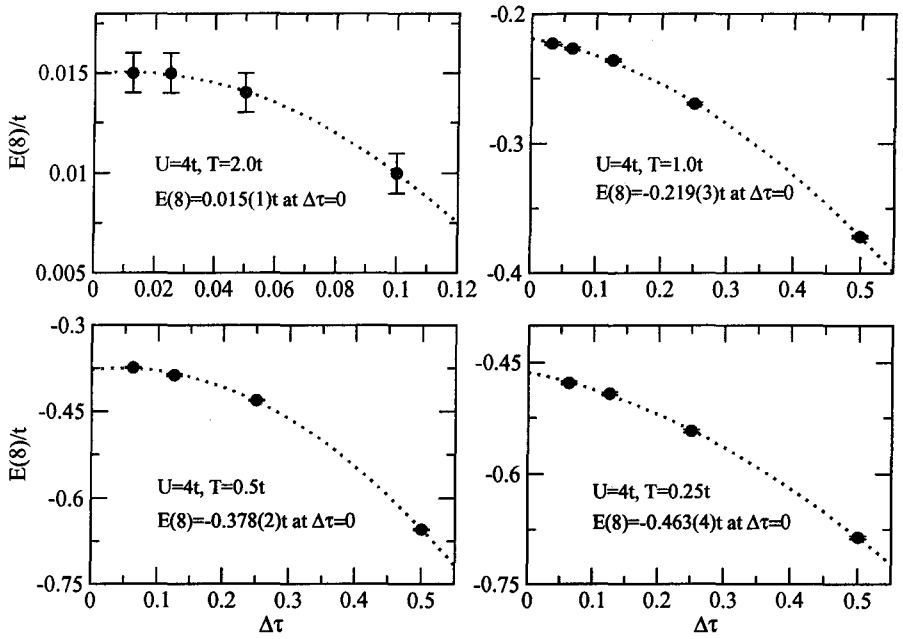
E(8)/t
U=4t, T=2.0t
E(8)=0.015(1)t at Δτ=0
U=4t, T=1.0t
E(8)=-0.219(3)t at Δτ=0
U=4t, T=0.5t
E(8)=-0.378(2)t at Δτ=0
U=4t, T=0.25t
E(8)=-0.463(4)t at Δτ=0
Δτ

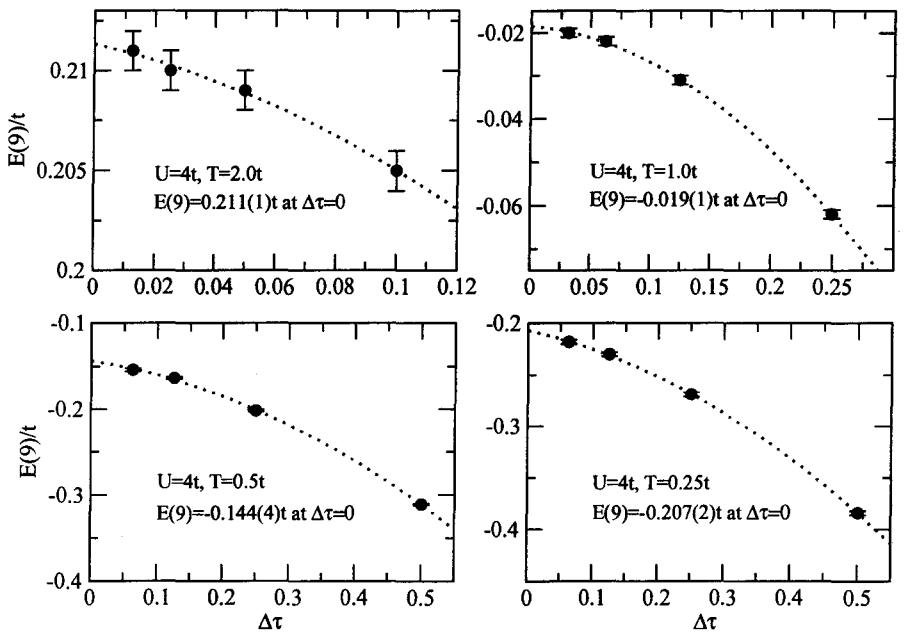
E(9)/t
U=4t, T=2.0t
E(9)=0.211(1)t at Δτ=0
U=4t, T=1.0t
E(9)=-0.019(1)t at Δτ=0
U=4t, T=0.5t
E(9)=-0.144(4)t at Δτ=0
U=4t, T=0.25t
E(9)=-0.207(2)t at Δτ=0
Δτ

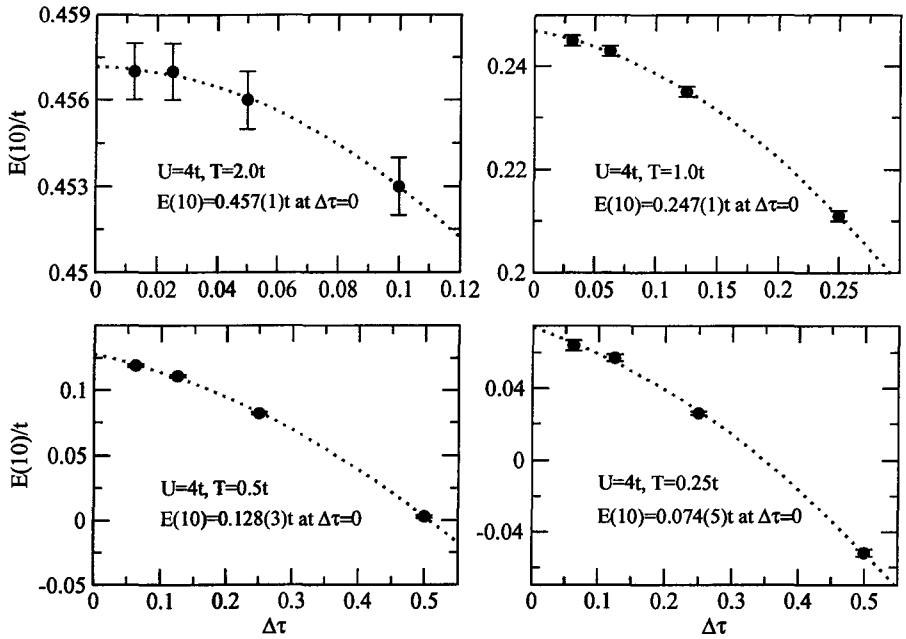

Figure K.3: Extrapolation of energy per bond with $\Delta\tau$ at different temperatures and electron fillings for $U = 4t$ in a cube molecule.

In Fig. K.9, K.10 and K.11, we extract the pair binding energy figures from Fig. K.4, K.6 and K.7, respectively for different temperatures (we have omitted the error bars for a clarity of the figures).

From Fig. K.4-K.11, we see the scatter points from auxiliary field Monte Carlo calculation are close to the exact diagonalization lines. The difference between them shows a systematic deviation, as seen in Fig. K.4-K.8. When the temperature goes down, the Monte Carlo data and exact diagonalization data becomes closer and closer, which means the correct tendency of Monte Calro data.

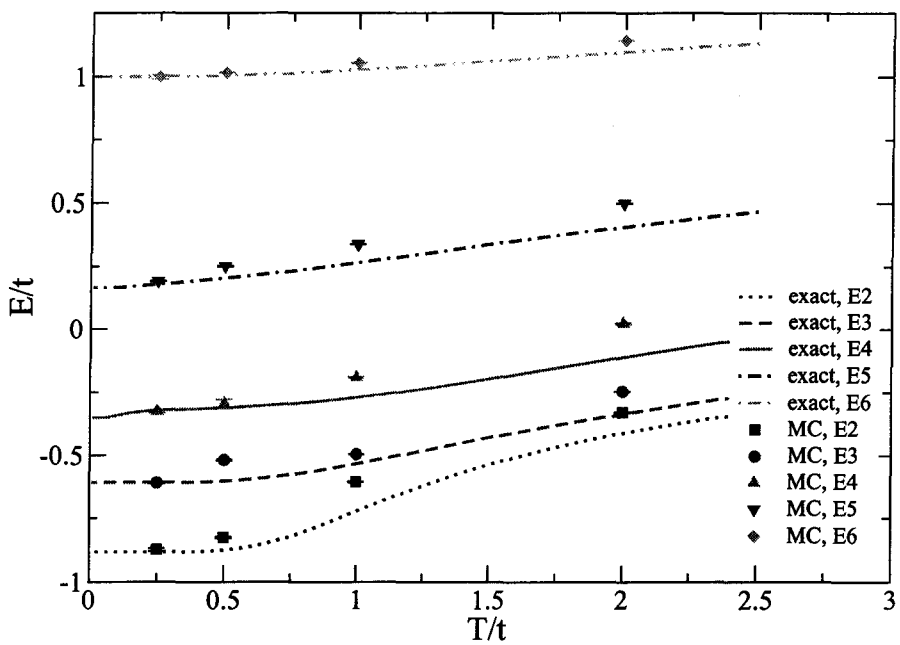

Figure K.4: Extrapolation of ground state energy per bond with temperature in a tetrahedron molecule for $U = 4t$. Scatter points are from auxiliary field Monte Carlo calculation and the lines are from exact diagonalization. We show in Fig. K.5 more details of the exact diagonalization result for half filling at low temperatures.

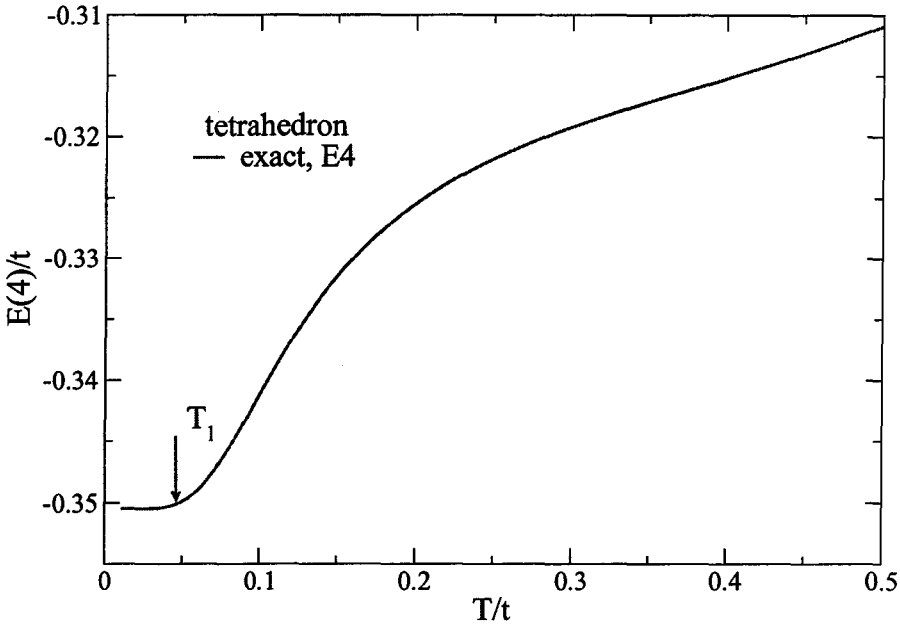

Figure K.5: Details of the exact diagonalization result for half filling at low temperatures. Note the onset of energy gap at T_1.

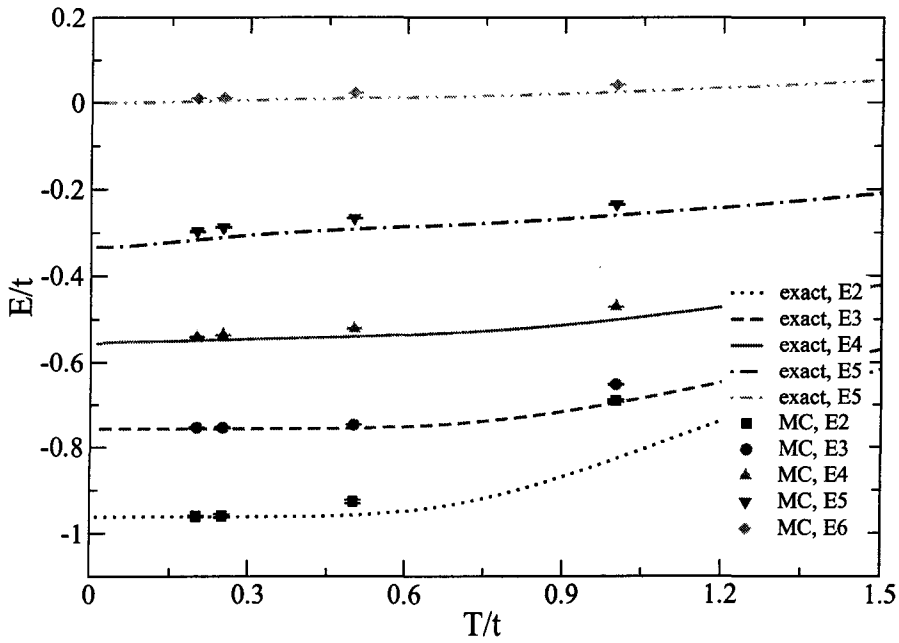

Figure K.6: Extrapolation of ground state energy per bond with temperature in a tetrahedron molecule for $U = 1t$. Scatter points are from auxiliary field Monte Carlo calculation and the lines are from exact diagonalization.

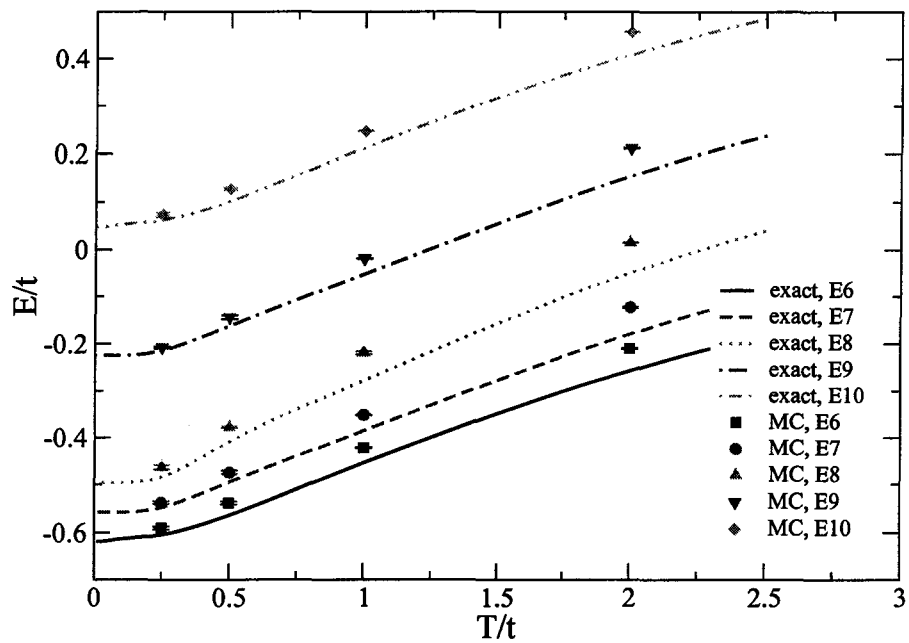

Figure K.7: Extrapolation of ground state energy per bond with temperature in a cube molecule for $U = 4t$. Scatter points are from auxiliary field Monte Carlo calculation and the lines are from exact diagonalization. We show in Fig. K.8 more details of the exact diagonalization result for cube doped with 2 holes at low temperatures.

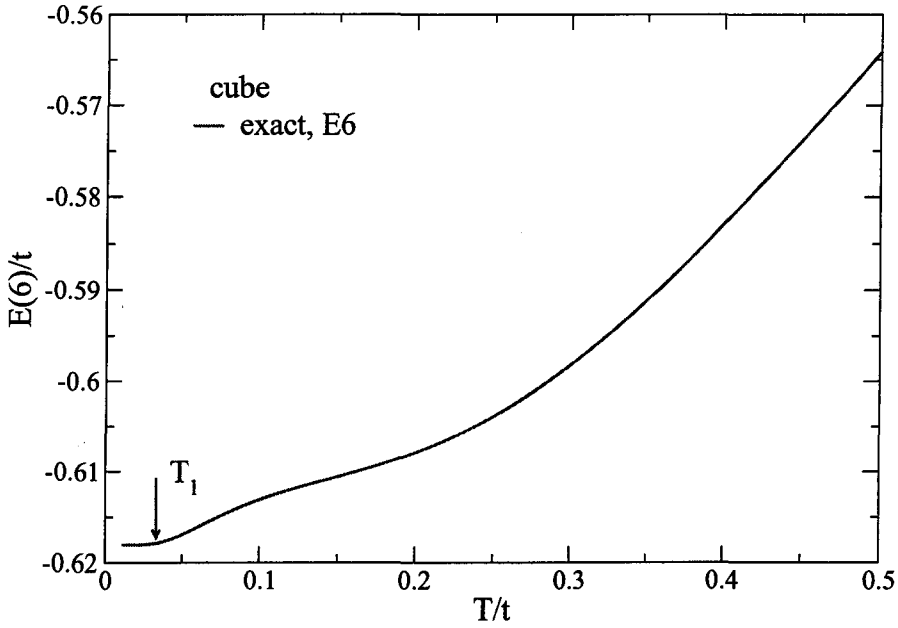

Figure K.8: Details of the exact diagonalization result for half filling at low temperatures. Note the onset of energy gap at T_1.

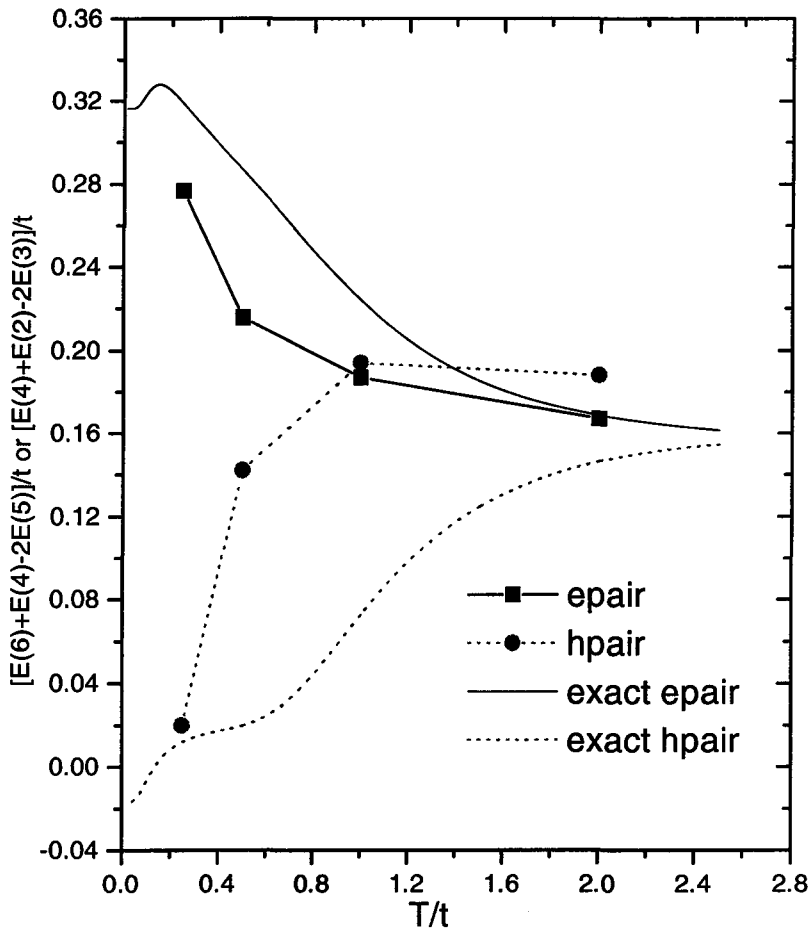

Figure K.9: Pair-binding energy for a tetrahedron molecule at different temperatures. Parameter $U = 4t$. Scatter points are from auxiliary field Monte Carlo calculation and the lines are from exact diagonalization.

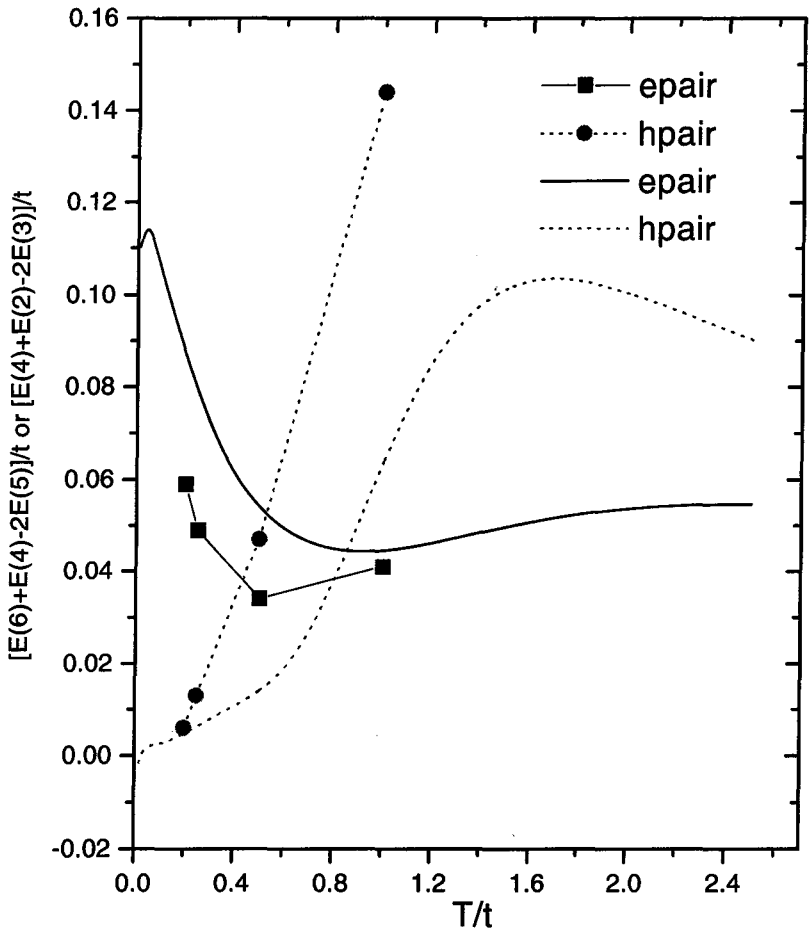

Figure K.10: Pair-binding energy for a tetrahedron molecule at different temperatures. Parameter $U = 1t$. Scatter points are from auxiliary field Monte Carlo calculation and the lines are from exact diagonalization.

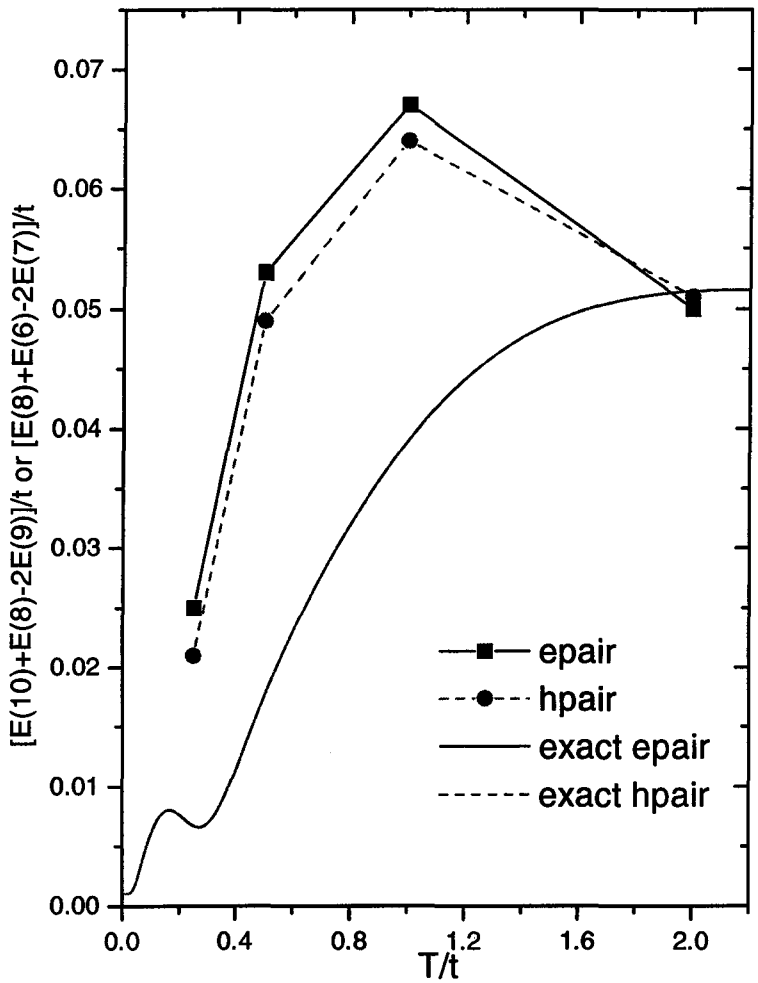

Figure K.11: Pair-binding energy for a cube molecule at different temperatures. Parameter $U = 4t$. Scatter points are from auxiliary field Monte Carlo calculation and the lines are from exact diagonalization.

Appendix L

Details on Hydrogen Calculation

In previous chapters, we have discussed the results on a hydrogen molecule from exact diagonalization, perturbation and Gutzwiller projection calculations. In this appendix, we will list the details on exact diagonalization and perturbation calculation which can be done analytically. This will also serve as an introduction on how to do perturbation on bigger and more complicated molecules, which certainly can not be done analytically but by computer techniques. Our exact diagonalization will include two models. One is the Hubbard model in Eq.(3.1), and the other is the $t-J$ model in Eq.(6.9).

L.1 Calculations on Hubbard Model

L.1.1 Exact Calculation in Half Filling

The Hamiltonian we are considering is still the Hubbard model in Eq.(3.1). We know that each site can have different occupations $(\uparrow\downarrow, \uparrow, \downarrow, 0)$, denoted as $(2, 1, -1, 0)$ respectively. Our basis wavefunctions can be divided into 3 different total spin sectors according to the symmetry of the Hubbard model: $S_z = 0$, $S_z = \hbar$ and $S_z = -\hbar$.

For $S_z = \hbar$, we have only one wavefunction:

$$\Psi_1 = (1, 1), \tag{L.1}$$

where the first number in the right hand side bracket denotes the occupation information in the first hydrogen atom, and the second number in the bracket denotes that of the second hydrogen atom. The expectation value of Hubbard Hamiltonian $\hat{H}$ is easily calculated and the result is simply

$$\epsilon_1 =< \Psi_1|\hat{H}|\Psi_1 >= 0. \tag{L.2}$$

For $S_z = -\hbar$, the calculation is basically the same

$$\Psi_{-1} = (-1,-1) \tag{L.3}$$

$$< \Psi_{-1}|\hat{H}|\Psi_{-1} > = 0, \tag{L.4}$$

or $\epsilon_2 = 0$.

The most interesting part comes from the $S_z = 0$ sector, where there are 4 basis wavefunctions:

$$\begin{cases} \phi_1 = (2,0) \\ \phi_2 = (1,-1) \\ \phi_3 = (-1,1) \\ \phi_4 = (0,2). \end{cases} \tag{L.5}$$

In units of t, we can write , according to the rules discussed in the exact diagonalization chapter, the matrix representation of $\hat{H}$

$$\hat{H} = \begin{pmatrix} \frac{U}{t} & -1 & 1 & 0 \\ -1 & 0 & 0 & -1 \\ 1 & 0 & 0 & 1 \\ 0 & -1 & 1 & \frac{U}{t}. \end{pmatrix}. \tag{L.6}$$

Exact disgonalization of Eq.(L.6) gives

$$\epsilon_3 = U/t, \tag{L.7}$$

$$\epsilon_4 = 0, \tag{L.8}$$

$$\epsilon_{5,6} = \frac{(\frac{U}{t}) \pm \sqrt{(\frac{U}{t})^2 + 16}}{2}. \tag{L.9}$$

Comparing the above eigenvalues, we find that the ground state energy of the hydrogen molecule is

$$E_0(2) = \frac{(\frac{U}{t}) - \sqrt{(\frac{U}{t})^2 + 16}}{2}, \tag{L.10}$$

and two wavefunction is in the spin-singlet sector.

L.1.2 Exact Calculation in Other Fillings

Now if the hydrogen molecule is filled with 3 electrons, we will have 4 different occupations, denoted by 4 wavefunctions:

$$\begin{cases} \phi_1 = (2,1) \\ \phi_2 = (2,-1) \\ \phi_3 = (1,2) \\ \phi_4 = (-1,2). \end{cases} \tag{L.11}$$

Then in units of t, we write the Hamiltonian $\hat{H}$ in matrix form

$$\hat{H} = \begin{pmatrix} U/t & 0 & 1 & 0 \\ 0 & U/t & 0 & 1 \\ 1 & 0 & U/t & 0 \\ 0 & 1 & 0 & U/t \end{pmatrix}. \tag{L.12}$$

Exact diagonalization of Eq.(L.12) gives

$$\epsilon_{1,2} = \frac{U}{t} + 1, \tag{L.13}$$

$$\epsilon_{3,4} = \frac{U}{t} - 1, \tag{L.14}$$

$$\tag{L.15}$$

Thus the ground state energy of the H_2^- molecule is

$$E_0(3) = \frac{U}{t} - 1. \tag{L.16}$$

Similar calculations are applied to the hydrogen molecules filled with 1, 4 or 0 electrons, and we list results below:

$$E_0(1) = -1, \tag{L.17}$$
$$E_0(4) = 2(\frac{U}{t}), \tag{L.18}$$
$$E_0(0) = 0. \tag{L.19}$$

Note all the energies are in units of t. The binding energies for electrons or holes are also extracted

$$\begin{aligned} E_e &= E_0(4) + E_0(2) - 2E_0(3) \\ &= \frac{1}{2}(\frac{U}{t}) - \frac{1}{2}\sqrt{(\frac{U}{t})^2 + 16} + 2, \end{aligned} \tag{L.20}$$
$$\begin{aligned} E_h &= E_0(2) + E_0(0) - 2E_0(1) \\ &= \frac{1}{2}(\frac{U}{t}) - \frac{1}{2}\sqrt{(\frac{U}{t})^2 + 16} + 2. \end{aligned} \tag{L.21}$$

L.1.3 Perturbation Calculation

If we treat the on-site Coulomb interaction term as a perturbation, then the unperturbed Hamiltonian is given by

$$\hat{H}_0 = -t \sum_{<i,j>\sigma} (c^+_{i\sigma} c_{j\sigma} + h.c.), \tag{L.22}$$

or in matrix representation

$$\hat{H}_0 = \begin{pmatrix} 0 & -t \\ -t & 0 \end{pmatrix}. \tag{L.23}$$

Diagonalization of Eq.(L.23) is trivial and we get two energy levels $\epsilon_1 = -1$ and $\epsilon_2 = 1$ (both in units of t). Thus to the 0^{th} order perturbation, the ground state energy of the hydrogen molecule is given by

$$E^{(0)} = -2, \tag{L.24}$$

and the unperturbed wavefunction is spin-singlet

$$\phi^{(0)} = \Psi_\beta|\uparrow> \Psi_\beta|\downarrow>, \tag{L.25}$$

where Ψ_β is the eigenfunction corresponding to eigenvalue ϵ_2 and is going to be introduced below.

The perturbation term is the on-site Coulomb interaction

$$\hat{H}' = U \sum_i n_{i\uparrow} n_{i\downarrow}. \tag{L.26}$$

In order to do perturbation calculation, we need the eigenfunctions of the unperturbed system. For $\epsilon_1 = 1$, the eigenfunction is

$$\Psi_\alpha = \frac{1}{\sqrt{2}} \begin{pmatrix} 1 \\ -1 \end{pmatrix}. \tag{L.27}$$

And for $\epsilon_2 = -1$,

$$\Psi_\beta = \frac{1}{\sqrt{2}} \begin{pmatrix} 1 \\ 1 \end{pmatrix}. \tag{L.28}$$

Thus, we have a transformation of operators between real space and k space

$$\begin{cases} c_{i\sigma} = \Psi_{\alpha,i} c_{\alpha\sigma} + \Psi_{\beta,i} c_{\beta\sigma} \\ c^+_{i\sigma} = \Psi_{\alpha,i} c^+_{\alpha\sigma} + \Psi_{\beta,i} c^+_{\beta\sigma} \end{cases} \tag{L.29}$$

The perturbation Hamiltonian is then transformed to

$$\begin{aligned} \hat{H}' &= U \sum_i n_{i\uparrow} n_{i\downarrow} \\ &= U\{(\Psi_{\alpha 1} c^+_{\alpha\uparrow} + \Psi_{\beta 1} c^+_{\beta\uparrow})(\Psi_{\alpha 1} c_{\alpha\uparrow} + \Psi_{\beta 1} c_{\beta\uparrow})(\Psi_{\alpha 1} c^+_{\alpha\downarrow} + \Psi_{\beta 1} c^+_{\beta\downarrow})(\Psi_{\alpha 1} c_{\alpha\downarrow} + \Psi_{\beta 1} c_{\beta\downarrow}) \\ &\quad +(\Psi_{\alpha 2} c^+_{\alpha\uparrow} + \Psi_{\beta 2} c^+_{\beta\uparrow})(\Psi_{\alpha 2} c_{\alpha\uparrow} + \Psi_{\beta 2} c_{\beta\uparrow})(\Psi_{\alpha 2} c^+_{\alpha\downarrow} + \Psi_{\beta 2} c^+_{\beta 1})(\Psi_{\alpha 2} c_{\alpha\downarrow} + \Psi_{\beta 2} c_{\beta\downarrow})\} \\ &= \frac{U}{2}\{n_{\alpha\uparrow} n_{\alpha\downarrow} + n_{\beta\uparrow} n_{\beta\downarrow} + 2 n_{\alpha\uparrow} n_{\beta\downarrow} + c^+_{\alpha\uparrow} c_{\beta\uparrow} c^+_{\alpha\downarrow} c_{\beta\downarrow} + c^+_{\beta\uparrow} c_{\alpha\uparrow} c^+_{\alpha\downarrow} c_{\beta\downarrow} + \\ &\quad c^+_{\alpha\uparrow} c_{\beta\uparrow} c^+_{\beta\downarrow} c_{\alpha\downarrow} + c^+_{\beta\uparrow} c_{\alpha\uparrow} c^+_{\beta\downarrow} c_{\alpha\downarrow}\}. \end{aligned} \tag{L.30}$$

With Eq.(L.30), first order perturbation is simply given by

$$\begin{aligned} E^{(1)} &= < \Psi_{\beta\uparrow} \Psi_{\beta\downarrow} | \hat{H}' | \Psi_{\beta\uparrow} \Psi_{\beta\downarrow} > \\ &= \frac{U}{2}\{0 + 1 + 0 + 0 + 0 + 0 + 0 + 0\} \\ &= \frac{U}{2}. \end{aligned} \tag{L.31}$$

$\Phi_1 = \Psi_{\beta\uparrow}\Psi_{\alpha\downarrow}$	$\Phi_2 = \Psi_{\beta\downarrow}\Psi_{\alpha\uparrow}$	$\Phi_3 = \Psi_{\alpha\uparrow}\Psi_{\alpha\downarrow}$
$E_1 = 0$	$E_2 = 0$	$E_3 = 2t$

Table L.1: Excited state of a hydrogen molecule.

For the second order perturbation, we have 3 different excited states, see Table 5. The second order perturbed energy is then easy to obtain

$$\begin{aligned} E^{(2)} &= \sum_{i=1}^{3} \frac{|<\Phi_i|\hat{H}'|\Phi_0>|^2}{E_0 - E_i} \\ &= \frac{|<\Phi_0|\hat{H}'|\Phi_3>|^2}{E_0 - E_3} \\ &= \frac{(\frac{U}{2})^2}{-2t-2t} \\ &= -\frac{U^2}{16t}. \end{aligned} \tag{L.32}$$

Thus in units of t, the ground state energy of a hydrogen molecule to the second order perturbation is

$$\begin{aligned} E &= E^{(0)} + E^{(1)} + E^{(2)} \\ &= -2 + \frac{1}{2}(\frac{U}{t}) - \frac{1}{16}(\frac{U}{t})^2. \end{aligned} \tag{L.33}$$

L.2 Calculations on $t - J$ Model

As the calculation is roughly the same as what we have done on the Hubbard model, we will only give details in the half-filling case.

Our basis wavefunctions can be divided into 3 different total spin sectors: $S_z = 0$, $S_z = \hbar$, and $S_z = -\hbar$. For $S_z = \hbar$, we have only one wavefunction:

$$\Psi_1 = (1, 1). \tag{L.34}$$

The expectation value of $t - J$ model Hamiltonian can then be easily evaluated

$$\epsilon_1 = <\Psi_1|\hat{H}|\Psi_1> = 0. \tag{L.35}$$

For $S_z = -\hbar$, the same calculation gives

$$\epsilon_2 =< \Psi_{-1}|\hat{H}|\Psi_{-1} >= 0, \tag{L.36}$$

where, $\Psi_{-1} = (-1, -1)$.

For $S_z = 0$ sector, we have two basis wavefunctions:

$$\begin{cases} \phi_1 &= (1, -1) \\ \phi_2 &= (-1, 1). \end{cases} \tag{L.37}$$

In units of J, we can write the matrix representation of the $t - J$ Hamiltonian $\hat{H}$

$$\hat{H} = \begin{pmatrix} -\frac{1}{2} & \frac{1}{2} \\ \frac{1}{2} & -\frac{1}{2} \end{pmatrix}. \tag{L.38}$$

Exact diagonalization of Eq.(L.38) gives

$$\epsilon_3 = 0, \tag{L.39}$$

$$\epsilon_4 = -J. \tag{L.40}$$

Comparing the above eigenvalues, we find the ground state energy of the hydrogen molecule, which is

$$E_0^{t-J} = -J = -\frac{4t^2}{U}. \tag{L.41}$$

This ground state energy of the $t - J$ model can also be obtained if we take the large U/t limit in Eq.(L.10).

Appendix M

C_{60} Molecule Coordinate Data

The following C_{60} molecule coordinate data are taken from the website: www.ccl.net/cca/data/fullerenes, where a lot of other molecular data can be found, too. These cartesian coordinate data can be converted to real length if we use the radius or diameter ($7\mathring{A}$) of a C_{60} molecule.

Table M.1: Cartesian coordinates of atoms in a C_{60} molecule. First column is the label of the 60 atoms, the fifth column is the nearest neighbor and last 2 columns are the 2 next nearest neighbors.

atom number	x	y	z	nl	nnl	nn2
1	0.000000	3.449997	0.684800	58	7	26
2	3.002716	1.408493	-1.170975	59	9	27
3	0.000000	-3.449997	0.684800	48	6	31
4	2.279007	-2.579483	-0.723694	60	10	28
5	-2.579483	-0.723694	2.279007	49	8	32
6	-1.170975	-3.002716	1.408493	56	3	29
7	-1.170975	3.002716	1.408493	50	1	33
8	-2.579483	0.723694	2.279007	57	5	30
9	2.279007	2.579483	-0.723694	46	2	34
10	3.002716	-1.408493	-1.170975	47	4	35
11	-3.002716	-1.408493	-1.170975	43	20	36
12	-3.002716	1.408493	-1.170975	44	16	37
13	-0.723694	2.279007	-2.579483	45	17	38
14	0.684800	0.000000	-3.449997	41	18	39
15	-0.723694	-2.279007	-2.579483	42	19	40

atom number	x	y	z	n1	nn1	nn2
16	-2.279007	2.579483	-0.723694	38	12	50
17	0.723694	2.279007	-2.579483	39	13	46
18	1.408493	-1.170975	-3.002716	40	14	47
19	-1.170975	-3.002716	-1.408493	36	15	48
20	-3.449997	-0.684800	0.000000	37	11	49
21	2.579483	0.723694	2.279007	53	22	25
22	2.579483	-0.723694	2.279007	54	21	23
23	1.408493	-1.170975	3.002716	55	22	24
24	0.684800	0.000000	3.449997	51	23	25
25	1.408493	1.170975	3.002716	52	21	24
26	1.170975	3.002716	1.408493	34	1	52
27	3.449997	0.684800	0.000000	35	2	53
28	2.279007	-2.579483	0.723694	31	4	54
29	-0.723694	-2.279007	2.579483	32	6	55
30	-1.408493	1.170975	3.002716	33	8	51
31	1.170975	-3.002716	1.408493	28	3	55
32	-1.408493	-1.170975	3.002716	29	5	51
33	-0.723694	2.279007	2.579483	30	7	52
34	2.279007	2.579483	0.723694	26	9	53
35	3.449997	-0.684800	0.000000	27	10	54
36	-2.279007	-2.579483	-0.723694	19	11	56
37	-3.449997	0.684800	0.000000	20	12	57
38	-1.170975	3.002716	-1.408493	16	13	58
39	1.408493	1.170975	-3.002716	17	14	59
40	0.723694	-2.279007	-2.579483	18	15	60
41	-0.684800	0.000000	-3.449997	14	42	45
42	-1.408493	-1.170975	-3.002716	15	41	43
43	-2.579483	-0.723694	-2.279007	11	42	44
44	-2.579483	0.723694	-2.279007	12	43	45
45	-1.408493	1.170975	-3.002716	13	41	44
46	1.170975	3.002716	-1.408493	9	17	58
47	2.579483	-0.723694	-2.279007	10	18	59
48	0.000000	-3.449997	-0.684800	3	19	60
49	-3.002716	-1.408493	1.170975	5	20	56
50	-2.279007	2.579483	0.723694	7	16	57
51	-0.684800	0.000000	3.449997	24	30	32
52	0.723694	2.279007	2.579483	25	26	33
53	3.002716	1.408493	1.170975	21	27	34
54	3.002716	-1.408493	1.170975	22	28	35
55	0.723694	-2.279007	2.579483	23	29	31
56	-2.279007	-2.579483	0.723694	6	36	49
57	-3.002716	1.408493	1.170975	8	37	50
58	0.000000	3.449997	-0.684800	1	38	46
59	2.579483	0.723694	-2.279007	2	39	47
60	1.170975	-3.002716	-1.408493	4	40	48